The potential of UAV-based remote sensing for the prediction of aboveground biomass and N fixation in legume-grass mixtures

---

Dissertation to obtain the academic degree
Doktor der Agrarwissenschaften
(Dr. agr.)

Submitted to the Faculty of Organic Agricultural Sciences
of the University of Kassel, Germany

By Esther Grüner

Witzenhausen, July 2020

This work has been accepted by the Faculty of Organic Agricultural Sciences of the University of Kassel as a thesis for acquiring the academic degree Doktor der Agrarwissenschaften (Dr. agr.).

- Supervisor: Prof. Dr. M. Wachendorf, University of Kassel, Germany
- Co-supervisor: Prof. Dr. A. Bürkert, University of Kassel, Germany

The oral defense day: 24th of September 2020

Preface

This dissertation was submitted to the Faculty of Organic Agricultural Sciences of the University of Kassel to fulfil the requirements for the degree Doctor of Agricultural Sciences (Dr. agr.). The dissertation comprises of two published articles in peer-reviewed international journals, which are included in Chapter 3 and 4. The list of the published articles referring to the chapters in the thesis is provided below.

Chapter 3: Grüner, E., Astor, T., & Wachendorf, M. (2019). Biomass prediction of heterogeneous temperate grasslands using an SfM approach based on UAV imaging. Agronomy, 9(2), 54. doi:10.3390/agronomy9020054

Chapter 4: Grüner, E.; Wachendorf, M.; Astor, T. (2020). The potential of UAV-borne spectral and textural information for predicting aboveground biomass and N fixation in legume-grass mixtures. PLoS ONE 15(6): e0234703. https://doi.org/10.1371/journal.pone.0234703

Acknowledgement

First of all, I am deeply grateful to my supervisor Prof. Dr. Michael Wachendorf for guiding me with his scientific knowledge, support, respect and motivation through the last three years and giving me the opportunity to do my PhD in his department. Moreover, I thank Prof. Dr. Andreas Bürkert for acceptance of the co-supervision.

I would like to thank Dr. Thomas Astor for all the supportive, inspiring discussions and for introducing me to the world of remote sensing. I also thank Dr. Rüdiger Graß for his great help and advice in the sometimes challenging project. Furthermore, I want to thank Wolfgang Funke for sharing his experiences in practical farming and his support in many days of field work. Special thanks to Andrea Gerke, who was so supportive and organized and always found a solution. In addition, I would like to thank Claudia Thieme-Fricke and Eva Wiegard for their reliable help on the field and in the laboratory and I also want to mention all the students who worked hard on this project.

I greatly thank my colleagues Jayan, Isaac, Ben, Supria, Matthias and especially Damian, being the best office partner, for this journey we all started together three years ago. You were a great source of inspiration, support and friendship. I further want to thank Susanne Günther, Dr. Thomas Fricke, Dr. Ilze Dzene, Dr. Frank Hensgen, Dr. Korbinian Kaetzl and Dr. Kathrin Stenchly for the unforgettable cooperation and the great fun during and outside of work. I will miss our coffee breaks!

Finally, I profoundly thank my family, especially my parents, who never stopped believing in me. I thank Stephan for giving me the confidence in my work on this thesis and all my closest friends who supported and motivated me in all ups and downs, as well as all other people who were part of this work.

Witzenhausen, July 2020 *Esther Grüner*

Table of Contents

List of figures ..... **VII**
List of tables ..... **IX**
List of abbreviations ..... **XI**
Summary ..... **XIII**
Zusammenfassung ..... **XV**
1 General introduction **1**
1.1 Grassland 2
1.2 Precision agriculture and grassland monitoring 4
1.3 Remote sensing in grassland 5
2 Research motivation and objectives **8**
3 Biomass Prediction of Heterogeneous Temperate Grasslands Using an SfM Approach Based on UAV Imaging **10**
3.1 Introduction 11
3.2 Material and Methods 14
3.2.1 Experimental Site and Design 14
3.2.2 RGB Remote Sensing and Data Acquisition 16
3.2.3 Data Processing and Analysis 17
3.2.4 Statistical Analysis 19
3.3 Results 21
3.3.1 Dry Matter Yield 21
3.3.2 Canopy Height 22
3.3.3 Prediction Models 24
3.4 Discussion 28
3.5 Conclusion 31
3.6 Appendix 33
4 The potential of UAV-borne spectral and textural information for predicting aboveground biomass and N fixation in legume-grass mixtures **34**
4.1 Introduction 35
4.2 Material and Methods 38
4.2.1 Experimental site and ground truth data 38
4.2.2 UAV image acquisition and data pre-processing 41
4.2.3 Data analysis and machine learning 42

4.2.4 Texture features of images 43
4.2.5 Vegetation index calculation 45
4.2.6 Partial Least Square and Random Forest regression 45
4.3 Results 47
4.3.1 Prediction models 49
4.4 Discussion 56
4.5 Conclusion 61
4.6 Appendix 62
5 Prediction of biomass and N fixation of legume-grass mixtures using sensor fusion 68
5.1 Introduction 69
5.2 Material and methods 72
5.2.1 Experimental site 72
5.2.2 Data acquisition 73
5.2.3 Data pre-processing 75
5.3 Results 78
5.3.1 Ground truth data 78
5.3.2 Biomass and N_{Fix} prediction 79
5.4 Discussion 86
5.5 Conclusion 89
5.6 Appendix 90
6 General discussion 93
6.1 Estimation models 94
6.1.1 Data acquisition 94
6.1.2 Choice of predictor variables 95
6.1.3 Model generation 97
6.2 Future perspectives 99
7 Conclusion 102
8 References 104

List of figures

Table 3.1: List of the treatments with functional groups, species and their ratio in the seed mixture of each treatment. 15

Table 3.2: Coefficients of determination (R^2), root mean square errors (RMSE) and relative RMSE (rRMSE) of linear regression analysis between manual height measurements (CH_R) and UAV-based RGB imaging (CH_D) for the whole dataset (All) and the different treatments: clover-grass (CG), lucerne-grass (LG) as well as the pure stands of legumes (L_{CG}, L_{LG}) and grass (G_{CG}, G_{LG}) of the mixtures, respectively. Values in brackets represent results for the dataset without pure grass swards of the second cut. 24

Table 3.3: Linear regression analysis of calibration (cal) and validation (val) dataset between dry matter yield and manual height measurements (CH_R) as well as UAV based RGB imaging (CH_D) for the whole dataset (All) and the different treatments: clover-grass (CG), lucerne-grass (LG) as well as the pure stands of legumes (L_{CG}, L_{LG}) and grass (G_{CG}, G_{LG}) of the mixtures, respectively. n = number of samples; R^2 = coefficient of determination; RMSE = root mean square error; rRMSE = relative RMSE; d = Willmott's refined index of agreement. Values in brackets represent results for the dataset without pure grass swards of the second cut. 25

Table 3.4: Linear regression analysis of calibration (cal) and validation (val) dataset between dry matter yield and manual height measurements (CH_R) as well as UAV based RGB imaging (CH_D) for clover-grass (CG) and lucerne-grass (LG) mixtures including corresponding pure stands of legumes (L) and grass swards (G). n = number of samples; R^2 = coefficient of determination; RMSE = root mean square error; rRMSE = relative RMSE; d = Willmott's refined index of agreement. Values in brackets represent results for the dataset without pure grass swards of the second cut. 27

Table 3.5: Measured total annual dry matter yield including four cuts (ADMY) and the difference between ADMY and the predicted values based on manual height measurement ($ADMY_R$) and UAV based RGB imaging ($ADMY_D$) for the whole dataset (All) and the different treatments: clover-grass (CG), lucerne-grass (LG) as well as the pure stands of legumes (L_{CG}, L_{LG}) and grass (G_{CG}, G_{LG}) of the mixtures, respectively. Values in brackets represent the relative deviation. For better understanding DMY data was re-transformed to the original scale. SD = standard deviation. 28

Table 3.6: Dry matter yield (DMY) of the different treatments: the clover-grass (CG) and lucerne-grass (LG) mixtures and pure stands of legumes (L) and grasses (G) for 10 sampling dates comprising four harvest cuts and six

sub-samplings every second week during sward growth between 17.05.17 and 09.10.17.....33

Table 4.1: Haralicks Grey Level Co-occurrence Matrix (GLCM) texture features.....44

Table 4.2: Median value of 100 randomly executed cross-validations of Partial Least Square (PLS) and Random Forest (RF) regression including multispectral variables and indices with and without texture features (T) for fresh (FM) and dry matter (DM) as well as fixed N (N_{Fix}) for the whole dataset as well as crop-specific: clover-grass (CG) and lucerne-grass (LG) mixtures including the pure stands of legumes (L_{CG}, L_{LG}) and grass (G_{CG}, G_{LG}); n = number of datapoints, R^2_{val} = coefficient of determination of validation, RMSEP = root mean square error of prediction, rRMSEP = relative RMSEP (%).....50

Table 4.3: Treatments. 62

Table 4.4: Vegetation indices. Vegetation indices calculated with four bands captured by the multispectral sensor used in this study: green, red, red edge (RE) and near infra-red (NIR). 63

Table 4.5: Photogrammetric processing information. 64

Table 5.1: Total rainfall, number of samples and UAV flight information for both research years.....72

Table 5.2: List of treatments.....90

Table 5.3: List of vegetation indices (VIs).....91

Table 5.4: Haralicks texture features.....92

List of tables

Table 3.1: List of the treatments with functional groups, species and their ratio in the seed mixture of each treatment. 15

Table 3.2: Coefficients of determination (R^2), root mean square errors (RMSE) and relative RMSE (rRMSE) of linear regression analysis between manual height measurements (CH_R) and UAV-based RGB imaging (CH_D) for the whole dataset (All) and the different treatments: clover-grass (CG), lucerne-grass (LG) as well as the pure stands of legumes (L_{CG}, L_{LG}) and grass (G_{CG}, G_{LG}) of the mixtures, respectively. Values in brackets represent results for the dataset without pure grass swards of the second cut. 24

Table 3.3: Linear regression analysis of calibration (cal) and validation (val) dataset between dry matter yield and manual height measurements (CH_R) as well as UAV based RGB imaging (CH_D) for the whole dataset (All) and the different treatments: clover-grass (CG), lucerne-grass (LG) as well as the pure stands of legumes (L_{CG}, L_{LG}) and grass (G_{CG}, G_{LG}) of the mixtures, respectively. n = number of samples; R^2 = coefficient of determination; RMSE = root mean square error; rRMSE = relative RMSE; d = Willmott's refined index of agreement. Values in brackets represent results for the dataset without pure grass swards of the second cut. 25

Table 3.4: Linear regression analysis of calibration (cal) and validation (val) dataset between dry matter yield and manual height measurements (CH_R) as well as UAV based RGB imaging (CH_D) for clover-grass (CG) and lucerne-grass (LG) mixtures including corresponding pure stands of legumes (L) and grass swards (G). n = number of samples; R^2 = coefficient of determination; RMSE = root mean square error; rRMSE = relative RMSE; d = Willmott's refined index of agreement. Values in brackets represent results for the dataset without pure grass swards of the second cut. 27

Table 3.5: Measured total annual dry matter yield including four cuts (ADMY) and the difference between ADMY and the predicted values based on manual height measurement ($ADMY_R$) and UAV based RGB imaging ($ADMY_D$) for the whole dataset (All) and the different treatments: clover-grass (CG), lucerne-grass (LG) as well as the pure stands of legumes (L_{CG}, L_{LG}) and grass (G_{CG}, G_{LG}) of the mixtures, respectively. Values in brackets represent the relative deviation. For better understanding DMY data was re-transformed to the original scale. SD = standard deviation. 28

Table 3.6: Dry matter yield (DMY) of the different treatments: the clover-grass (CG) and lucerne-grass (LG) mixtures and pure stands of legumes (L) and grasses (G) for 10 sampling dates comprising four harvest cuts and six

sub-samplings every second week during sward growth between 17.05.17 and 09.10.17.....33

Table 4.1: Haralicks Grey Level Co-occurrence Matrix (GLCM) texture features.....44

Table 4.2: Median value of 100 randomly executed cross-validations of Partial Least Square (PLS) and Random Forest (RF) regression including multispectral variables and indices with and without texture features (T) for fresh (FM) and dry matter (DM) as well as fixed N (N_{Fix}) for the whole dataset as well as crop-specific: clover-grass (CG) and lucerne-grass (LG) mixtures including the pure stands of legumes (L_{CG}, L_{LG}) and grass (G_{CG}, G_{LG}); n = number of datapoints, R^2_{val} = coefficient of determination of validation, RMSEP = root mean square error of prediction, rRMSEP = relative RMSEP (%).....50

Table 5.1: Total rainfall, number of samples and UAV flight information for both research years.....72

List of abbreviations

2D	two dimensional
3D	three dimensional
ADMY	annual dry matter yield
ANOVA	analysis of variance
CG	clover-grass
CH	canopy height
CH_D	canopy height (drone-based)
CH_R	canopy height (ruler-based)
CSH	crop surface height
d	Willmott's refined index of agreement
DEM	digital elevation model
DM	dry matter
DMY	dry matter yield
DPGS	differential global positioning system
DSM	digital surface model
FM	fresh matter
G	grass
GCP	ground control point
GIS	geographic information system
GLCM	grey level co-occurrence matrix
GPS	Global Positioning System
L	legume
LAI	leaf area index
LG	lucerne-grass
LiDAR	Light Detection And Ranging
N	nitrogen
N_2	atmospheric nitrogen
N_{Fix}	nitrogen fixation
NDVI	Normalized Difference Vegetation Index
NIR	near infrared
MS	multi-spectral
MSE	mean of squared residuals
OLS	ordinary least square
PLS	Partial Least Square
QGIS	Quantum Geographic Information System
R^2	coefficient of determination
RE	red edge
RF	Random Forest
RGB	red, green, blue
RMA	reduced major axis
RMSE	root mean square error
rRMSE	relative root mean square error
RMSEP	root mean square error of prediction
rRMSEP	relative root mean square error of prediction

RTK	real time kinetics
SD	standard deviation
SfM	Structure from Motion
SR	Simple Ratio
TLS	terrestrial laser scanning
UAV	unmanned aerial vehicle
VI	vegetation index

Summary

The world population is growing steadily and with it the demand for meat and animal protein. A major source of feed for livestock is grassland, which serves as high quality and protein rich forage. In addition to permanent grassland, temporary grassland is a valuable crop rotation element, especially in organic farming, since legumes in legume-grass mixtures can fix atmospheric nitrogen (N_{Fix}). To further increase the intensification in agriculture, reliable non-destructive measurement techniques are needed as an alternative to traditional labor- and time-consuming methods in grasslands. Precision agriculture offers an efficient information-based and site-specific approach to support farm management decisions. In this context, remote sensing is the key driver for precision agriculture to gain these goals. Especially unmanned aerial vehicle (UAVs) are a low-cost and flexible platform for different sensor applications.

Temporary grassland management in precision agriculture plays only a secondary role compared to other agricultural crops. To further close this research gab, this thesis aimed to examine whether remote sensing measurements can be used to estimate biomass and N fixation under field conditions in two legume-grass mixtures including varying proportions of legumes (0-100%). In this thesis three different approaches were tested with three multi-temporal studies: (i) point cloud-based canopy surface height measurement, (ii) multispectral information and (iii) the combination of both in form of sensor fusion.

The first approach was based on the strong correlation between canopy surface height (CSH) and aboveground biomass (Chapter 3). Photogrammetric structure from motion (SfM) processing of UAV-based red, green, blue (RGB) images into point clouds can be used to generate 3D spatial information about CSH. The study showed that biomass estimation by SfM-based UAV RGB imaging provided similar accuracies across all treatments as the ruler height measurements, even under extreme weather conditions (drought). Nevertheless, the high variability of the canopy surface required supplementary spectral and structural information. The second approach used UAV-based multispectral information and vegetation indices for aboveground biomass and

N_{Fix} estimation (Chapter 4). To include also horizontal spatial relationships of pixels to each other in the images, texture features where calculated. The study compared the estimation models with and without the inclusion of texture features. The results showed, that biomass prediction accuracy for the whole dataset as well as for crop-specific models were substantially improved by the inclusion of texture features. The third approach combined point cloud-based CSH measurement with multispectral data and texture features (Chapter 5). This study included two-year data and to increase the spatial resolution, a terrestrial laser scanner was used for a high-density point cloud. Sensor fusion was found to provide better estimates of aboveground biomass and N_{Fix} than separate data analysis of point clouds and multispectral information. Furthermore, the study showed the important role of texture based on multispectral data, but also based on CSH data, which contributed greatly to the estimation model generation.

The results of this thesis showed the challenges and diverse possibilities of the UAV-based biomass and N_{Fix} estimation of two legume-grass mixtures (Chapter 6). The rapid technical development of sensors, platforms and information technology offers constant improvements in precision agriculture and grassland monitoring. The approaches used in this work offer an interesting method for new possibilities at field and farm level.

Zusammenfassung

Die Weltbevölkerung wächst stetig und damit auch die Nachfrage nach Fleisch und tierischem Eiweiß. Eine Hauptfutterquelle für Nutztiere ist Grünland, das als hochwertiges und proteinreiches Futter dient. Neben Dauergrünland ist temporäres Grünland oder Futterbau ein wertvolles Fruchtfolgeglied, insbesondere im ökologischen Landbau, da Leguminosen in Leguminosen-Gras-Gemenge Luftstickstoff (N_{Fix}) binden können. Um die Intensivierung in der Landwirtschaft weiter zu steigern, sind zuverlässige zerstörungsfreie Messtechniken als Alternative zu herkömmlichen arbeits- und zeitaufwändigen Methoden in Grünland erforderlich. Die Präzisionslandwirtschaft (Precision Agriculture) bietet einen effizienten informationsbasierten und standortspezifischen Ansatz zur Unterstützung von Entscheidungen zur Betriebsführung. In diesem Zusammenhang ist die Fernerkundung der Haupttreiber für die Präzisionslandwirtschaft, um diese Ziele zu erreichen. Insbesondere unbemannte Luftfahrzeuge (UAVs) sind eine kostengünstige und flexible Plattform für verschiedene Sensoranwendungen.

Der Futterbau spielt im Vergleich zu anderen Kulturen in der Präzisionslandwirtschaft nur eine untergeordnete Rolle. Um diese Forschungslücke weiter zu schließen, soll untersucht werden, ob Fernerkundungsmessungen verwendet werden können, um die Biomasse und N-Fixierung unter Feldbedingungen in zwei Leguminosen-Gras-Gemengen mit unterschiedlichen Anteilen an Leguminosen (0-100%) abzuschätzen. In dieser Arbeit wurden drei verschiedene Ansätze mit drei multitemporalen Studien getestet: (i) punktwolkenbasierte Messung der Oberflächenhöhe, (ii) multispektrale Informationen und (iii) die Kombination beider in Form einer Sensorfusion.

Der erste Ansatz basierte auf der starken Korrelation zwischen der Pflanzenhöhe (CSH) und der oberirdischen Biomasse (Kapitel 3). Die photogrammetrische Prozessierung (Struktur from Motion (SfM)) von UAV-basierten rot, grün, blau (RGB) Bildern zu Punktwolken kann verwendet werden, um räumliche 3D-Informationen über CSH zu generieren. Die Studie zeigte, dass die Biomasseschätzung durch SfM-basierte UAV-RGB-Bildgebung bei allen Behandlungen ähnliche Genauigkeiten ergab

wie die Messungen der Zollstockhöhe, selbst unter extremen Wetterbedingungen (Dürre). Die hohe Variabilität der Pflanzenhöhe erforderte jedoch zusätzliche spektrale und strukturelle Informationen. Der zweite Ansatz verwendete UAV-basierte multispektrale Informationen und Vegetationsindizes für die oberirdische Biomasse- und N_{Fix}-Schätzung (Kapitel 4). Um auch horizontale räumliche Beziehungen von Pixeln zueinander in Bildern aufzunehmen, wurden Texturmerkmale berechnet. Die Studie verglich die Schätzmodelle mit und ohne Einbeziehung von Texturmerkmalen. Die Ergebnisse zeigten, dass die Genauigkeit der Biomassevorhersage für den gesamten Datensatz sowie für kulturspezifische Modelle durch die Einbeziehung von Texturmerkmalen erheblich verbessert wurde. Der dritte Ansatz kombinierte punktwolkenbasierte CSH-Messung mit multispektralen Daten und Texturmerkmalen (Kapitel 5). Diese Studie umfasste Zweijahresdaten. Um die räumliche Auflösung zu erhöhen, wurde ein terrestrischer Laserscanner für eine Punktwolke mit hoher Dichte verwendet. Es wurde festgestellt, dass die Sensorfusion bessere Schätzungen der oberirdischen Biomasse und von N_{Fix} liefert als die separate Datenanalyse von Punktwolken und multispektralen Informationen. Darüber hinaus zeigte die Studie die wichtige Rolle der Textur auf der Basis von multispektralen Daten, aber auch auf der Basis von CSH Daten, welche einen großen Beitrag zur Erzeugung der Schätzmodelle leistete.

Die Ergebnisse dieser Arbeit zeigten die Herausforderungen und vielfältigen Möglichkeiten der UAV-basierten Biomasse- und NFix-Schätzung von zwei Leguminosen-Gras-Gemengen (Kapitel 6). Die schnelle technische Entwicklung von Sensoren, Plattformen und Informationstechnologie bietet ständige Verbesserungen in der Präzisionslandwirtschaft und der Grünlandüberwachung. Die in dieser Arbeit verwendeten Ansätze bieten eine interessante Methode für neue Möglichkeiten auf Feld- und Betriebsebene.

1 General introduction

The worlds human population reached more than seven billion in the year 2019 and is predicted to exceed ten billion at the end of this century (United Nations 2019). The growing population and welfare are leading to a change in diet towards a higher consumption of meat and animal protein (Kearney 2010). To fulfill the current demand of livestock production in Europe, 188 million ha of arable land is utilized for producing forage, which makes 72% of the overall European agricultural area (Lesschen et al. 2011). More than 40% of the agricultural used area is grassland, which serves as high quality and protein rich forage (O'Mara 2012).

An improved intensification in agriculture to cover the worlds food demand is challenging, due to changing environmental, economic and social impacts and must be adjusted continuously (Oenema et al. 2014). To handle the environmental variability, precision agriculture, also called “precision farming” is an efficient information-based approach to support farm management decisions (Schellberg et al. 2008). Precision agriculture is defined as sustainable and side-specific crop management including a precise application of fertilizer and pesticides, tillage, drilling and yield mapping (Auernhammer 2001). Oenema et al. (2014) identified lack of knowledge about grassland management as one main reason for limited intensification of grasslands. Although grassland takes up the majority of the agricultural area used, little of the new precision agriculture technology has been transferred from arable crops to grassland management (Schellberg et al. 2008). Research in precision agriculture can help to sustainably promote the intensification of grassland and ensure a sufficient livelihood. Remote sensing is the key driver for precision agriculture to gain these goals (Bhakta et al. 2019). These new technologies could help to reach and improve farm management and yield to meet the growing global demands for food.

1.1 Grassland

Grassland in temperate regions is defined as vegetation with more than 10% vegetation cover mainly by grasses and herbs and with less than 10% cover of trees (Dixon et al. 2014). There exist three types of grassland: natural (non-agricultural), extensive (permanent) and intensive (temporary) grasslands (Figure 1.1).

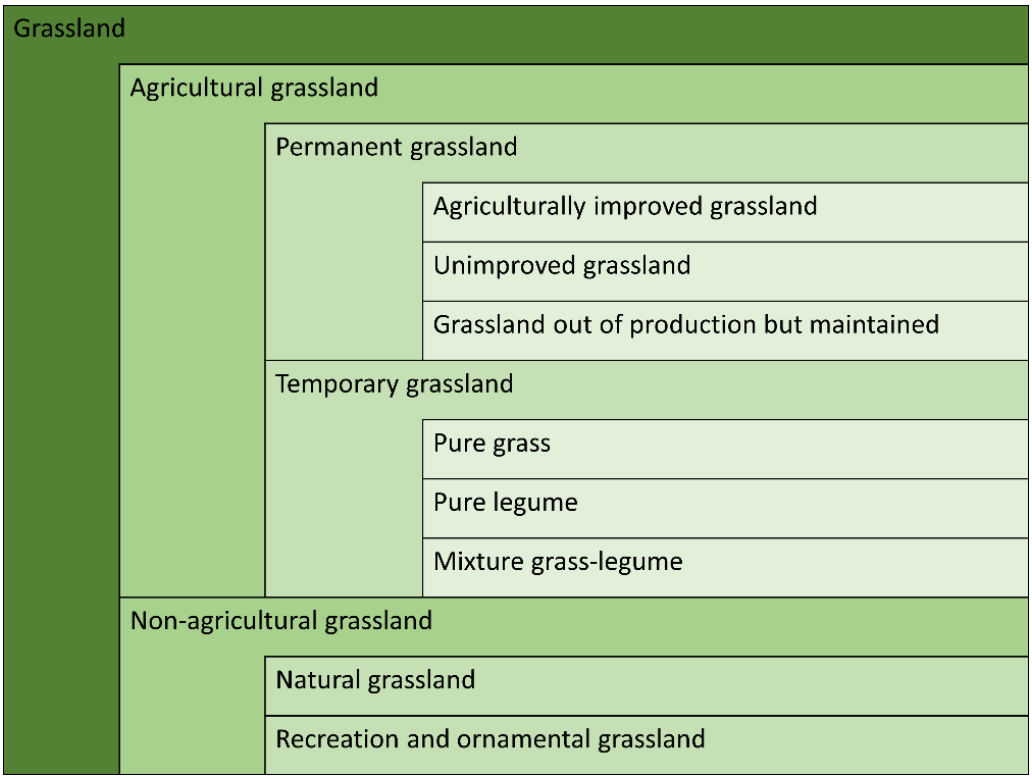

Figure 1.1: EUROSTAT grassland classification (Velthof et al. 2014, modified)

Detailed definitions for different types of grasslands are given by Allen et al. (2011). The amount of species richness and biodiversity decreases with intensification (Bengtsson et al. 2019). For animal production, agricultural permanent and temporary grasslands are the main fodder sources. Permanent grassland is used for grazing as pastures and cutting for hey or silage as meadows. In contrast, temporary grassland is regularly sown, as it is part of the arable crop rotation, which ranges in short phase as winter cover crop (Kuo and Jellum 2002) to several years (Kayser et al. 2010). In Europe from five years of cultivation it is considered as permanent grassland and may no longer be plowed. The species composition can range from monocultures of

legumes and pure grass to legume-grass mixtures (Figure 1.1). The utilization of fertilizer, pesticides, irrigation and the cutting frequency varies strongly within permanent and temporary grasslands (Gierus et al. 2012). Annual yield ranges between 2 t ha^{-1} for grazed extensive grassland and 20 t ha^{-1} for intensive managed grasslands (Peeters 2009). These aspects make clear how diverse and heterogeneous grasslands are.

The main role of temporary grassland is feeding herbivores and ruminants as fodder, but its biomass also serves as substrate for biogas plants (Stinner et al. 2008) and as green manure (Olesen et al. 2009). Furthermore, the cultivation of temporary grasslands provides several additional positive effects on the following cash crop. Beside an increasing yield, the advantages are: increased cash crop quality (Eriksen et al. 2006; Shah et al. 2017), enhanced soil fertility (van Eekeren et al. 2009) and suppression of weed (Melander et al. 2016).

Although, dinitrogen (N_2) is the most frequent gas in air, nitrogen (N) is the most limiting element and factor in agriculture as most plants cannot absorb it (Galloway et al. 1995). Legumes are an exception, as one of their major benefits is their ability to fix atmospheric N (Fustec et al. 2010). Therefore, especially organic farmers add legume-grass mixtures to the crop rotation, as the use of chemical fertilizers is prohibited in this agricultural system. Though, also conventional farmers use legumes to reduce mineral N fertilizer, since an excess leads to negative environmental impacts, like water eutrophication and pollution (Schröder et al. 2004), as well as air pollution and climate change by nitrous oxide (Reay et al. 2012). The amount of fixed N varies strongly and is affected by environmental impacts, and the proportion and species of legumes in the mixture (Boller and Nösberger 1987). Prominent legume species in Europe are white clover (*Trifolium repens* L.), alfalfa (*Medicago sativa* L.) and red clover (*Trifolium pratense* L.) (Gierus et al. 2012). Higher biomass yield can be obtained in combination with grasses as legume-grass mixtures compared to monocultures (Nyfeler et al. 2011). By the symbiosis with *Rhizobium* bacteria, grassland-legumes are able to fix up to 300 kg N ha^{-1} (Carlsson and Huss-Danell 2003; Ledgard and Steele 1992), which has to be taken into account in the N balance of the farm (Möller et al. 2008). Therefore, the quantification of total grassland biomass and the amount of fixed N is necessary.

1.2 Precision agriculture and grassland monitoring

Precision agriculture promotes a sustainable farm management, which helps the farmer to decrease the input while increasing the output factor (Zhang et al. 2002). With the introduction of the Global Positioning System (GPS) and geographic information system (GIS) side-specific farming and ecological monitoring was revolutionized (Crookston 2006; Boyd and Foody 2011). To operate in precision agriculture, data collection and monitoring are essential procedures to support decision making. Vegetation monitoring is the repeated measurement and detection of even small changes between observations of the same location (Critchley et al. 1998). Grassland monitoring includes the assessment of biomass productivity and quality through the entire growing season, as in contrast to other agricultural crops (in Europe), several harvests per year are possible.

The measurement of biomass and quality of grassland is divided in two approaches: destructive and non-destructive. Destructive methods are based on biomass sampling by clipping and weighing or laboratory analysis, which is seen as the most accurate method, whereas non-destructive methods only measure parameters. So far, for biomass estimation traditional methods are carried out by farmers based on visual observation, ruler height and raising plate meter/disc meter and destructive biomass sampling (Catchpole and Wheeler 1992; Sanderson et al. 2001). Visual observations need trained observers, and though, this method is still subjective (Campbell and Arnold 1973).

Beside biomass, the measurement of symbiotically fixed N by legumes is of high interest, as it contributes to the N-cycle and reduces additional fertilization. There exist two different laboratory methods to estimate the amount of fixed N: the ^{15}N natural abundance and ^{15}N isotope dilution technique. The first method is based on the natural isotope discrimination, where the amount of ^{15}N in the soil is higher than in the atmosphere. Therefore, the ratio of ^{15}N and ^{14}N can be measured and compared with a non-fixing reference plant (Carlsson and Huss-Danell 2003). For the isotope dilution method additional ^{15}N is applied to the soil, so the ratio is wider and more precise. A simpler and less expensive method is the difference method based on Stülpnagel

(1982), where the amount of total N uptake of the legume and the non-fixing reference plant is measured and subtracted. The extended difference method subtracts additionally the amount of mineral soil N, for a more precise result.

To detect changes in grassland monitoring, the scale of observation is of great importance (Critchley et al. 1998). The object and parameter of interest as well as the research objectives set the special and temporal scale of measurements. Vegetation monitoring can be done on a worldwide scale for land-cover changes (Green et al. 1994; Kyere et al. 2019) down to single plant observations (Biewer et al. 2008; Jay et al. 2015; Lati et al. 2013). The monitoring methods need a substantial repetition in the area of interest for an equal distribution of measurements, especially for very heterogenic locations. Grassland is a very heterogenous crop with varying species compositions in mixture and phenological and structural differences (Schellberg et al. 2008). Therefore, spatial and temporary resolution as well as scale play a decisive role in grassland monitoring concerning infield spatial variability (Critchley et al. 1998). Nevertheless, all before mentioned methods are time consuming and labor intensive for large areas, what limits its operation to a local scale. An increase of computer-aided evaluation and data collection up to total automation of measurements and analysis is of high interest. Remote sensing, using flexible platforms, offers new possibilities for grassland monitoring and modelling to replace field measurements.

1.3 Remote sensing in grassland

Plants use amongst other things light to produce energy and biomass by photosynthesis (McKendry 2002). The solar reflection and absorption is affected by the plant properties and therefore, green vegetation has a specific spectral signature, similar to a fingerprint, which differs from other material (Wachendorf et al. 2018). This spectral signature is characterized by a low reflection in the visible (red, green, blue; RGB) region by absorption (except of a small peak in the green area), turning to high reflection for near infrared (NIR). The region between red and NIR is called red edge (RE), which marks the typical course of the curve (Ollinger 2011). This pattern or parts

of it can be detected by remote sensing techniques, as a non-destructive measurement method.

Optical sensors, to capture the spectral reflectance, range from RGB cameras to multi- and hyperspectral sensors, which cover also bands beyond the visible and differ in the number of bands, bandwidth as well as – range (Schellberg et al. 2008; Wachendorf et al. 2018). To increase the spectral reflection information specific bands can be combined to calculate vegetation indices (VIs) (Mulla 2013). The most known VI is the Normalized Difference Vegetation Index (NDVI), which includes the before mentioned low red and high NIR reflection characteristics (Rouse et al. 1974). NDVI has successfully been used to measure quantity and quality of grassland traits (Cho et al. 2007; Fan et al. 2009; Wijesingha et al. 2020). Although there exist more than 100 VIS for several plant traits (Xue and Su 2017), due to the influence of local environment and different grass conditions, there is no uniform feasibility of one particular index (Gao 2006). Furthermore, experience with N_{Fix} is still missing.

Sensors can be used ground-based or mounted on different platforms like satellites, airplanes or unmanned aerial vehicles (UAVs) (Wachendorf et al. 2018). Ground-based methods like spectrometry are already common monitoring tools in grassland (Biewer et al. 2009; Mutanga and Skidmore 2004; Psomas et al. 2011). This technique can cover wide range of spectral wavelengths and due its light weight, it is portable and easy to handle within the field (Künnemeyer et al. 2001). Nevertheless, similar to destructive measurement methods, ground-based field spectrometry is time-consuming for larger areas.

Satellites offer so far a good solution for high temporal and constant grassland monitoring on national and global scale (Ali et al. 2016), but need radiometric and atmospheric corrections due to the large distance to the area of interest and image quality can be affected by clouds (Gao 2006; Mulla 2013). Since manned airplane missions are very cost-intensive, UAVs got very prominent in precision agriculture, due to their flexibility, low-costs and easy maintenance. Furthermore, sensors attached to UAVs can offer higher image resolution compared to airplanes or satellites, due to a lower flight altitude, which is beneficial to observe on a local scale.

Beside spectral information also structural or height information can be revealed by remote sensing. Since plant height correlates with biomass ultra-sonic sensor (Fricke et al. 2011), Light Detection and Ranging (LiDAR) and Structure from Motion (SfM) are methods used in grassland monitoring (Cooper et al. 2017; Wijesingha et al. 2018). LiDAR is an active sensor, where areas of shadows can be better captured than with passive optical sensors, which is in particular important at very high spatial resolutions (Wallace et al. 2017). SfM is based on overlapping images, which can be captured by low-cost RGB UAVs. Recent studies have demonstrated the advantage of SfM in permanent grasslands for biomass estimation (Forsmoo et al. 2018; Lussem et al. 2019; Wijesingha et al. 2018). Bareth and Schellberg (2018) showed good results for SfM based on low-cost UAV imaging as an alternative for rising plate meter measurements.

Biophysical and -chemical traits have an huge impact on the spectral expression and its intensity (Ollinger 2011). Therefore, research with ground truth data is still required (Gao 2006). Most existing studies monitoring grassland with remote sensing methods focused on permanent grassland (Schellberg et al. 2008; Wachendorf et al. 2018), while temporary grassland so far received less attention.

2 Research motivation and objectives

Reliable non-destructive measurement techniques are needed as an alternative to traditional methods for grasslands. As mentioned in Chapter 1, there exist phenological, phenotypical and structural differences between permanent and temporary grasslands (Toupet et al. 2020). So far, most studies ignored variable conditions in practical arable farming, which occur due to topographic differences in the field. This heterogeneity can affect species composition, especially the proportion of legumes from 0-100% in the mixtures, which has also an impact on the amount of fixed N. As grassland heterogeneity not only changes in space but also in time due to season and weather conditions (Peterson et al. 2002), multi-temporal studies play a decisive role in grassland monitoring to understand changes in productivity throughout the vegetation phase. Knowledge on aboveground biomass yield and N_{Fix} in temporary grassland, as an important crop rotation element, can be effectively used for sustainable farm management decisions. To close the above-mentioned research gabs, this thesis leads to the following question:

Can remote sensing measurements be used to estimate biomass and N fixation under field conditions in temporary grasslands including varying proportions of legumes?

The aim of this doctoral thesis was to focus on the evaluation of canopy surface height (CSH), based on 3D point cloud, and multispectral information in two in temperate European climate common legume-grass mixtures (clover- and lucerne-grass) over three vegetation periods (2017-2019). This thesis consists of three successive studies. In a first attempt CSH based on SfM was assessed as an alternative to ruler height measurement to predict biomass. In the second study multispectral information was used to evaluate biomass and N_{Fix}. The final study combines both approaches in a sensor fusion, where two-year data of TLS and multispectral information was analyzed. All these studies were carried out on the experimental farm of the Universität Kassel in Witzenhausen, Neu-Eichenberg, which is managed organically. To cover a wide

range of legume proportion, pure stands of legumes and grasses of both mixtures, were investigated in all three studies, which makes the studies comparable.

In conclusion, key research questions are:

- Are UAV-based point clouds suitable for CSH measurement as an alternative to manual ruler height measurement to estimate aboveground biomass? (Chapter 3)
- Is UAV-based multispectral data suitable for aboveground biomass and N_{Fix} estimation? (Chapter 4)
- Does sensor fusion based on both, CSH and multispectral information, improve aboveground biomass and N_{Fix} estimation? (Chapter 5)
- What are the limitations of these methods and their future applications in temporary grassland? (Chapter 3, 4, 5, 6)

3 Biomass Prediction of Heterogeneous Temperate Grasslands Using an SfM Approach Based on UAV Imaging

Abstract

An early and precise yield estimation in intensive managed grassland is mandatory for economic management decisions. RGB (red, green, blue) cameras attached on an unmanned aerial vehicle (UAV) represent a promising non-destructive technology for the assessment of crop traits especially in large and remote areas. Photogrammetric structure from motion (SfM) processing of the UAV-based images into point clouds can be used to generate 3D spatial information about the canopy height (CH). The aim of this study was the development of prediction models for dry matter yield (DMY) in temperate grassland based on CH data generated by UAV RGB imaging over a whole growing season including four cuts. The multi-temporal study compared the remote sensing technique with two conventional methods, i.e., destructive biomass sampling and ruler height measurements in two legume-grass mixtures with red clover (*Trifolium pratense* L.) and lucerne (*Medicago sativa* L.) in combination with Italian ryegrass (*Lolium multiflorum* Lam.). To cover the full range of legume contribution occurring in a practical grassland, pure stands of legumes and grasses contained in each mixture were also investigated. The results showed, that yield prediction by SfM-based UAV RGB imaging provided similar accuracies across all treatments (R^2 = 0.59–0.81) as the ruler height measurements (R^2 = 0.58–0.78). Furthermore, results of yield prediction by UAV RGB imaging demonstrated an improved robustness when an increased CH variability occurred due to extreme weather conditions. It became apparent that morphological characteristics of clover-based canopies (R^2 = 0.75) allow a better remotely sensed prediction of total annual yield than for lucerne-grass mixtures (R^2 = 0.64), and that these crop-specific models cannot be easily transferred to other grassland types.

Keywords: grassland; yield prediction; canopy height; remote sensing; unmanned aerial vehicle; RGB imaging; structure from motion

3.1 Introduction

Legume-grass mixtures with red clover (*Trifolium pratense* L.) and lucerne (*Medicago sativa* L.) in combination with Italian ryegrass (*Lolium multiflorum* Lam.), grown for 1–3 years, play an important role in crop rotations, particularly in organic farming in temperate European climates. Such crops serve as green manure by fixing nitrogen or as feedstock for animals and biogas plants. These intensive grasslands are harvested three to five times per year and, therefore, an early and precise yield estimation is mandatory for management decisions and economic optimizations at the field and farm level (Sanderson et al. 2001). An emerging and promising technology in grassland faming is remote sensing, and especially the use of different sensors on unmanned aerial vehicles (UAV) show great potential for improving agricultural use of grasslands (Schellberg et al. 2008; Wachendorf et al. 2018).

Destructive biomass sampling is considered to be the most accurate yield estimation method but can also be considered as the most labor-intensive method (Catchpole and Wheeler 1992). Another approach for estimating biomass in grasslands is the assessment of canopy height (CH), which was frequently found to be positively correlated with crop biomass (Fricke and Wachendorf 2013; Holman et al. 2016). Traditional height measurements in grassland are often conducted with a rising plate meter, determining the compressed sward height, or with a ruler stick (Hakl et al. 2012; Cudlín et al. 2018). Furthermore, several portable technical devices for non-destructive biomass estimation were developed in the recent years, which so far were not widely distributed in agricultural practice, e.g., leaf area meter to asses leaf area index (LAI) (Harmoney et al. 1997), electronic capacitance meter, which measures the difference of capacitance between air and biomass (Sanderson et al. 2001) and a reflectometer, which measures intensity of spectral reflectance by light emitting diodes (LED) (Künnemeyer et al. 2001). Biomass sampling, manual height measurement and the above-mentioned technical devices need a substantial number of repetitions in

combination with a spatially uniform distributions of the measurements to generate a reliable yield estimation (Lu 2006). Therefore, much time and effort is required to receive reliable data especially on large areas.

Sensors attached on UAVs are useful non-destructive tools for obtaining spatial information from large and remote areas. There exist different sensor systems, such as LiDAR, ultrasound and RGB (red, green, blue) imaging to collect spatial data for a rapid quantification of aboveground biomass (Forsmoo et al. 2018; Moeckel et al. 2017; Wachendorf et al. 2018; Wallace et al. 2017). A UAV in combination with a consumer-grade digital camera for RGB imaging represents a low-cost approach for estimating yield, which may be affordable und workable for farmers. By photogrammetric structure from motion (SfM) processing of the UAV-based images into point clouds, 3D spatial data can be easily generated. Forsmoo et al. (2018) calculated in a grassland sward, that for a plot of 8 m^2 a CH assessment with a ruler needed 550 single height measurements to receive the same accuracy as a SfM-based CH assessment based on UAV RGB imaging. Therefore, the high spatial resolution makes UAV RGB imagery in combination with an SfM approach an interesting tool for yield estimation in practical grassland farming.

SfM derived height measurement based on UAV RGB imaging was successfully used in forestry (Dittmann et al. 2017), and, to a lower degree also in agricultural crops, such as wheat (Holman et al. 2016; Schirrmann et al. 2016), barley (Bendig et al. 2014), maize (Geipel et al. 2014; Li et al. 2016) and vegetable crops (Moeckel et al. 2018). All these studies found strong relationships between biomass and RGB imaging in homogeneous crops. Contrary, grassland represents a mixed crop containing legumes and grasses of several species. Additionally, species contribution and yield changes in the field throughout the growing season and is affected by many factors, such as cutting intensity, soil features, fertilization and climate conditions (Elgersma and Søegaard 2018; Ergon et al. 2016). So far, only a few studies exist using SfM based on RGB imaging in grassland. Cooper et al. (2017) and Wallace et al. (2017) compared height measurements in permanent grasslands based on terrestrial SfM and terrestrial LiDAR and observed similar relationships between these two methods and the grassland biomass. Van Iersel et al. (2018) showed the potential of modeling temporal

dynamics of CH in a floodplain grassland and of classifying different vegetation types (pixel size = 5 cm) with a consumer-grade camera attached on a UAV. Viljanen et al. (2018) worked in an intensive grassland with four harvest cuts and different nitrogen applications rates. The latter used a high-resolution camera (pixel size = 1 cm) mounted on a UAV and combined CH with spectral vegetation indices (VI), resulting in highly significant correlations with biomass. VIs from multi- or hyperspectral sensors also show promising potential for qualitative and quantitative biomass estimation; however extensive spectral calibration work is necessary for these technique (Wachendorf et al. 2018).

To understand the spatial variability and dynamics in grasslands over the entire growing season multi-temporal studies are needed. So far, no study using yield prediction models by SfM considered different proportions of legumes (including pure legume and grass stands as well as legume-grass mixtures), which frequently occur in practical grassland farming. The aim of this study is the development of estimation models for dry matter yield (DMY) in mixed grassland by CH generated by UAV RGB imaging over a whole growing season. The study compares this novel remote sensing technique with ruler height measurements, an established conventional method and uses destructive biomass sampling as a reference data. All measurements were conducted in two different legume-grass mixtures. To cover the wide range of legume contribution in practical grassland, pure stands of legumes (100% legumes) and grasses (0% legumes) were investigated as well as their mixtures. The specific objectives of this study were: (1) the assessment of CH by RGB imaging in two legumes-grass mixtures over the whole growing season; (2) the comparison of prediction models based on an SfM approach with a conventional measurement method; (3) the development of a yield prediction model containing also pure stands of legumes and grasses; (4) assessment of the prediction accuracy for the total annual DMY based on SfM including all harvest cuts during one complete growing season.

3.2 Material and Methods

3.2.1 Experimental Site and Design

The study was carried out at the experimental farm in Neu-Eichenberg of the Universität Kassel (51°23’ N, 9°54’ E, 227 m above sea level) in northern Hesse, Germany. The soil is a silty clay loam with 3.6% sand, 73% silt, 23.4% clay and 2% humus. Summer barley was cultivated as a preceding crop. The mean annual precipitation and daily temperature of the site is 728 mm and 8°C, respectively (Figure 3.1 A, B).

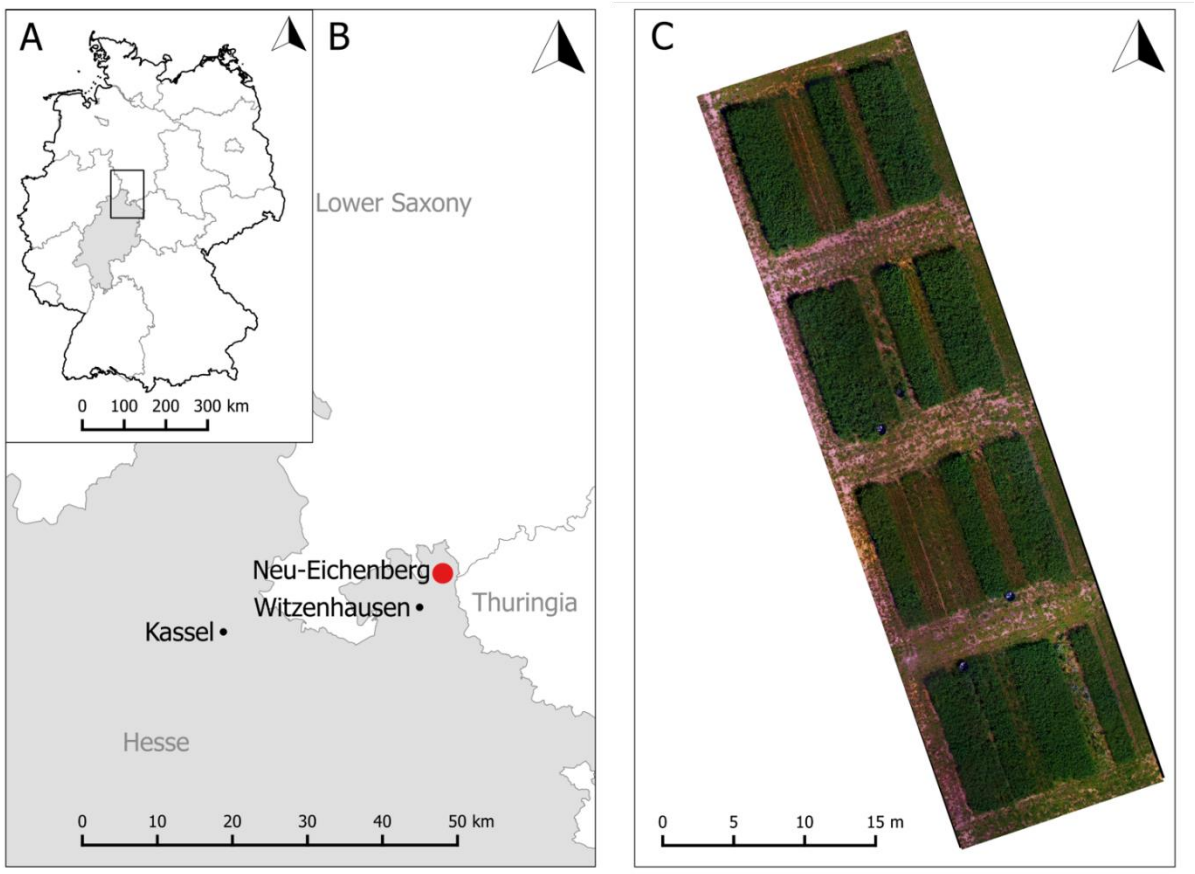

Figure 3.1: (A) Germany’s political map showing the location of Hesse; (B) North-Hesse’s political map showing the location of the experimental site in Neu-Eichenberg; (C) Orthomosaic of the experimental field showing the different plots on 7 August 2017, at the time of the third cut.

Field plots (1.5 m × 10 m) of clover-grass (CG) and lucerne-grass (LG) in mixtures as well as of pure stands of legumes (L; 100% legumes) and grasses (G; 0% legumes) (Table 3.1) were sown in autumn of 2016 in four randomized replicate blocks, giving a total of 24 plots (Figure 3.1 C). All treatments were sown with a total seed rate of 35 kg ha^{-1}. CG contained 60% *Lolium multiflorum*, 30% *Trifolium pratense*, 5% *Trifolium hybridum* L. and 5% *Trifolium repens* L., whereas LG included 40% *Medicago sativa*, 20% *Festuca pratensis* Huds., 15% *Lolium perenne* L., 10% *Lolium multiflorum*, 10% *Trifolium pretense* and 5% *Phleum pretense* L. Consequently, the treatments formed a set of heterogenous vegetation which differed largely in their morphological and optical characteristics. As the experimental farm is managed organically, no fertilizer or pesticides were applied.

Table 3.1: List of the treatments with functional groups, species and their ratio in the seed mixture of each treatment.

Treatment		Functional group	Species	Ratio (%)
Clover-grass mixture	CG	Legumes (L)	*Trifolium pratense*	30
			Trifolium hybridum	5
			Trifolium repens	5
		Grass (G)	*Lolium multiflorum*	60
Lucerne-grass mixture	LG	L	*Medicago sativa*	40
			Trifolium pratense	10
		G	*Festuca pratensis*	20
			Lolium perenne	15
			Lolium multiflorum	10
			Phleum pratense	5
Pure clover legumes	L_{CG}	L from CG mixture	*Trifolium pratense*	75
			Trifolium hybridum	12.5
			Trifolium repens	12.5
Pure lucerne and clover legumes	L_{LG}	L from LG mixture	*Medicago sativa*	80
			Trifolium pratense	20
Pure grass sward	G_{CG}	G from CG mixture	*Lolium multiflorum*	100
Pure grass sward	G_{LG}	G from LG mixture	*Festuca pratensis*	40
			Lolium perenne	30
			Lolium multiflorum	20
			Phleum pratense	10

The total amount of rainfall (762 mm in 2017) was higher than the mean annual precipitation (728 mm), though early summer was characterized by a severe drought. Precipitation for the first cut (17 May 2017) revealed 66 mm compared to long-term average of 91 mm and for the second cut (26 June 2017) 47 mm compared to long-term average of 95 mm. This drought caused an accelerated maturation of the grasses with pronounced stem formation and little leaf growth especially in the second cut.

3.2.2 RGB Remote Sensing and Data Acquisition

RGB images were taken with a low-cost quadrocopter (DJI Phantom 3 Advanced; Shenzhen, China). The flight plan was done with autopilot by means of Pix4Dcapture software (App version 4.4.0, Pix4D SA, Lausanne, Switzerland). All missions were carried out in the morning to ensure equal sun position (8:00–12:00 a.m.). RGB images were taken one day before every harvest (4 flights) and during growth every second week (6 flights). A standard digital camera (DJI FC300S, DJI, Shenzhen, China) was mounted on a gimble and had a f/2.8 lens with a 94° field of view and 12 megapixels. For each mission, images with a forward and side overlap of 80% were taken in a grid pattern at a constant flying height of 20 m, resulting in 300 to 400 individual images with a spatial ground resolution between 7 and 8 mm per pixel. Seven wooden targets, painted black and white (10 × 10 cm, cross-centered) and mounted on small tripods, were used as portable ground control points (GCPs) for georeferencing the generated point clouds at each flight. The GCPs were evenly distributed and set up into balance on the pathways between the experimental plots. The GPS (global positioning system) coordinates were measured using a Leica RTK DGPS with a horizontal and vertical precision of 2 cm. Additionally, the whole experimental field was georeferenced once by recording the coordinates of the corners of each plot.

Subsequent to each flight mission, manual height measurements (CH_R) and destructive biomass samples were taken. The mean grassland height per plot resulted from 50 randomly distributed measurements, which were conducted with a ruler at a precision of 0.01 m. The height was defined as the vertical distance from the soil surface to the highest point of the plant which touched the ruler (Heady 1957). Plots

were harvested four times (17 May 2017, 26 June 2017, 8 August 2017, 9 October 2017) with a Haldrup forage plot harvester at a stubble height of 5 cm and a cutting width of 1.50 m. Prior to harvest two biomass samples for fresh and dry matter yield were taken manually in every plot on an area of 50 × 50 cm each. To enrich the calibration database with data from less mature sward conditions sub-samples were taken every second week during sward growth between 17 May 2017 and 9 October 2017 on an area of 25 × 25 cm in every plot (Appendix Table 3.6). To avoid sampling effects, sub-samples were taken in the first 1.50 m of the plots, whereas the remaining plot area remained untouched during growth. All biomass samples were dried at 105°C to constant weight (~ 48 h), to determine dry matter content and to calculate dry matter yield (DMY).

3.2.3 Data Processing and Analysis

Three-dimensional (3D) point clouds were generated from the RGB images for each dataset using the SfM approach. The software Agisoft PhotoScan Professional (Agisoft LLC, St. Petersburg, Russia) was used to calculate the digital surface model (DSM) from the RGB images. The SfM algorithm obtains 3D information from 2D images and converts the images automatically into a DSM. All processing steps were executed separately for a better control, using uniform settings on a high-performance computer (Figure 3.2).

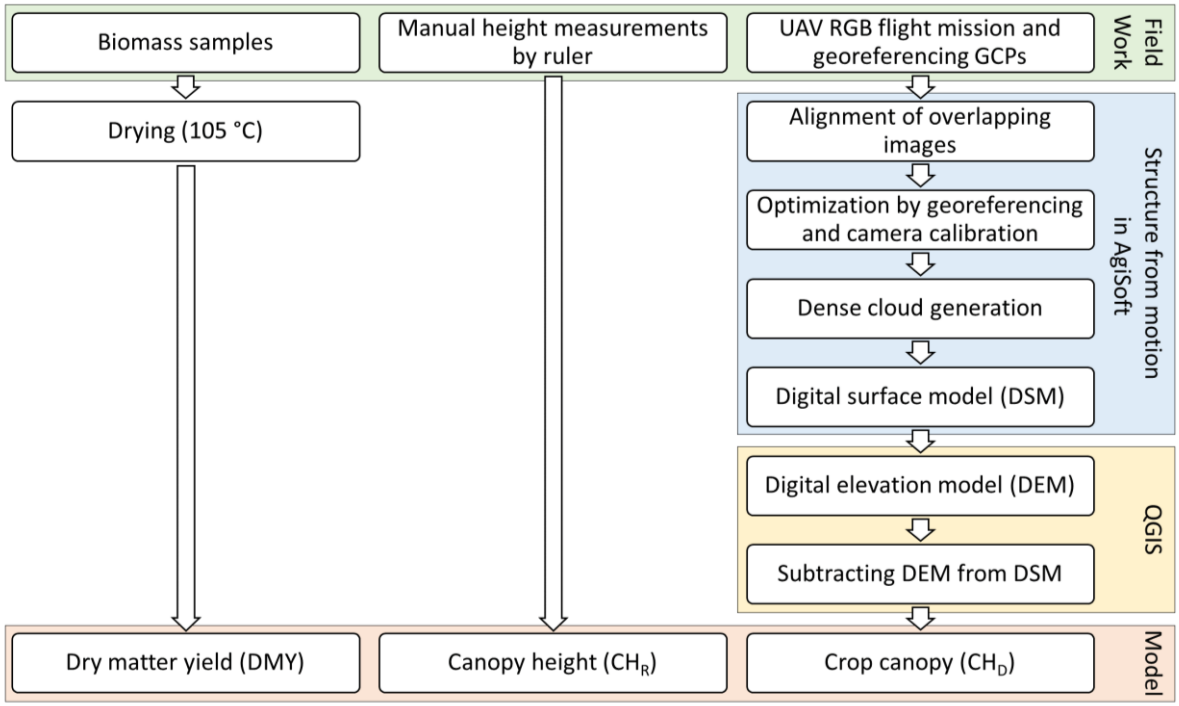

Figure 3.2: Workflow of biomass sampling, manual and UAV-based structure from motion (SfM) height measurement.

After importing a dataset, the overlapping images were aligned by internal image matching techniques and algorithms. Location and orientation of the individual images of the moving camera were automatically determined. The alignment was done with the accuracy setting “medium” and a key point limit of 40,000 and tie point limit of 4000. The output was a sparse point cloud containing a certain amount of paired multidimensional points of all images, which were linked together by identical features.

For the optimization step, the GPS coordinates of the GCPs were imported using the coordinate system WSG 84. The sparse point cloud was georeferenced manually by determining three pictures for each of the seven GCPs and placing the renumbered GCP marker on the cross center of the targets. After that, the software estimated the positions of the GCP marker for the other images automatically and, when needed, the markers were adjusted and placed manually. The spatial error of the GCPs varied between 1 and 2 cm. Additional optimizing of the sparse cloud was done by enhancing the camera lens parameters. With these optimized settings, the image alignment, the

location and orientation of images and, eventually, the sparse point cloud was updated and corrected.

In the next step the georeferenced sparse point cloud was converted into a dense point cloud. The software computed the depth information by the image alignment for all points of the images. For that, medium quality settings were used to keep the processing time at an acceptable level and depth filtering was set to “aggressive” to sort out outlier points due to noise or inaccurate focusing. These steps resulted in one single point cloud, which was much denser and more detailed.

In the last step the dense point cloud was exported in the form of a DSM as a TIFF file with a resolution between 1 and 3 cm per pixel. The DSM represented the recorded surface as a raster data.

Further processing was done with Quantum Geographical Information System (QGIS 2.18.14, QGIS Development Team, Raleigh, NC, USA) software to provide a digital elevation model (DEM). After importing the raster image, ground points in the pathways next to the plots were selected from the DEM, which were interpolated by an inverse interpolation with a power of 3 to provide a continuous ground surface model over the whole field. CH was calculated by subtracting DEM from DSM. The coordinates of the plot corners were used to delimit each plot area. The mean height value for each plot from the drone-based RGB imaging (CH_D) was extracted by zonal statistics. These processes were done for every flight mission separately. From the whole dataset seven CH_D values had to be removed due to unrealistic negative height values.

3.2.4 Statistical Analysis

Statistical analysis was performed using R programming language version 3.5.1 (R Foundation for Statistical Computing, Vienna, Austria). DMY was tested for normal distribution and its residuals for homoscedasticity. As these assumptions were not fulfilled, DMY was square root transformed. ANOVA was used to detect differences among yields of the four cuts in each treatment.

For creating estimation models for the whole dataset (including the subsamples), CH and DMY were used for linear regression models. One main assumption for an ordinary least square (OLS) regression (Type-I regression model) is the allocation of *y* as dependent variable and *x* as independent variable. Another assumption for OLS is the measurement of the independent variable *x* without error. In our study it was not feasible to distinguish between *x* and *y* for CH and DMY and as *x* (i.e., is CH) was measured both manually and by RGB imaging, the height measurements cannot be considered as error-free. In this case, a reduced major axis (RMA) regression, which is a Type-II regression model, was suggested by (Cohen et al. 2003) for analysis in the field of remote sensing. Though slope, intercept and root mean square error (RMSE) are calculated differently, RMA shows the same coefficient of determination (R^2) as OLS. In the current study, RMA was used to predict DMY by CH_R and CH_D for the whole dataset and for the treatments separately. For a better understanding of the graphical presentation of the yield estimation model, the equations were re-transformed to the original scale.

For an assessment of the model accuracy, cross-validation was carried out. The dataset was split into a calibration (training) and validation dataset. To generate an even distribution of the randomly chosen validation dataset, one value was withdrawn from each treatment and sampling date, resulting in a 75% calibration and 25% validation dataset. The calibration dataset was used to generate the corresponding models and the coefficient of determination (R^2_{cal}), the root mean square error ($RMSE_{cal}$) were calculated. The validation dataset was used as an independent dataset to verify the calibrated models by linear regression between measured and predicted DMY, represented by coefficient of determination (R^2_{val}) and root mean square error ($RMSE_{val}$) as well as relative $RMSE_{val}$ ($rRMSE_{val}$). Additionally, to determine the accuracy of the validation between measured and predicted DMY Willmott's refined index of agreement (d) was generated. Willmott's refined index of agreement is a dimensionless value between 0 and 1 indicating no agreement and total agreement, respectively (Willmott 1981).

3.3 Results

Ten datasets of DMY, CH_R and CH_D were collected throughout the vegetation period from May to October 2017. From the datasets of RGB images, which were processed by Agisoft PhotoScan into 3D models and further into CH_D values, seven mean CH_D values from the third and fourth sub-sampling, were negative and were, therefore, excluded from further analysis.

3.3.1 Dry Matter Yield

As the mixtures and pure stands were investigated at various growth stages throughout the growing season, DMY varied widely and declined in most cases with progressing growing season from first to fourth cut (Figure 3.3). DMY of pure grass swards exhibited a particularly strong decrease after the first cut. The mean DMY for the whole dataset including sub-samples ranged from 0.09 to 6.32 t ha^{-1} (Appendix Table 3.6).

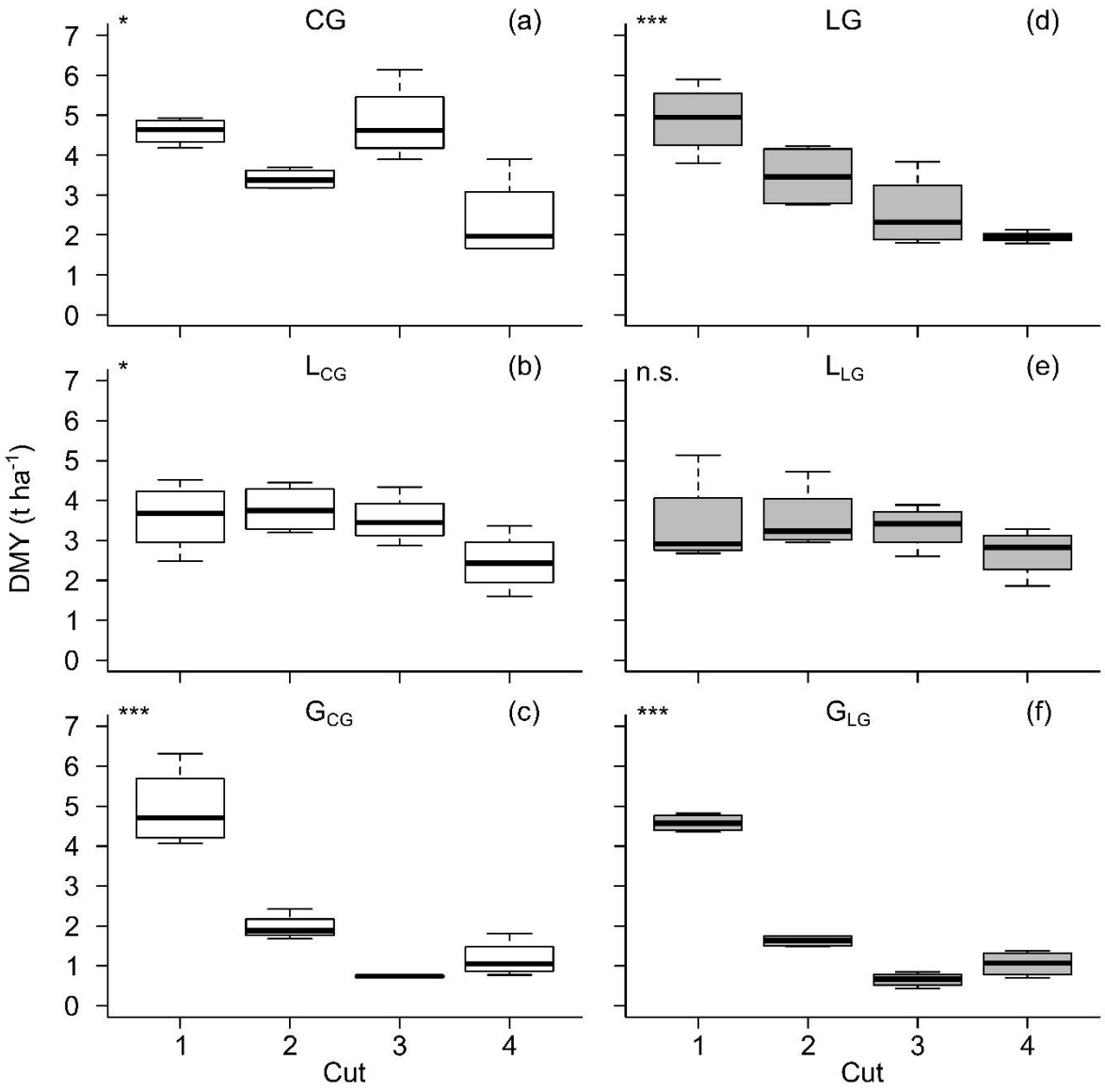

Figure 3.3: Dry matter yield (DMY) at four cuts of clover-grass (CG, left) and lucerne-grass (LG, right) mixtures (a, d) as well as pure stands of legumes (L) (b, e) and grasses (G) (c, f). *** = $p < 0.001$; * = $p < 0.05$; n.s. = not significant.

3.3.2 Canopy Height

The average height values per treatment and date of CH_R and CH_D varied from 9.42 to 89.54 cm and 1.01 to 71.06 cm respectively (Figure 3.4 a). On average, CH_D was more than 4 cm lower than CH_R. CH of sub-samplings and of the fourth cut were lower compared to the first, second and third cut. The linear relationship between CH_R and CH_D showed an R^2 of 0.56 with an RMSE of 13.39 cm. CH_R values of grass from the

second cut were remarkably higher than the corresponding CH_D values. If the data of the grass of the second cut were excluded from analysis, R^2 and RMSE improved to 0.70 and 10.32 cm respectively (Figure 3.4 b).

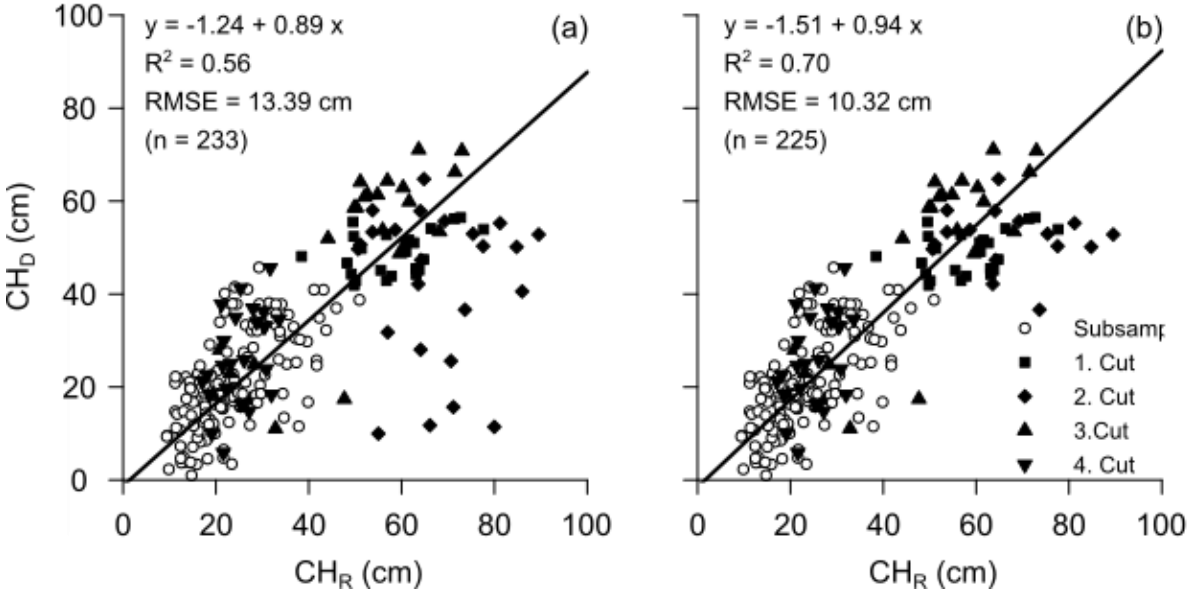

Figure 3.4: Linear relationship between canopy height from manual height measurements (CH_R) and UAV-based RGB imaging (CH_D) for the whole dataset (a) and for the whole dataset excluding pure grass stands of the second cut (b). The different symbols indicate sub-samples (○), which were taken between the first (■), second (♦), third (▲) and fourth (▼) harvest.

Considering the individual treatments, R^2 for the mixtures and pure legume stands varied between 0.70 and 0.84 and rRMSE between 11 and 16% (Table 3.2). The pure grass treatments G_{CG} and G_{LG} showed a lower R^2 of 0.47 (RMSE = 16.51 cm) and 0.29 (RMSE = 16.91 cm) respectively. Similarly to the complete dataset, when the second cut was also excluded from the analysis of the pure grass data, relationship between manual and UAV-based measurements were much better.

Table 3.2: Coefficients of determination (R^2), root mean square errors (RMSE) and relative RMSE (rRMSE) of linear regression analysis between manual height measurements (CH_R) and UAV-based RGB imaging (CH_D) for the whole dataset (All) and the different treatments: clover-grass (CG), lucerne-grass (LG) as well as the pure stands of legumes (L_{CG}, L_{LG}) and grass (G_{CG}, G_{LG}) of the mixtures, respectively. Values in brackets represent results for the dataset without pure grass swards of the second cut.

Treatment	R^2	RMSE (cm)	rRMSE (%)
All	0.56 (0.70)	13.39 (10.32)	17 (13)
CG	0.79	10.19	13
LG	0.70	11.14	16
L_{CG}	0.84	6.08	11
L_{LG}	0.72	8.70	16
G_{CG}	0.47 (0.70)	16.51 (9.17)	22 (14)
G_{LG}	0.29 (0.57)	16.91 (9.35)	24 (17)

3.3.3 Prediction Models

CH as measured by ruler and UAV-based imaging was used as a predictor for DMY. Models were developed based on a calibration and validation dataset for the whole dataset as well as separately for the different treatments (Table 3.3). Regression analysis with the entire dataset and CH_R as regressor resulted in an R^2_{cal} of 0.62 and an R^2_{val} of 0.64 and a corresponding $RMSE_{val}$ of 0.28 t ha^{-1} ($rRMSE_{val}$ = 18%). Model performance for CH_D was slightly better with R^2_{cal} = 0.69 and an R^2_{val} of 0.72 (rRMSE = 17%). Considering the individual treatments, R^2_{cal} varied between 0.58 and 0.80 and R^2_{val} between 0.42 and 0.68 ($rRMSE_{val}$ =0.23-0.34 t ha-1) for CH_R, while for CH_D R^2_{cal} (R^2_{cal} = 0.62-0.80) and R^2_{val} (R^2_{val} = 0.46-0.87, $rRMSE_{val}$ = 0.23-0.36 t ha^{-1}) was somewhat higher. Willmott's refined index of agreement (d) of CH_R and CH_D varied on a similar high level between 0.82 and 0.92. Exclusion of the pure grass data of the second cut resulted in higher R^2_{cal} and R^2_{val} values, but only the $rRMSE_{val}$ values G_{GL} of CH_R ($rRMSE_{val}$ = 15%) and both grass treatments of CH_D ($rRMSE_{val}$ = 16-19%) were

lower. However, d yielded in a higher value for both, CH_R and CH_D by excluding pure grass data from the second cut (0.88-0.94).

Table 3.3: Linear regression analysis of calibration (cal) and validation (val) dataset between dry matter yield and manual height measurements (CH_R) as well as UAV based RGB imaging (CH_D) for the whole dataset (All) and the different treatments: clover-grass (CG), lucerne-grass (LG) as well as the pure stands of legumes (L_{CG}, L_{LG}) and grass (G_{CG}, G_{LG}) of the mixtures, respectively. n = number of samples; R^2 = coefficient of determination; RMSE = root mean square error; rRMSE = relative RMSE; d = Willmott's refined index of agreement. Values in brackets represent results for the dataset without pure grass swards of the second cut.

Treatment	Calibration		Validation				
	n_{cal}	R^2_{cal}	n_{val}	R^2_{val}	$RMSE_{val}$ (t ha^{-1})	$rRMSE_{val}$ (%)	d
				CH_R			
All	180 (174)	0.62 (0.71)	53 (51)	0.64 (0.65)	0.28 (0.29)	18 (19)	0.90 (0.90)
CG	30	0.80	10	0.66	0.34	19	0.90
LG	30	0.71	9	0.50	0.33	19	0.85
L_{CG}	30	0.68	10	0.56	0.26	21	0.87
L_{LG}	30	0.77	8	0.68	0.23	19	0.91
G_{CG}	30 (27)	0.64 (0.82)	8 (7)	0.42 (0.51)	0.33 (0.34)	21 (22)	0.83 (0.88)
G_{LG}	30 (27)	0.58 (0.82)	8 (7)	0.43 (0.73)	0.29 (0.20)	22 (15)	0.82 (0.94)
				CH_D			
All	180 (174)	0.69 (0.73)	53 (51)	0.72 (0.62)	0.27 (0.30)	17 (20)	0.92 (0.89)
CG	30	0.80	10	0.87	0.23	13	0.96
LG	30	0.63	9	0.68	0.35	20	0.89
L_{CG}	30	0.81	10	0.46	0.29	24	0.83
L_{LG}	30	0.62	8	0.51	0.36	30	0.82
G_{CG}	30 (27)	0.68 (0.69)	8 (7)	0.54 (0.64)	0.35 (0.30)	23 (19)	0.85 (0.90)
G_{LG}	30 (27)	0.67 (0.71)	8 (7)	0.48 (0.77)	0.30 (0.20)	23 (16)	0.86 (0.94)

A major aim of the study was to generate prediction models for DMY based on CH_D, which are valid across the entire range of legume contribution possibly occurring in practical grassland farming (i.e. 0 to 100% of DMY). It turned out that models perform better when developed separately for the two legume species (data of the entire

dataset not shown). Figure 3.5 shows the legume-specific linear models, each including the respective mixture as well as the corresponding pure legume and grass sward. For better understanding DMY data was re-transformed to the original scale. DMY of clover-grass was predicted better by CH_D with an R^2_{cal} of 0.75 compared to CH_R with R^2_{cal} of 0.60 (Table 3.4). Also the validation for clover-grass by CH_D showed a higher R^2_{val} of 0.75 ($rRMSE_{val}$ = 17%) compared to CH_R with an R^2_{val} of 0.58 ($rRMSE_{val}$ = 22%). In contrast, DMY of lucerne-grass was predicted and validation was performed somewhat better by CH_R (R^2_{cal} = 0.67, R^2_{val} = 0.69) than by CH_D (R^2_{cal} = 0.64, R^2_{val} = 0.62). The d value varied on a high level for all models between 0.87 and 0.93.

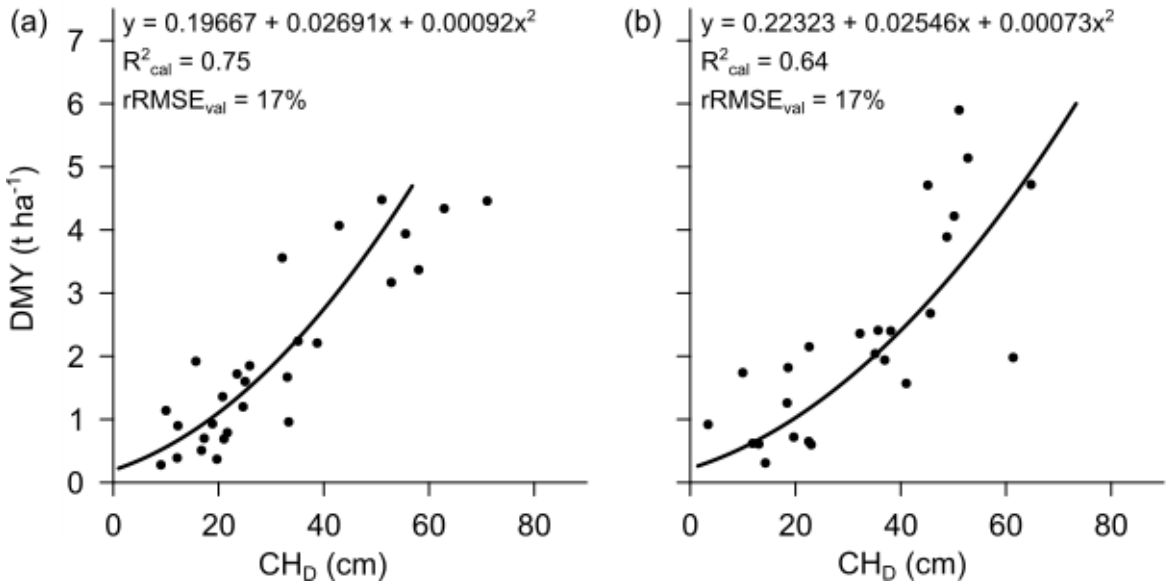

Figure 3.5: Legume-specific regression models of the calibration dataset with validation dataset (•) for dry matter yield (DMY) based on canopy height from UAV-based RGB imaging (CH_D). For better understanding DMY data was re-transformed to the original scale. Models for clover-grass (a) and lucerne-grass (b) both include the respective mixtures as well as the corresponding pure legume and grass swards. R^2 = coefficient of determination; rRMSE = relative root mean square error (calculated with square root-transformed data).

Table 3.4: Linear regression analysis of calibration (cal) and validation (val) dataset between dry matter yield and manual height measurements (CH_R) as well as UAV based RGB imaging (CH_D) for clover-grass (CG) and lucerne-grass (LG) mixtures including corresponding pure stands of legumes (L) and grass swards (G). n = number of samples; R^2 = coefficient of determination; RMSE = root mean square error; rRMSE = relative RMSE; d = Willmott's refined index of agreement. Values in brackets represent results for the dataset without pure grass swards of the second cut.

	Calibration		**Validation**				
Treatment	**n_{cal}**	**R^2_{cal}**	**n_{val}**	**R^2_{val}**	**$RMSE_{val}$ (t ha^{-1})**	**$rRMSE_{val}$ (%)**	**d**
			CH_R				
Clover-grass (CG, L_{CG}, G_{CG})	90	0.60	28	0.58	0.34	22	0.87
Lucerne-grass (LG, L_{LG}, G_{LG})	90	0.65	25	0.69	0.29	16	0.90
			CH_D				
Clover-grass (CG, L_{CG}, G_{CG})	90	0.75	28	0.75	0.26	17	0.93
Lucerne-grass (LG, L_{LG}, G_{LG})	90	0.64	25	0.62	0.32	17	0.88

For practical implementation it is relevant to know the accuracy of the novel methodology for the prediction of the total annual DMY (ADMY), which is the total DMY of a crop over the entire growing season. In the present study ADMY was calculated by accumulating the harvest yield of all four cuts. ADMY varied between 11.85 and 15.18 t ha^{-1} for the whole dataset and the mixtures with a standard deviation (SD) between 2.01 and 2.37 (Table 3.5). By applying the prediction models (Table 3.4) and accumulating the estimated yields of the four cuts, estimates were produced for ADMY based on manual height measurement ($ADMY_R$) as well as based on UAV based RGB imaging ($ADMY_D$) (Table 3.5). Similar results were predicted by CH measurement, which varied for $ADMY_R$ between 12.38 and 16.85 t ha^{-1} (SD = 1.92-2.17) and for $ADMY_D$ between 11.77 and 15.71 t ha^{-1} (SD = 1.76-2.62).

Table 3.5: Measured total annual dry matter yield including four cuts (ADMY) and the difference between ADMY and the predicted values based on manual height measurement ($ADMY_R$) and UAV based RGB imaging ($ADMY_D$) for the whole dataset (All) and the different treatments: clover-grass (CG), lucerne-grass (LG) as well as the pure stands of legumes (L_{CG}, L_{LG}) and grass (G_{CG}, G_{LG}) of the mixtures, respectively. Values in brackets represent the relative deviation. For better understanding DMY data was re-transformed to the original scale. SD = standard deviation.

Treatment	ADMY (t ha^{-1})		$ADMY_R$ (t ha^{-1})		$ADMY_D$ (t ha^{-1})	
	Mean	SD	Mean	SD	Mean	SD
All	11.85	2.01	12.38	1.92	11.77	2.09
CG	15.18	2.25	16.85	2.14	15.71	2.62
LG	12.88	2.37	13.73	2.17	12.30	1.76

3.4 Discussion

The primary aim of this study was to develop and evaluate a prediction model for DMY of heterogeneous temperate grasslands by means of SfM using UAV-based RGB imaging. CH was successfully predicted both by manual and SfM height measurement. SfM-based CH was on average 4 cm lower than the manually measured values. The same tendency was found in previous studies with barley with a difference of 10 cm (Bendig et al. 2014) and 19 cm (Aasen et al. 2015), respectively, though both investigations used a higher resolution of 1 cm per pixel. In our study, manual measurements represented 50 single points from the ground soil to the highest point touching the ruler. In contrast, SfM datasets covered the whole area of interest, scanning the complete visible canopy surface and not only the top of single plants (Bendig et al. 2014; Li et al. 2016). Furthermore, the nadir position of the camera with a resolution of 2 cm per pixel may not have captured every single grass tiller, especially at windy conditions, and the strong depth filtering during the generation of dense point clouds may have already caused an exclusion of single outlying points. All this led to a generally lower average CH compared to the manual measurements and is also supported by the finding that the correlation between SfM-based and manual height measurement improved, when the data of the extreme mature grasses of the second cut were excluded. Cunliffe et al. (2016) showed that in dryland vegetation ultra-fine resolution of less than 1 cm of the height model was able to depict single grass stems.

The prediction models for DMY based on the calibration dataset of CH_R and CH_D showed similar accuracies across all treatments with R^2 = 0.58–0.80 and R^2 = 0.62–0.81, respectively. Most other multi-temporal studies reporting on SfM-based prediction models by means of UAV RGB imaging were conducted with arable crops. Correlation results were comparable for barley with an R^2 = 0.82 (Bendig et al. 2014), for winter wheat (R^2 = 0.68–0.95) (Schirrmann et al. 2016) and for maize and sorghum (R^2 = 0.68–0.78) (Malambo et al. 2018). Moeckel et al. (2018) achieved substantially higher R^2 values with stands of tomato, eggplant and cabbage (R^2 = 0.89–0.97), which represent more heterogeneous crops. Roth and Streit (2018) examined different cover crops, including also two clover species, and achieved an R^2 of 0.58. When plants, which were growing close to the ground or even lodging, were excluded from the regression model, R^2 increased to 0.74. In a permanent timothy-dominated grassland Viljanen et al. (2018) obtained a Pearson correlation coefficient between 0.77 and 0.97. They showed that the quality of the estimation model depended on plant density and growth stage of the sward. Bendig et al. (2015) achieved the best results in summer barley prior to heading of the crop. Malambo et al. (2018) and Grenzdörffer (2014) showed that the SfM approach worked better for uniform crops than for crops with a heterogeneous canopy surface. Compared to other arable crops, which are usually grown in monocultures (e.g., cereals, maize), clover- and lucerne-grass mixtures form a rather heterogeneous canopy with a wide range of coverage of the two components, which above all, have a very different stature.

Several studies indicated that plant density influences the estimation of plant height (Gillan et al. 2014; Holman et al. 2016; Watanabe et al. 2017). In our study, the second cut was markedly affected by drought, which resulted particularly for grasses in a low tiller density and less leaf biomass. The exclusion of the data of the pure grass stands of the second cut improved the correlations for both methods. A camera with a higher resolution to capture more details of the canopy surface (Cunliffe et al. 2016) and the integration of plant density as additional information may further improve the prediction accuracy in heterogeneous crops. In a study of Schut et al. (2018) the combination of spectral indices with remotely sensed CH information showed promising results at small-scaled farm level. In other studies fusion of 3D LiDAR and spectral data substantially improved biomass prediction in extensively manage permanent

grasslands compared to the use of single sensors (Fricke and Wachendorf 2013; Moeckel et al. 2017).

Accuracy of biomass estimation by RGB imaging may be reduced due to errors and uncertainties during the image and point cloud generation. The seven negative CH_D values, which were excluded from the present analysis, were located in an area of the experimental site, where a slight slope occurred. In our study, the DEM was generated by the interpolation of z-values from points located in the pathways between the plots. As the biomass at the erased points were extremely low, negative height values may, thus, have been caused by an inadequate representation of the true ground surface in the interior of the plots. With a small and rather flat area like our experimental field the error due to insufficient interpolation is relatively low, whereas for practical and possibly uneven fields of several hectares explicitly generated DEM point clouds may be necessary for a sound calculation of canopy heights. This can e.g., be done during periods of bare soil, e.g., before sowing or after harvest of the crop. However, the production of additional pre-sowing or post-harvest point clouds requires extra flight missions and a considerable effort of data analysis. Tests which were conducted prior to the experiment indicated that extremely diligent georeferencing of the point clouds with an adequate number of georeferenced control points is necessary to avoid errors and uncertainties in the CH data.

In practical forage production strategic decisions (e.g., for adjusting the number of farm animals to the amount of available roughage) are usually taken based on data from one year or growing season. Thus, generating reliable data on the expected total annual biomass produced from single fields would substantially support farmers' decisions. As a first approach models were developed to predict total annual yield separately for the clover- and lucerne-grass stands. As the legume contribution of legume-grass mixtures varies greatly in farming practice (Ledgard and Steele 1992), the corresponding pure stands of legumes and grasses were also included in both models. The fact, that model accuracy was different for clover- (R^2 = 0.75) and lucerne-grass (R^2 = 0.64) data indicates that, morphological characteristics (e.g., leaf position, vertical or horizontal distribution) of clover canopies allow a better prediction of biomass than for lucerne-grass mixtures, and that these crop-specific models cannot

be easily transferred to other grassland types. The reasons behind this finding cannot be determined with the present study and, thus, further investigations (also considering model evaluation on the field scale) are needed. However, it is encouraging that averaged across all treatments, the accuracy between measured yield and UAV-based yield assessment was similar to manual height measurement.

Data acquisition by UAV can be done in a relative short time, whereas data processing by SfM is a computationally intensive process, depending on computer performance and number of images. In our study, data acquisition for each sampling date by manual height measurement, which was a rather high number of measurements (50 measurements per plot ~ 3 h) and UAV-based RGB imaging including data processing yielded in a similar amount of time (~ 3–4 h). So far, a practical implementation does not seem feasible, but as flight time of UAVs, computer performance and automation of data processing steadily increases, this method is seen to have great potential. To summarize, the results indicate that UAV-based RGB imaging may serve as a suitable estimator for total annual yield of heterogeneous legume-grass mixtures, which future studies should evaluate.

3.5 Conclusion

Accurate yield estimation in temporal grassland farming is an essential prerequisite for management decisions. The present study showed, that SfM-based RGB imaging in combination with a UAV provides a promising alternative to the time- and effort-consuming yield prediction based on conventional manual methods. Furthermore, yield estimation by RGB imaging proved similar prediction of DMY at extreme weather conditions compared to manual height measurements by ruler. Our new approach to yield assessment by SfM showed great potential and was also able to successfully estimate total annual yield. The use of UAVs serves as a fast, non-destructive tool for multi-temporal data acquisition.

However, the large variability of canopy surface in legume-grass mixtures causes lower prediction accuracies than in more homogeneous arable crops. Therefore,

instead of using single sensors, research should focus on fusion of complementary sensor data, e.g., by including spatial and spectral information. The fast-emerging technologies in remote sensing have a great potential to develop such sensor systems integrated on one UAV platform.

3.6 Appendix

Table 3.6: Dry matter yield (DMY) of the different treatments: the clover-grass (CG) and lucerne-grass (LG) mixtures and pure stands of legumes (L) and grasses (G) for 10 sampling dates comprising four harvest cuts and six sub-samplings every second week during sward growth between 17.05.17 and 09.10.17.

	DMY (t ha^{-1})									
Cut	**1st harvest**	1st sub-sample	2nd sub-sample	**2nd harvest**	3rd sub-sample	**3rd harvest**	4th sub-sample	5th sub-sample	6th sub-sample	**4th harvest**
Date	**17.05.17**	02.06.17	13.06.17	**26.06.17**	11.07.17	**08.08.17**	23.08.17	05.09.17	20.09.17	**09.10.17**
Treatment										
CG	4.60	0.78	2.29	3.40	0.73	4.82	0.44	1.15	1.79	2.37
LG	4.90	0.60	2.21	3.47	0.67	2.57	0.78	1.70	1.87	1.95
L_{CG}	4.95	0.35	1.49	1.97	0.29	0.74	0.33	0.87	1.35	1.17
L_{LG}	3.59	1.12	2.59	3.79	1.03	3.53	0.78	2.06	2.93	2.46
G_{CG}	4.58	0.57	1.59	1.62	0.21	0.66	0.41	0.86	1.08	1.05
G_{LG}	3.41	0.76	1.97	3.53	0.95	3.33	0.52	1.81	1.81	2.70

4 The potential of UAV-borne spectral and textural information for predicting aboveground biomass and N fixation in legume-grass mixtures

Abstract

Organic farmers, who rely on legumes as an external nitrogen (N) source, need a fast and easy on-the-go measurement technique to determine harvestable biomass and the amount of fixed N (N_{Fix}) for numerous farm management decisions. Especially clover- and lucerne-grass mixtures play an important role in the organic crop rotation under temperate European climate conditions. Multispectral sensors mounted on unmanned aerial vehicles (UAVs) are new promising tools for a non-destructive assessment of crop and grassland traits on large and remote areas. One disadvantage of multispectral information and derived vegetations indices is, that both ignore spatial relationships of pixels to each other in the image. This gap can be filled by texture features from a grey level co-occurrence matrix. The aim of this multi-temporal field study was to provide aboveground biomass and N_{Fix} estimation models for two legume-grass mixtures through a whole vegetation period based on UAV multispectral information. The prediction models covered different proportions of legumes (0-100% legumes) to represent the variable conditions in practical farming. Furthermore, the study compared prediction models with and without the inclusion of texture features. As multispectral data usually suffers from multicollinearity, two machine learning algorithms, Partial Least Square and Random Forest (RF) regression, were used. The results showed, that biomass prediction accuracy for the whole dataset as well as for crop-specific models were substantially improved by the inclusion of texture features. The best model was generated for the whole dataset by RF with an rRMSE of 10%. For N_{Fix} prediction accuracy of the best model was based on RF including texture (rRMSEP = 18%), which was not consistent with crop specific models.

4.1 Introduction

The production of industrial fertilizer containing nitrogen (N) as an essential element of plant growth increased global food production in the last decades. Nevertheless, the excessive use of N in agriculture caused different environmental problems, like e.g. eutrophication and pollution of water (Schröder et al. 2004) and is also linked to air pollution and climate change (Reay et al. 2012). To reduce these negative impacts on the environment, organic agriculture uses a reduced N supply as it follows the idea of a closed nutrient cycle and, thus, is considered as a sustainable and low-input agricultural system (Köpke 1995). As mineral N fertilizer is prohibited in organic agriculture, N is the primary limiting nutrient for many farms (Berry et al. 2002). Beside organic fertilizer, organic farmers rely on legumes as an external N supplier, due to the ability of fixing atmospheric N in symbiosis with *Rhizobium* bacteria (Fustec et al. 2010). Especially, legume-grass mixtures, like e.g. clover-grass or lucerne-grass, cultivated for 1-3 years and cut 3-5 times a year, are an inherent part of the organic crop rotation in temperate European climates. These mixtures detain even higher amounts of N than the same solely cultivated legume (Nyfeler et al. 2011) and are used as green manure or forage for livestock as well as for biogas plants. Total annual N fixation varies strongly and can reach up to over 300-500 kg N ha^{-1} $year^{-1}$ depending on the legume species (Carlsson and Huss-Danell 2003; Ledgard and Steele 1992; Rasmussen et al. 2012). Beside N acquisition, legume-grass mixtures provide additional positive effects on the subsequent cash crop, i.e. enhanced product quality and soil fertility as well as weed suppression (Eriksen et al. 2006; Melander et al. 2016; Shah et al. 2017; van Eekeren et al. 2009). For an efficient nutrient management on farm level both with and without livestock, knowledge on the actual amount of biomass harvested as well as on the total annual biomass is necessary (Elgersma and Søegaard 2018). Furthermore, the amount of fixed N (N_{Fix}) is a valuable information, as it contributes to the N cycle of the farm. In order to understand the dynamics of legume-grass mixtures over the entire growing season, multi-temporal studies are required. It is well known that legume proportion varies strongly in practical farming which substantially affects total annual N_{Fix} (Suter et al. 2015).

Traditional methods and devices to estimate biomass in practical grassland management, like destructive biomass sampling, ruler height or rising plate meter measurements are commonly used but are labour and time consuming. Methods to estimate N_{Fix} are very expensive and need a lot of laboratory work, like isotope measurement of the $^{15}N/^{14}N$ ratio of the natural abundance or by the isotope dilution method (Thilakarathna and Raizada 2018). Another method is the nitrogen difference method, where the N content in the aboveground biomass of a N-fixing plant and a non-N-fixing plant as reference is analyzed and the difference is calculated (Stülpnagel 1982). Høgh-Jensen et al. (2004) generated a model for legume-grass mixtures, which includes additional sinks of fixed N, like the amount of fixed N in the below-ground biomass of the fixing plant, as well as of the grass. Nevertheless, farmers need efficient on-the-go measurement techniques for biomass and N_{Fix} estimation for short-term management decisions.

Solutions for new non-destructive measurement techniques, covering large areas in short time, can be found in the field of remote sensing, which developed rapidly in the last decades in agricultural and grassland science. An overview about different applications of remote sensing in grasslands is given in Schellberg et al. (2008) and Wachendorf et al. (2018). A very promising platform for sensors are unmanned aerial vehicles (UAVs), which are becoming increasingly important for agricultural crops (Aasen et al. 2018; Yao et al. 2019). There exists a variety of different optical sensors, to be mounted on UAVs for the assessment of agricultural crops. These sensors capture the reflecting light of vegetation, ranging from low-cost costumer-grade cameras for RGB (red, green, blue) images to multi- and hyperspectral sensors, which cover also non-visible spectral bands (Bueren et al. 2015; Cho et al. 2007; Grüner et al. 2019).

To compensate background noise from soil or atmosphere in the spectral reflection and to increase the sensitivity for vegetation traits, vegetation indices (VIs) can be calculated (Jackson and Huete 1991). The most known VI, which uses the red and near infrared (NIR) bands, is the Normalized Difference Vegetation Index (NDVI) (Rouse et al. 1974). Nevertheless, NDVI has its limitations, as it saturates at high biomass and LAI values (Cho et al. 2007; Rasmussen et al. 2016) and is varying with

soil colour (Huete et al. 1985) and due to atmospheric effects (Kaufman et al. 1992). In the recent decades more than 100 VIs were developed, which vary in calculation and proportion of different spectral bands for specific applications and utilization for biophysical and -chemical features of vegetation (Xue and Su 2017). For estimating different vegetation features in grassland, VIs are already well-studied tools like for biomass yield (Ali et al. 2017; Capolupo et al. 2015), leaf area index (LAI) (He et al. 2006) and quality (Askari et al. 2019).

One aspect with the common use of spectral bands and VIs is that they ignore spatial variability of the grey level values (pixels) within the neighbourhood of each pixel. This gap can be covered by texture analysis, which is more complex to quantify than spectral information (Coburn and Roberts 2004). Texture is the spatial variation within an image, which correlates with the structure and heterogeneity of vegetation (Gallardo-Cruz et al. 2012). Furthermore, Culbert et al. (2009) documented that texture features can vary depending on the observed vegetation and its phenological stage, which makes it an interesting tool for multi-temporal studies. These facts are gaining more attention in research studies, mainly focusing on land cover classification (Kupidura 2019; Wan and Chang 2018; Wang et al. 2019), vegetation modelling (Bellis et al. 2008; Zhou et al. 2017) and structure (Wood et al. 2012, 2013) as well as forest biomass estimation (Lu 2005; Wijaya et al. 2010). For agricultural crops, there exist, to our best knowledge, only two studies using texture features in combination with UAV multispectral information. In a multi-temporal study over two years, Zheng et al. (2019) and Li et al. (2019) used a multispectral sensor on a UAV to estimate rice biomass and LAI including different cultivars, varying seed densities and N levels. The authors concluded that the combination of spectral and texture information is a promising method for biomass estimation. Few studies have explored the effectiveness of texture features in permanent grass- and rangeland and mainly focused on the classification of vegetation (Laliberte and Rango 2009). Gebhardt and Kühbach (2007) as well as van Evert et al. (2009) found a high detection accuracy for *Rumex obtusifolius* in grasslands by using texture features. Guo et al. (2004) compared two grassland management systems (i.e. grazed and non-grazed) and successfully described differences in spatial heterogeneity of these grasslands. The most popular method of gaining texture information of remotely sensed images follows a statistical approach,

named Grey Level Co-occurrence Matrix (GLCM), which can be used to calculate so-called second order texture features (Haralick et al. 1973). While first-order texture features are calculated directly from occurring grey level values (e. g. variance) within a certain area (window), second-order texture features consider the spatial relationship between these pixels, also called co-occurrence. Therefore, these features are more computationally intensive, but have a greater potential to represent the structure of vegetation. Nevertheless, there exist no studies which estimate biomass in terms of aboveground biomass and N_{Fix} of legume-grass mixtures using texture features in combination with multispectral information.

The aim of this study is to develop harvestable biomass and aboveground N_{Fix} estimation models from UAV multispectral imaging of legume-grass mixtures with varying legume proportions (0-100%). To deal with multispectral data, which usually suffers from multicollinearity, machine learning algorithms can be a solution, especially when the number of predictors is higher than the number of samples in the dataset. The specific objectives of this study were: (1) to develop harvestable biomass and aboveground N_{Fix} prediction models for mixtures with two different legumes by machine learning algorithms for a whole growing season; (2) to compare the prediction accuracy of these models with and without the inclusion of texture features; (3) to identify key variables of the resulting models; (4) to compare the measured and predicted total annual dry matter biomass and N_{Fix} including all cuts in one growing season.

4.2 Material and Methods

4.2.1 Experimental site and ground truth data

The field experiment was conducted in 2017 and 2018 in Neu-Eichenberg at the experimental farm of the Universität Kassel, which is located in northern Hesse, Germany (51°23’ N, 9°54’ E, 227 m above sea level). The soil is characterized as a silty clay loam and oil radish was cultivated as a preceding crop. As the experimental farm is managed organically, no pesticides or mineral N fertilizer were applied. Long-

term average annual precipitation at the site is 687 mm, but the amount of rainfall in 2018 was unusually low (350 mm) and led to severe drought throughout the whole vegetation period.

Field plots were established in autumn 2017 with a size of 1.50 m × 12 m and sown with a total seed rate of 35 kg ha^{-1}. The treatments consisted of two legume-grass-mixtures, clover- (CG) and lucerne-grass (LG), and additionally pure stands of legumes (L_{CG}, L_{LG}) and grass (G_{CG}, G_{LG}) of both mixtures. These six treatments were sown in four randomized replicates, resulting in 24 plots in total (Figure 4.1). CG contained 60% *Lolium multiflorum*, 30% *Trifolium pratense*, 5% *Trifolium hybridum* L. and 5% *Trifolium repens* L., whereas LG included 40% *Medicago sativa*, 20% *Festuca pratensis* Huds., 15% *Lolium perenne* L., 10% *Lolium multiflorum*, 10% *Trifolium pratense* and 5% *Phleum pratense* L (Appendix Table 4.3).

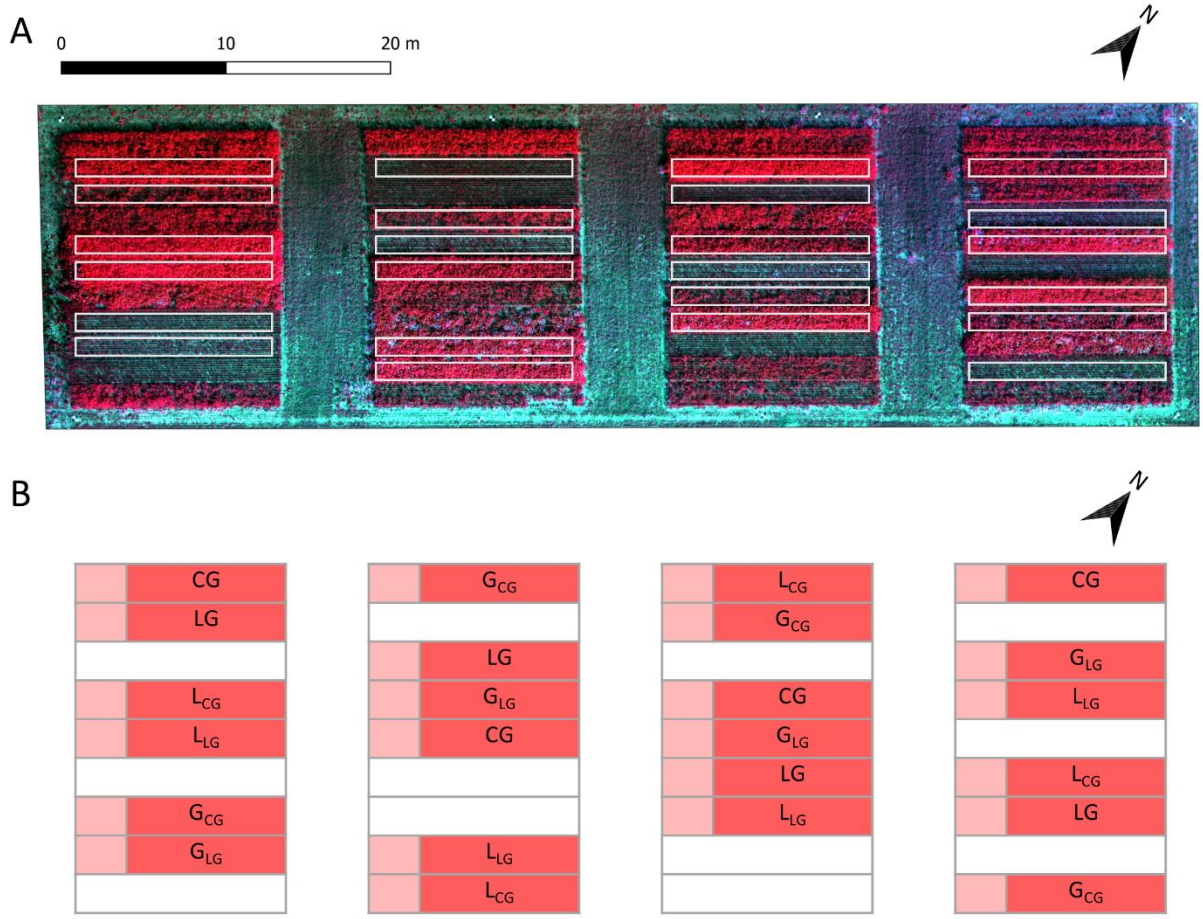

Figure 4.1: Overview of experimental field and treatments. (A) Orthomosaic of the experimental field showing the different plots (white border) one day before the third main harvest (02.08.2018) in false colours (NIR, red, green); (B) Design of experimental layout with treatments in four replicates: clover- (CG) and lucerne-grass (LG) and pure stands of legumes (L_{CG}, L_{LG}) and grasses (G_{CG}, G_{LG}) of the mixtures. Sampling area for main harvests (red) and the first 1.5 m for sub-sampling (light red).

In total eight biomass datasets for fresh (FM) and dry matter (DM) were obtained from three main harvests (17.05.2018, 20.06.2018, 03.08.2018) and to cover the whole vegetation period from five additional sub-sampling dates, whereas N_{Fix} was determined only at main harvests. At each main harvest two aboveground biomass samples were collected in each plot on an area of 50 cm × 50 cm and cut at a stubble height of 5 cm. Biomass samples were weighed, dried for 48 h at 105 °C and weighed again to determine DM. The remaining aboveground biomass was removed with a Haldrup forage plot harvester. Two additional samples of fresh biomass were taken. One sample of all plots was dried at 60 °C for a later N content analysis. The second

sample was taken only from the mixtures to determine the different fractions: legumes, grass, herbs and senesced material. The five sub-samples were taken between the main harvests at an area of 25 cm × 25 cm, restricted to the first 1.5 m of every plot to leave the remaining area undisturbed for the main harvests (Figure 4.1 B).

N concentration in the biomass was assessed by an elemental microanalyzer (Elementar vario MAX CHN, Langenselbold, Germany) and N content in the aboveground biomass was determined by multiplication of N concentration and DM biomass. The difference method according to Stülpnagel (1982) was used to quantify N_{Fix} of the legumes (Equation 4.1):

$$N_{Fix} = N_L - N_R \quad (4.1)$$

where the N content of the mixtures and the pure stand of legumes were defined as the N fixing crop (N_L) and the pure stands of grass were used as the non-fixing reference crop (N_R).

4.2.2 UAV image acquisition and data pre-processing

UAV flight missions were conducted before each cut (eight flights in total) in the morning at a nearly equal sun position. A low-cost quadrocopter (DJI Phantom 3 Advanced, Shenzhen, China) was used equipped with a multispectral sensor (Parrot Sequoia, MicaSense Inc, Seattle, USA). The sensor captured the reflected light in four separate bands: green (530-570 nm), red (640-680 nm), red edge (730-740 nm) and near-infrared (NIR; 770-810 nm) with a spatial resolution of 1.2 Megapixel (MP) as well as red, green, blue (RGB) images with a spatial resolution of 16 MP. The sensor was supplied with an additional sunshine sensor, which was mounted on the top of the drone to capture the at-the-sensor irradiance for automatic calibration of every picture. This radiometric calibration is done to eliminate variation in sunlight conditions during flight for the subsequent analysis. For two cuts the drone was flown at a flight altitude of 50 m above ground, where image overlap was 100%. Therefore, as a compromise between flight height and time, remaining cuts were flown at 20 m. All flight missions were flown manually, as due to the removal of the original camera automatic flight

missions created major internal technical problems. The UAV was steered in a grid pattern through the experimental field at a speed of less than 1 m/s and the time trigger of the sensor was set to one image per 1.5 sec, resulting in about 1000 to 2000 images. Eight portable ground control points (GCPs; 25 cm × 25 cm) were evenly distributed in the pathways next to the plots and georeferenced by a differential global positioning system (DGPS, Leica, Germany) with a mean horizontal and vertical error of 0.02 m (Appendix Table 4.5). Additionally, the plot corners were georeferenced once to delimit the individual plots.

Photogrammetric processing was done by means of structure from motion (SfM) with Agisoft PhotoScan Professional (Agisoft LLC, St. Petersburg, Russia) to generate multispectral orthomosaics for every flight mission. The overlapping images, including more than nine images for the area of interest, of each imported dataset were aligned with internal algorithms and image fitting techniques of the software. The position and orientation of each image was adjusted, and a sparse point cloud was created with the accuracy setting “high”, a key point limit of 40,000 and tie point limit of 1,000. Coordinates of the GCPs had to be placed in five images manually and automatic camera calibration was used to improve the accuracy of the sparse point cloud. In the next step a dense point cloud was created with “high” quality settings and a “mild” depth filtering to achieve a detailed image. The resulting output was a multispectral orthomosaic including the reflectance values of each band. Due to different flight altitude (50 and 20 m), ground resolution ranged between 2-4 cm. Therefore, orthomosaics were exported as a TIFF file with 4.5 cm resolution for unified conditions for subsequent analysis.

4.2.3 Data analysis and machine learning

Extraction of reflectance information of the four bands and calculation of the texture features was achieved by Quantum Geographical Information System (QGIS 2.18.14, QGIS Development Team, Raleigh, NC, USA). Coordinates of the plot corners were used to create polygons, avoiding the first 1.5 m which were disturbed by biomass sub-sampling (Figure 4.1 B). For the remaining area of 15.75 m^2 zonal statistic was applied

for polygons of each plot and band to generate average values of every variable. An overview of the workflow including the variables and analysis is given in Figure 4.2.

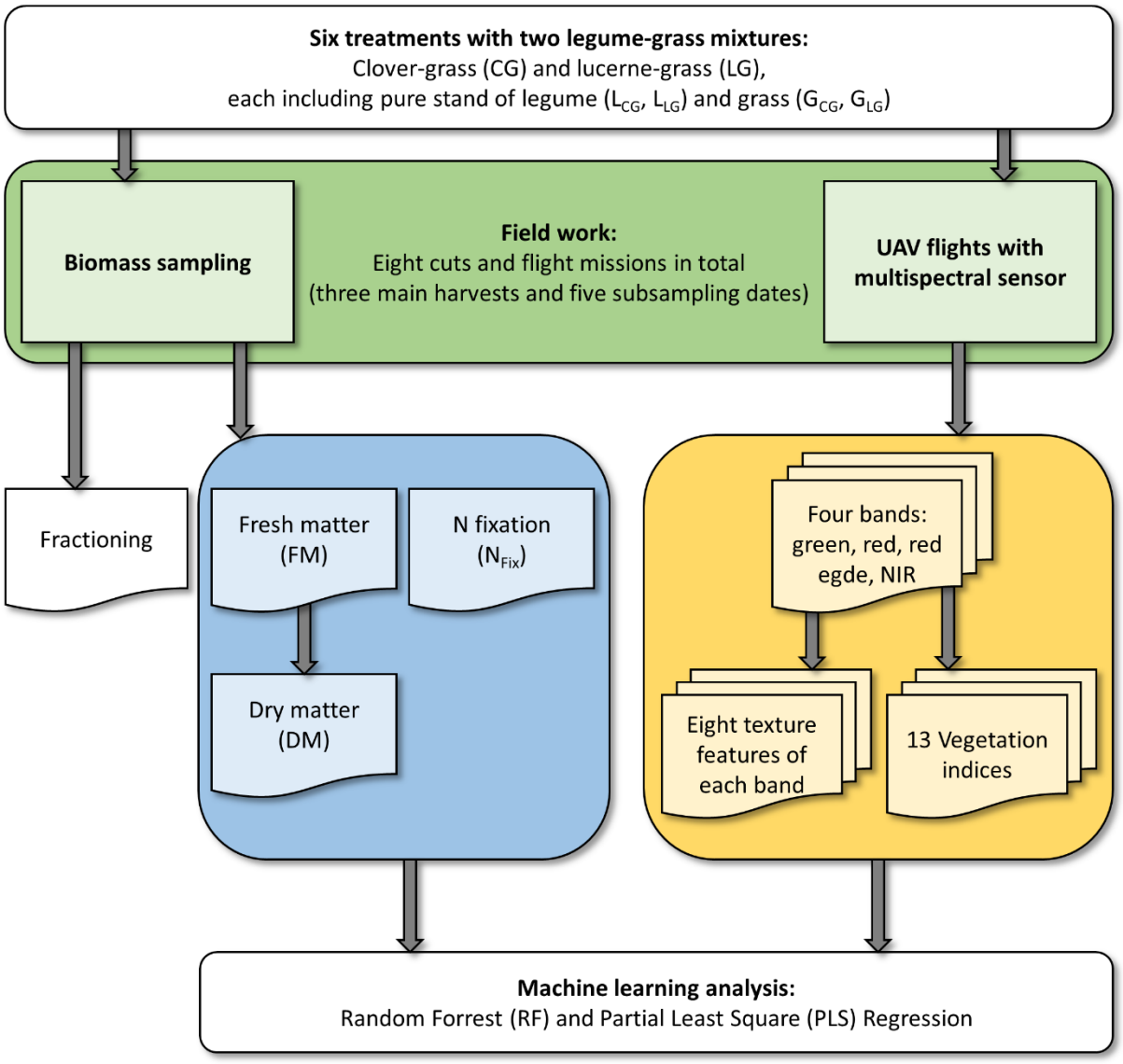

Figure 4.2: Workflow. Workflow of data acquisition and processing with fieldwork (green), dependent variables (blue) and independent variables (yellow) for data analysis.

4.2.4 Texture features of images

Image texture can be described as the spectral and spatial variability of grey level values of an image. Haralick suggested a GLCM using 14 second order textural features of remotely sensed images (Haralick et al. 1973). As there exists no evidence

in literature which features are best suitable for biomass prediction in grassland or legume-grass mixtures, eight of these GLCM texture features were used (Table 4.1), which were provided by the processing tool HaralickTextureExtraction of the Orfeo Toolbox library (OTB, open source, (Morin et al. 2019)) in QGIS. The eight Haralick texture parameters were computed for all four spectral bands separately with settings on default (window size: 2 × 2) and a texture set selection on “simple”. The radiometric resolution was set to 16 bit.

Table 4.1: Haralicks Grey Level Co-occurrence Matrix (GLCM) texture features.

Texture feature	Explanation (adapted from Haralick et al. 1973; Yang et al. 2012)
1. Energy	Measures the local steadiness of the grey levels
2. Entropy	Measures randomness or degree of disorder
3. Correlation	Shows the linear dependency of grey level values in the GLCM
4. Inverse Difference Moment	Measures the local homogeneity
5. Inertia	Measures the local contrast or amount of variations
6. Cluster Shade	Measures skewness of the GLCM
7. Cluster Prominence	Measures the asymmetry of the GLCM
8. Haralick Correlation	Shows the probability of two pixels with similar grey level

4.2.5 Vegetation index calculation

The spectral information of the orthomosaics was used to calculate a set of common VIs. Thirteen VIs using visible and red edge as well as NIR reflectance were selected (Appendix Table 4.4), which were reported in literature for structural or biochemical characteristics of vegetation and grasslands (Askari et al. 2019; Xue and Su 2017). VIs were calculated in R (R 3.5.1, R Foundation for Statistical Computing, Vienna, Austria) based on the mean value of the original reflectance of the spectral bands for each plot.

4.2.6 Partial Least Square and Random Forest regression

Further analysis and model calculation were done with R. Two machine learning methods were used for model calibration by means of the caret package (Kuhn 2008) for modelling FM and DM biomass and N_{Fix}: Partial Least Square (PLS) and Random Forest (RF) regression. PLS reduces the number of highly correlated independent variables (i.e. spectral bands) by linear combinations to a few latent vectors (principal components), which cover the maximum of covariance between independent and dependent variables (i.e. FM, DM, or N_{Fix}) to build a regression model (Geladi and Kowalski 1986). Another machine learning algorithm, which in contrast observes non-linear relationships, is RF regression. RF, introduced by Breiman (2001), builds multiple decision trees for regression with a random selection of sub-datasets as input variables. Both regression algorithms, PLS and RF, are common techniques for spectral analysis, including highly correlated independent variables, to estimate biomass yield and quality, also in the field of grassland and forage production (Askari et al. 2019; Barrett et al. 2014; Capolupo et al. 2015).

For an internal training and validation of the PLS and RF models, a leave-one-out-cross-validation (LOOCV) was performed. For PLS the tuning parameter *ncomp*, which defines the number of principal components to be tested, was set to 10% of the number of samples with 4 as a minimum (for DM and FM: 19 for the whole dataset and 10 for both CG and LG; for N_{Fix}: 5 for the whole dataset and 4 for CG and LG). Two tuning

parameters were set for RF in order to produce decision trees: *mtry*, which is the number of randomly selected variables and *ntree*, which represents the number of trees to grow. In this study, *mtry* was determined by the square root of the number of variables (here without texture: 5; with texture: 8) and *ntree* is automatically set to 500, as commonly recommended (Belgiu and Drăgut 2016).

The four spectral bands together with eight texture parameters for each band and the 13 vegetation indices resulted in a total of 49 variables, which were used as independent variables, while FM, DM and N_{Fix} were considered as dependent variables (Figure 4.2). To measure the accuracy of the PLS and RF models a cross-validation (CV) was implemented. Therefore, the whole dataset was divided into a training (75%) dataset for calibration of the model and a test dataset (25%). The test dataset included at least one datapoint of each treatment (CG, LG, L_{CG}, L_{LG}, G_{CG}, G_{LG}) and cut (three main harvests and five sub-sampling dates) for a later validation. To avoid bias by dividing the dataset, CV was run 100 times with randomly chosen training and test datasets. Performance of model prediction quality by CV was indicated by average coefficient of determination of the validation (R^2_{val}) (Equation 4.2), root mean square error of prediction (RMSEP) (Equation 4.3) and relative RMSEP (rRMSEP) (Equation 4.4):

$$R^2_{val} = \left[1 - \frac{\sum_{i=1}^{n}(y_i - \hat{y}_i)^2}{\sum_{i=1}^{n}(y_i - \bar{y}_i)^2}\right] \quad (4.2)$$

$$RMSEP = \sqrt{\frac{\sum_{i=1}^{n}(y_i - \hat{y}_i)^2}{n}} \quad (4.3)$$

$$rRMSEP = \frac{RMSEP}{\max(y_i) - \min(y_i)} \quad (4.4)$$

where y_i is the measured variable (i. e. FM, DM, N_{Fix}), $\hat{y}_i$ is the predicted variable, $\bar{y}_i$ is the average measured variable and *n* is the number of samples.

This was done for the whole dataset, as well as crop-specific for clover- and lucerne-grass, each including the mixture and the pure stands of the corresponding legumes and grasses. Furthermore, PLS and RF were compared with and without texture parameters and the best machine learning algorithm was selected based on the lowest median rRMSEP value for further analysis. To determine the variable importance for biomass and N_{Fix} prediction, the best model out of the 100 cross-validated machine learning algorithms was identified based on the lowest rRMSE value.

4.3 Results

Due to severe drought through the whole vegetation period, both biomass and N fixation were at a relatively low level. Nevertheless, the experimental set up with two legume-grass-mixtures (CG, LG) including the pure stands of legumes (L_{CG}, L_{LG}) and grass (G_{CG}, G_{LG}) as well as the various sampling dates through the vegetation period generated a wide range in biomass (Figure 4.3). In this multi-temporal study, the range of FM for CG and LG (0-100% legumes) was 0.38-33.95 and 0.23-28.56 t ha^{-1}, whereas the range of DM was 0.07-5.41 and 0.07-5.33 t ha^{-1}, respectively. N_{Fix}, which was calculated only for the main harvests, was 3.84-118.09 kg ha^{-1} for CG and 4.57-121.48 kg ha^{-1} for LG.

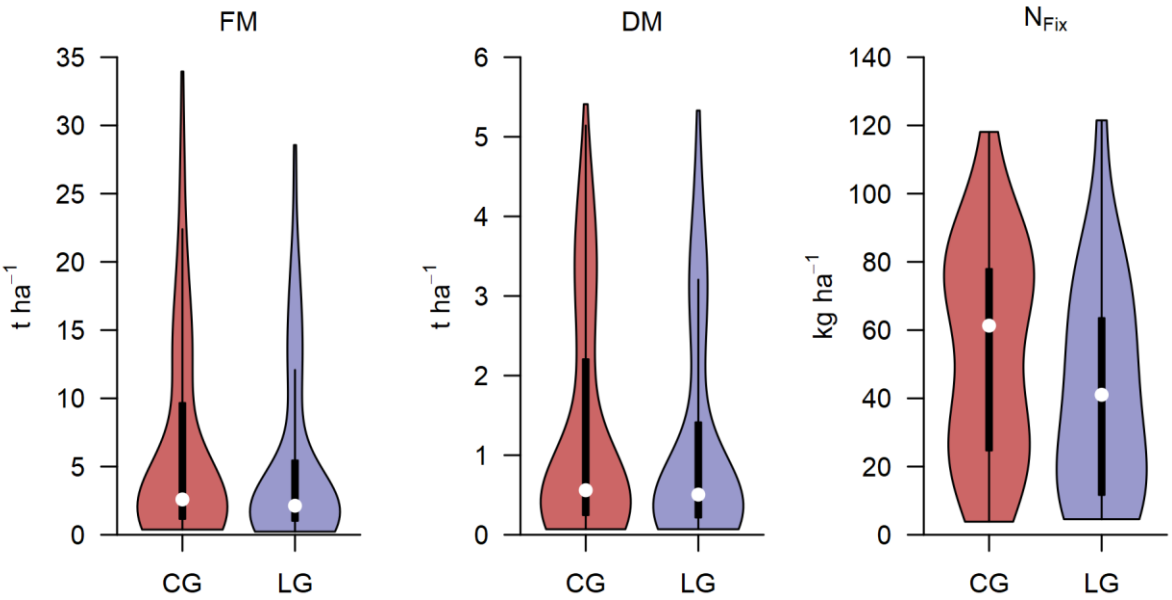

Figure 4.3: Violin plot of ground truth data. Violin plots of measured fresh (FM) and dry matter (DM) biomass and fixed N (N^{Fix}) of clover- (CG) and lucerne-grass (LG) mixtures including pure stands of legumes and grasses. Biomass data (FM, DM) were obtained at 3 main harvests and 5 sub-sampling dates, whereas N_{Fix} was determined only at main harvests. Black boxes show the 25 and 75% percentile, white circles indicate the median, whiskers represent the 5 and 95% percentile, violins show point density.

For every main harvest, the percentage of the different fractions (legumes, grass, herbs, senesced material) in the mixtures was determined to point out differences in the proportions of legumes (Figure 4.4). There were only slight differences between the two treatments CG and LG, but they differed between the three cuts. The proportion of legumes accounted for over 80% in the first cut and decreased for the second cut to about 40% and to 20% in the third cut. In contrast, the percentage of grass increased for every cut. Proportions of herbs and senesced material was negligible.

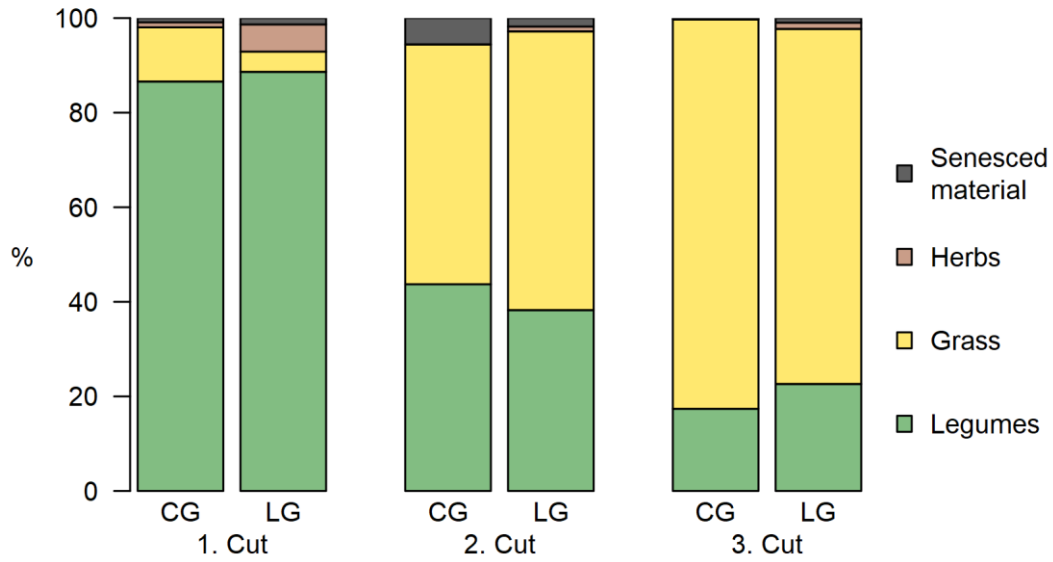

Figure 4.4: Fractions of the mixtures. Dry matter (DM) contribution of the legumes, grass, herbs and senesced material fractions for the three main cuts in the clover- (CG) and lucerne-grass (LG) mixtures.

4.3.1 Prediction models

Prediction models for biomass and N_{Fix} were built with four spectral bands as well as 13 VIs and were compared with models including additional eight texture features for each band. Separate models were developed for the whole dataset (CG, LG, G_{CG}, G_{LG}, L_{CG}, L_{LG}) as well as specifically for the two legume-grass mixtures, including the corresponding pure stands of legumes and grass to cover the whole range of legume proportions occurring in farming practice (Table 4.2).

Table 4.2: Median value of 100 randomly executed cross-validations of Partial Least Square (PLS) and Random Forest (RF) regression including multispectral variables and indices with and without texture features (T) for fresh (FM) and dry matter (DM) as well as fixed N (N_{Fix}) for the whole dataset as well as crop-specific: clover-grass (CG) and lucerne-grass (LG) mixtures including the pure stands of legumes (L_{CG}, L_{LG}) and grass (G_{CG}, G_{LG}); n = number of datapoints, R^2_{val} = coefficient of determination of validation, RMSEP = root mean square error of prediction, rRMSEP = relative RMSEP (%).

Variable	Texture (T)	Model	Whole dataset				Clover-grass (CG, L_{CG}, G_{CG})				Lucerne-grass (LG, L_{LG}, G_{LG})			
			n	R^2_{val}	RMSEP	rRMSEP	n	R^2_{val}	RMSEP	rRMSEP	n	R^2_{val}	RMSEP	rRMSEP
FM (t ha^{-1})	Without T	PLS	192	0.46	5.18	18.54	96	0.44	5.9	21.51	96	0.42	4.85	21.69
		RF	192	0.62	4.23	15.22	96	0.55	5.32	19.21	96	0.54	4.52	19.04
	With T	PLS	192	0.77	3.6	12.13	96	0.7	4.3	15.75	96	0.7	3.56	16.58
		RF	192	**0.86**	**2.79**	**9.76**	96	**0.76**	**3.95**	**14.08**	96	**0.74**	**3.27**	**14.62**
DM (t ha^{-1})	Without T	PLS	192	0.53	0.96	20.05	96	0.51	1.03	21.88	96	0.49	0.96	21.94
		RF	192	0.62	0.86	17.3	96	0.56	0.98	21.28	96	0.55	0.93	20.41
	With T	PLS	192	0.76	0.72	15.09	96	0.66	0.89	18.68	96	0.68	0.78	19.04
		RF	192	**0.87**	**0.52**	**10.78**	96	**0.79**	**0.71**	**15.05**	96	**0.77**	**0.66**	**15.28**
N_{Fix} (kg ha^{-1})	Without T	PLS	48	0.72	18.12	18.98	24	**0.69**	**19.87**	**24.46**	24	0.81	18.56	22.25
		RF	48	0.74	17.01	17.91	24	0.73	18.46	25.39	24	0.6	20.03	26.33
	With T	PLS	48	0.7	17.86	19.56	24	0.49	27.73	36.86	24	**0.83**	**19.86**	**20.9**
		RF	48	**0.76**	**16.77**	**17.88**	24	0.67	18.99	26.41	24	0.79	17.34	23.75

Inclusion of texture features generally improved cross validation results of both FM and DM models (Table 4.2). The lowest rRMSEP was found in the RF models with the whole dataset, where texture features reduced the relative error from 15.22 to 9.76% rRMSEP (R^2_{val} = 0.62 to 0.86). For the crop-specific RF models texture features improved rRMSEP from 19.21 to 14.08% (R^2_{val} = 0.55 to 0.76) for CG and from 19.04 to 14.62% (R^2_{val} = 0.54 to 0.74) for LG. The same trends were obtained from the PLS models, but rRMSEP values were 2-3% higher (Table 4.2).

In general, N_{Fix} prediction showed no consistent improvement and preferable model algorithm by the integration of texture features. For RF with LG, where rRMSEP was reduced from 26.33 to 23.75%, although it could not outperform the PLS model (Table 4.2). In contrast CG showed the best model by RF without texture (rRMSEP = 25.39%). The lowest rRMSEP of 17.88% was found for the whole dataset by RF with texture features, whereas rRMSEP excluding texture was 17.91%. Considering the crop-specific models, the best performance was found for PLS with texture, where the model for LG (rRMSEP = 20.90%; R^2 = 0.80) performed better than for CG without texture features (rRMSEP = 24.46%; R^2 = 0.69).

The best prediction model algorithm (i. e. RF or PLS) was chosen by lowest rRMSEP value for further assessment. Coefficient of determination of validation (R^2_{val}) for the best models varied between 0.69 and 0.87. The plots of fit in Figure 4.4 for measured versus predicted biomass and N_{Fix} show the 100 times randomly repeated prediction models for the whole dataset as well as crop-specifically. As the validation dataset contained at least one data point from each treatment and cut, a wide range of crop conditions was covered by the models. Despite of that all models showed an underestimation at higher biomass levels (Figure 4.5), while this trend was not as clearly visible for N_{Fix}.

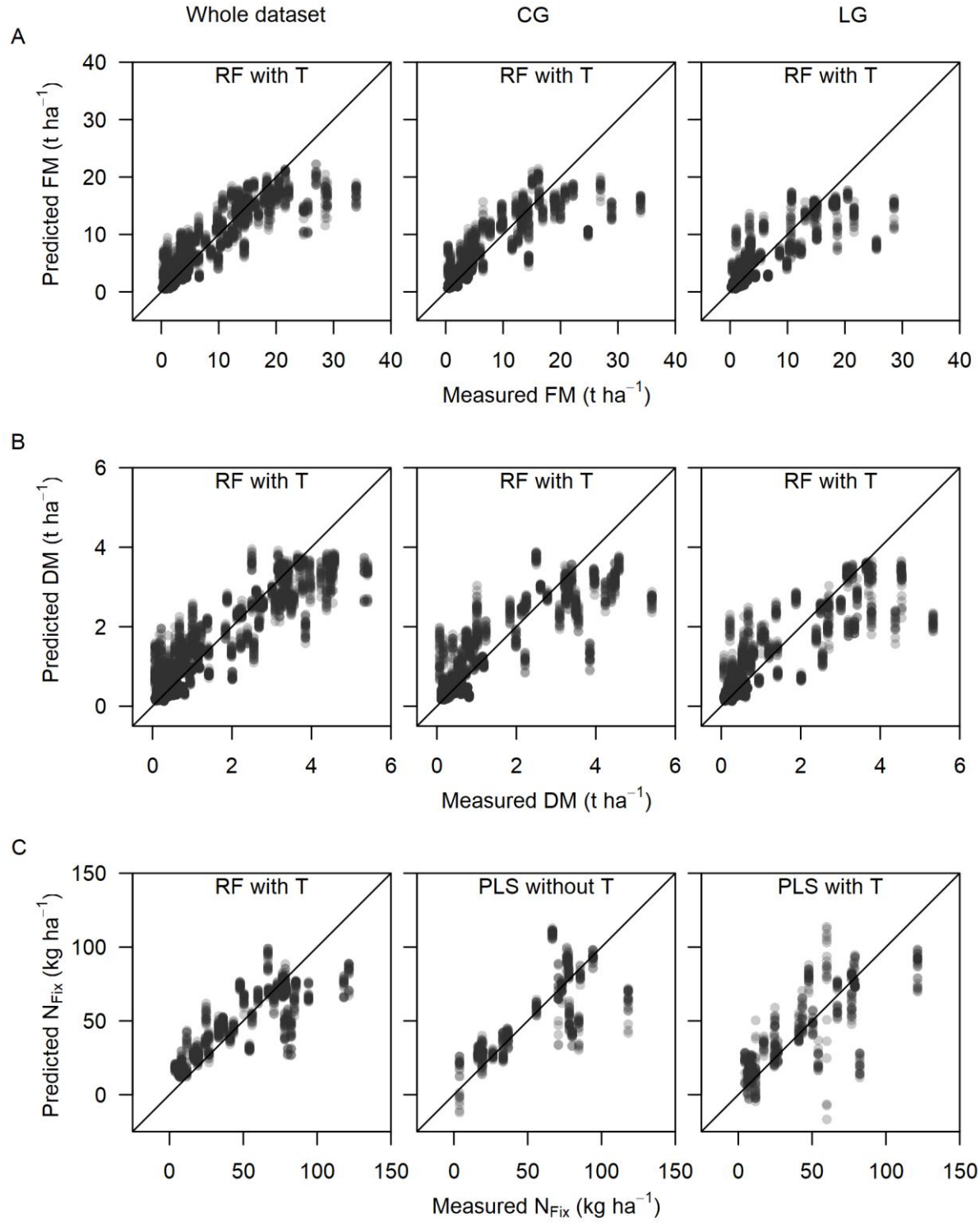

Figure 4.5: Plot of fit. Scatterplot for measured and predicted fresh (FM) (A) and dry matter (DM) (B) and fixed N (N_{Fix}) (C) for the whole dataset as well as crop-specific: clover-grass (CG) and lucerne-grass (LG) mixtures including the pure stands of legumes and grass. Plots show the best prediction algorithm, Partial Least Square or Random Forest (RF), with 100 randomly selected test and training data sets based on data from 3 main harvests and 6 sub-sampling dates, whereas N_{Fix} contains only main harvests.

To identify the contribution of texture features compared to single bands and VIs in the developed prediction models, the variable importance was calculated (Figure 4.6). Therefore, out of the 100 CV-models the best model based on the lowest rRMSEP was chosen and compared with and without texture for the whole dataset (Figure 4.6). For FM without texture features the three most important variables were MCARI, NDRE and GCI, which changed with the inclusion of texture features to G_Tex_3, R_Tex_7 and CVI. A similar trend is visible for DM, where GCI, GNDVI and R were the most important variables, whereas GCI, R_Tex_7 and G_Tex_3 contributed the most to the model when texture features were included. Particularly texture features of the red band ranked relatively high, which also applied for crop-specific models (Appendix Figure 4.9 and Figure 4.10). For N_{Fix} without texture features the three most important variables were RE, NIR and CVI, which changed to RE, NIR_Tex_8 and RE_Tex_8 after including texture features.

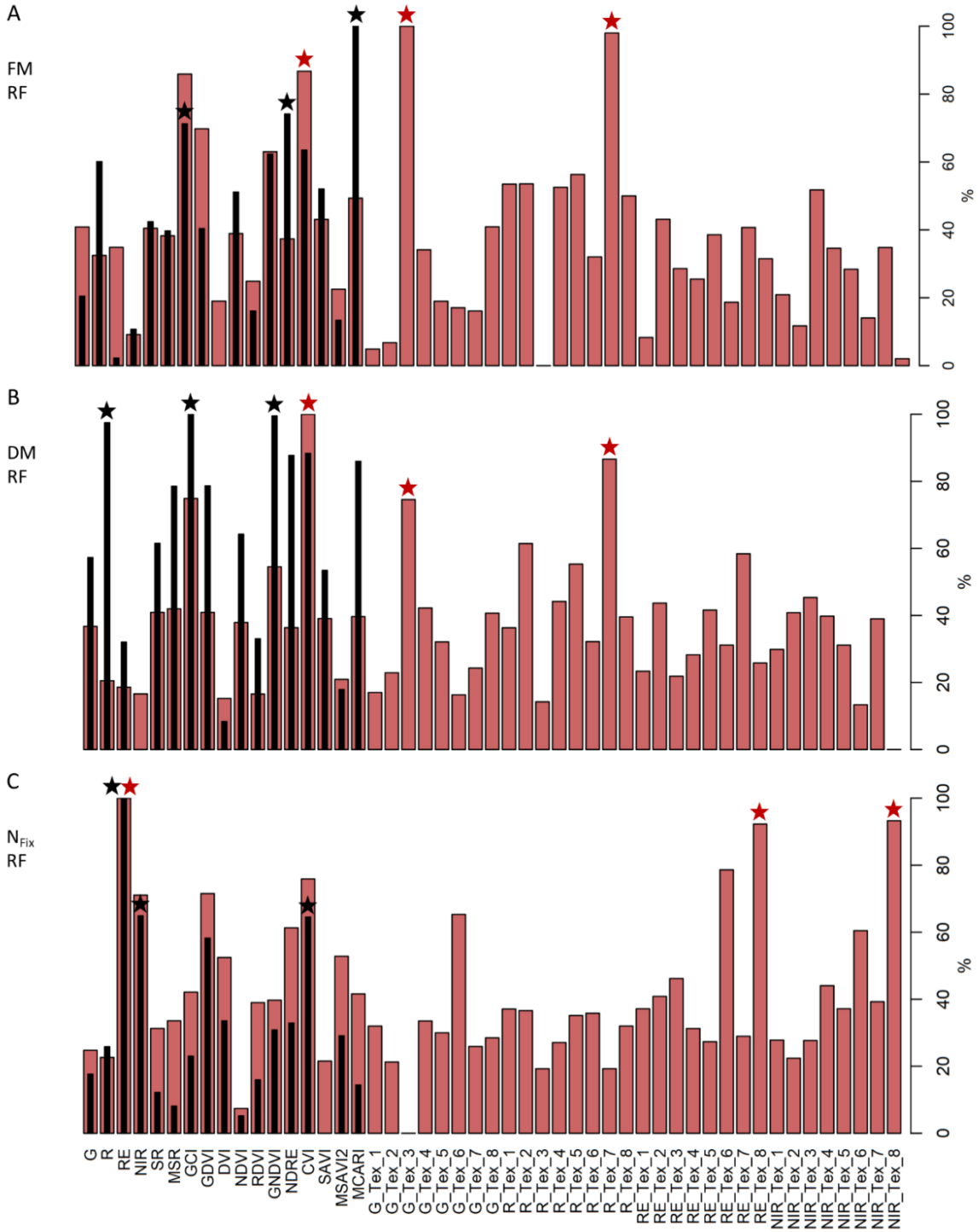

Figure 4.6: Variable importance. Variable importance of prediction models for fresh (FM) (A) and dry matter (DM) (B) as well as fixed N (N_{Fix}) (C) for the whole dataset built with four spectral bands, 13 vegetation indices and with (red) and without (black) 8 texture features of each band. Stars indicate the three highest rankings of variables with (red) and without texture features (black) in the model. Plots show the best prediction algorithm, Partial Least Square (PLS) or Random Forest (RF), with the best of 100 randomly selected test and training data sets based on data from 3 main harvests and 6 sub-sampling dates, whereas N_{Fix} contains only main harvests.

For practical farming the accuracy of total annual biomass is relevant, which is the cumulated biomass of the main harvests of one year. Therefore, biomass (FM, DM) and N_{Fix} measured and predicted by the best prediction algorithm for the two mixtures CG and LG is shown in Figure 4.7 with cumulated data. Though the two legume-grass mixtures were on different biomass and N_{Fix} levels, they showed very similar patterns concerning the trend of observed and predicted values. In total after the third harvest (H3) predicted FM and DM was underestimated by 1.18 and 1.25 t ha^{-1} for CG as well as 1.52 and 2.38 t ha^{-1} for LG respectively. N_{Fix} was overestimated at all cuts with annual N_{Fix} (H3) was overestimated by 13.69 kg ha^{-1} for CG and by 9.96 kg ha^{-1} for LG.

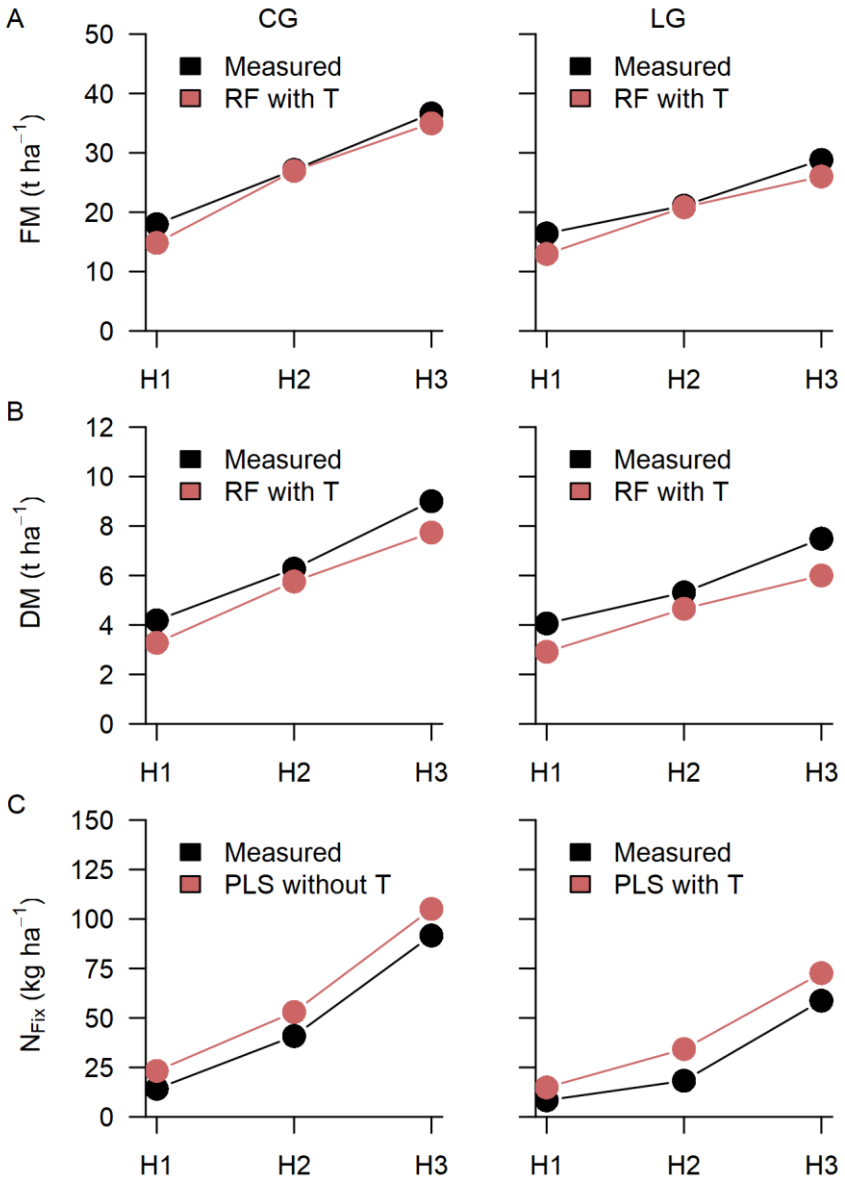

Figure 4.7: Annual biomass. Measured (black) and predicted (red) cumulated biomass for fresh (FM) (A) and dry matter (DM) (B) as well as fixed N (N_{Fix}) (C) for clover-grass (CG) and lucerne-grass (LG) mixtures, after the first (H1), second (H2: H1+H2) and third (H3: H1+H2+H3) cut. Best machine learning algorithm is shown of Partial Least Square (PLS) and Random Forest (RF) regression with and without texture features (T).

4.4 Discussion

The aim of this study was to provide aboveground biomass and N_{Fix} estimation models in two legume-grass mixtures through a whole vegetation period based on

multispectral information. The prediction models covered different proportions of legumes to represent the variable conditions in practical farming and the multi-temporal data acquisition offered a wide range of biomass levels, which is a prerequisite for robust and generalized models (Psomas et al. 2011). All multispectral information, containing also VIs and texture features, arose from four spectral bands. Consequently, no additional sensors were needed, which reduced measurement errors (Assmann et al. 2019) and makes this method time and cost efficient.

The first specific objective of this study was the development of biomass and N_{Fix} prediction models for two common legume-grass mixtures. Though differences in model performance between the two machine learning algorithms (i.e. PLS and RF) were minor, biomass prediction by RF performed better (in terms of rRMSE) than by PLS both for the whole as well as for the crop-specific dataset. Similar findings were reported by Zhou et al. (2019), who found Support Vector Machine (SVM) to perform better than PLS with hyperspectral reflectance data captured with a radiometer (400-1000 nm) in different legume-grass mixtures. The authors pointed out, that there might exist a non-linear relationship between spectral information and biomass, which could not be captured by PLS modelling. For N_{Fix} the best model for the whole dataset was given by RF, whereas the crop-specific regression analysis was better with PLS. Morin et al. (2019) stated that RF showed weaknesses in dealing with small sample sizes. In our study the dataset for model calibration of N_{Fix} was limited to three main harvests only, which may have decreased model robustness.

In contrast to findings by Grüner et al. (2019), where biomass prediction models by UAV height measurement showed substantial crop-specific differences, no clear differences were found in this study between clover- and lucerne-grass mixtures. Interestingly, for biomass and N_{Fix} the best models with an average rRMSEP of 10% (FM), 11% (DM) and 18% (N_{Fix}) were obtained based on the whole dataset, which produced rather universal and crop-unspecific models. Model validation by a preferably independent test dataset is desirable for the assessment of prediction accuracy. However, our models were created based on datasets from one experimental site only and a limited variety of plant species which may limit the transfer to other locations and time periods (Wood et al. 2013).

N_{Fix} models were less accurate with a relative error of 18-24%. To our best knowledge, no other studies investigated the relationships between spectral information and N fixation by legume-grass mixtures. The relationships between N_{Fix} and multispectral information with R^2 from 0.69 to 0.84 found in our study must be interpreted with caution, as different impacts of N flux in the soil, air and plant affect N fixation of forage legumes in mixtures with grasses (Thilakarathna and Raizada 2018). Knoblauch et al. (2017) could not capture N dynamics of the soil by a multispectral sensor with two bands (red, NIR) or by calculating NDVI and SR (Simple Ratio) in a greenhouse experiment with perennial ryegrass (*Lolium perenne* L.). The authors concluded that the above mentioned effects cause problems to measure N_{Fix} so far by optical remote sensing, as it only obtains spectral information of the biomass and the top soil surface, but furthermore, does not consider the root tissue which also contains atmospherically fixed N (Carlsson and Huss-Danell 2003). N_{Fix} model accuracy may also depend on the methodology for measuring reference data. N_{Fix} calculation by the difference method, which is widely-spread and relatively simple to use, assumes that grass and legumes have the same intensity of soil N absorption. However, grass usually absorbs more soil N, which leads to an underestimation of the method (Carlsson and Huss-Danell 2003). For this reason, Thilakarathna and Raizada (2018) suggested to include non-N-fixing legumes of the same species as a reference, not only for a more precise difference method, but also to calibrate the spectral information and to use it for an improved classification of N fixation.

The second and third objective of our study was to compare the performance of the biomass and N_{Fix} prediction models with and without texture features and to identify the importance of the variables. Models for FM and DM showed poor accuracies without texture features with an rRMSEP between 15 to 22%. Due to missing rainfall through the whole vegetation period and as no fertilizer was applied, especially pure stands of grass were growing poorly after the first cut. Biewer et al. (2008) found that models build with VIs solely (i. e. NDVI and SR) showed weaknesses in predicting mature and dry grass swards due to alteration of the spectral information. Though mixed stands with plants of varying chemical (e. g. pigments and water) and morphological traits (e. g. angle and structure of leaves) may show similar spectral reflection patterns (Ollinger 2011), texture features may help to distinguish single plant

species by considering the spatial heterogeneity (Simin et al. 2010). Our results clearly demonstrated that inclusion of texture features reduced rRMSEP by almost the half (rRMSEP = 10-15%) and resulted in improved model accuracies (R^2 = 0.75-0.87). Furthermore, texture features showed high rankings in the variable importance of the models, especially for those of the red band. The latter finding is confirmed by the work of Gallardo-Cruz et al. (2012) who found texture features from red and NIR bands as the most important in satellite-based remote sensing for vegetation classification and modelling of height and biodiversity.

Thus far, only one study included texture analysis for biomass prediction of agricultural crops. Using multispectral UAV images Zheng et al. (2019) found rather poor relationships between different texture features and DM over two vegetations periods. However, model accuracy could be improved by using a new Normalized Difference texture index (NDTI) instead of single texture features (R^2 = 0.44-0.75 for the whole dataset). A comparison to legume-grass mixtures, which form more heterogeneous canopies, is difficult. Nevertheless, Zheng at al. point out that a normalization of texture information by an index excludes background noises like soil reflection and varying sun position and, thus, may improve biomass prediction in multi-temporal studies with legume-grass mixtures, but more research is required in this area.

N_{Fix} was improved by texture features except for CG, although texture showed high rankings for variable importance. As N_{Fix} depends on several different conditions (e.g. soil variability), this plant trait cannot be captured easily by spectral information of the plant canopy. Such limited information may be the reason for the inconsistent effects of texture features on model accuracy. A broader spectral range or hyperspectral information from additional sampling dates as well as from bare soil areas at the time of measurement, which act as a reference for the soil N content (Kusumo et al. 2011) may improve model accuracy.

The last objective of our study was the assessment of total annual biomass and N_{Fix} for CG and LG. Total annuals represent the level at which farmers, plant breeders and advisory services usually conduct the evaluation of crop performance and where data are available as a basis for feeding plans for ruminants or biogas plants. Annual FM and DM was underestimated for both CG and LG by around 1 to 2 t ha^{-1}, with slightly

better accuracy for FM. Surprisingly, a prediction of annual biomass by crop height, which was estimated from drone-based RGB imaging and photogrammetric analysis, showed greater potential (Grüner et al. 2019). Contrary, annual total N_{Fix} for CG and LG was slightly overestimated by 10-14 kg ha^{-1}. Compared to data reported for CG and LG, which indicate a total annual N fixation of up to 300 kg ha^{-1} (Boller and Nösberger 1987; Carlsson and Huss-Danell 2003; Rasmussen et al. 2012), total annual N_{Fix} in our study was generally on a relatively low level, which in combination with a small sample size may have created difficulties in the modelling process. Annual biomass and N_{Fix} prediction by multispectral information, thus, should be considered as a first approach for the support of farm management decisions, which still needs further improvement.

In general, accurate biomass prediction by multispectral UAV data depends on several parameters during data acquisition, like recording time, image quality and model tuning. Though the sensor used in our study had an integrated sunshine sensor for automatic calibration of every picture, multi-temporal data acquisition requires stable and calm weather conditions and equal time points of flight missions (Bendig et al. 2015), which was difficult to comply with even under experimental conditions and all the more so poses challenges under farming conditions. Changing atmospheric condition between the sampling dates might also affect data quality, which can only be compensated by proper atmospheric correction (Yu et al. 2017). Nevertheless, atmospheric algorithms are complex and intense atmospheric measurements have to be done simultaneously for each flight, which increases measurement time (Aasen et al. 2018; Laliberte et al. 2011; Yu et al. 2017). Moreover, moving plant leaves by wind or blurred images need to be avoided to keep texture accuracy high (van Evert et al. 2009). As flight speed in our study was very slow (1 m/s) image quality was high and no image had to be excluded from the analysis. Especially for texture features, image quality and resolution play a decisive role (Coburn and Roberts 2004), which depends on the sensor resolution in combination with the flight altitude. With the sensor used in our study a flight height of 50 and 20 m resulted in an image resolution of 2-4 cm, which was then resampled to 4.5 cm. Different ground resolutions should be avoided in future studies to keep unified conditions for data analysis As plant and especially grass leaves can be thinner than 2 cm, a higher spatial resolution may improve texture resolution

and, therefore, biomass prediction accuracy. Furthermore, in our study only default parameter settings for texture processing were used. The impact and versatility of tuning parameters and window size for texture processing was shown elsewhere (Coburn and Roberts 2004; Lu 2005; Morin et al. 2019) and should be considered in future research to improve quality of biomass estimation in legume-grass mixtures. Further work is needed to assess the potential of this promising tool at other sites and different legume-grass mixtures.

4.5 Conclusion

Non-destructive and fast aboveground biomass and N_{Fix} prediction tools are desirable for practical farm management, especially for organic farmers who are depending on legumes as an N source. For this purpose, the aim of this multi-temporal field study was to provide aboveground biomass and N_{Fix} estimation models based on UAV-borne multispectral information. Two machine learning methods were tested (PLS and RF) using data from two different legume-grass mixtures and associated pure legume and grass through a whole vegetation period. We successfully developed a procedure for biomass prediction by inclusion of texture features from a grey level co-occurrence matrix. RF produced the best results for the whole dataset based on the two legume-grass mixtures including the pure stands of legumes and grass, both for biomass and N_{Fix}. Although prediction of fixed N seemed to be more complex, strong relationships were found between N_{Fix} and multispectral information under field conditions. In conclusion, multispectral information including texture features from one single sensor on a UAV proved to be a very promising tool for biomass and N_{Fix} prediction in legume-grass mixtures.

4.6 Appendix

Table 4.3: Treatments.

Treatment		Functional group	Species	Ratio (%)
Clover-grass mixture	CG	Legumes (L)	*Trifolium pratense*	30
			Trifolium hybridum	5
			Trifolium repens	5
		Grass (G)	*Lolium multiflorum*	60
Lucerne-grass mixture	LG	L	*Medicago sativa*	40
			Trifolium pratense	10
		G	*Festuca pratensis*	20
			Lolium perenne	15
			Lolium multiflorum	10
			Phleum pratense	5
Pure clover legumes	L_{CG}	L from CG mixture	*Trifolium pratense*	75
			Trifolium hybridum	12.5
			Trifolium repens	12.5
Pure lucerne and clover legumes	L_{LG}	L from LG mixture	*Medicago sativa*	80
			Trifolium pratense	20
Pure grass sward	G_{CG}	G from CG mixture	*Lolium multiflorum*	100
Pure grass sward	G_{LG}	G from LG mixture	*Festuca pratensis*	40
			Lolium perenne	30
			Lolium multiflorum	20
			Phleum pratense	10

CG = Clover-grass; LG = Lucerne-grass.

Table 4.4: Vegetation indices. Vegetation indices calculated with four bands captured by the multispectral sensor used in this study: green, red, red edge (RE) and near infra-red (NIR).

Name	Definition	Reference
Simple Ratio	$SR = \frac{NIR}{Red}$	Jordan 1969 [72]
Modified Simple Ratio	$MSR = \frac{\frac{NIR}{Red} - 1}{\sqrt{\frac{NIR}{Red}} + 1}$	Chen 1996 [73]
Green Chlorophyll Index	$GCI = \left(\frac{NIR}{Green}\right) - 1$	Gitelson et al. 2005 [74]
Difference Vegetation Index	$DVI = NIR - Red$	Tucker 1979 [75]
Normalized Difference Vegetation Index	$NDVI = \frac{NIR - Red}{NIR + Red}$	Rouse et al. 1974 [27]
Renormalized Difference Vegetation Index	$RDVI = \frac{NIR - Red}{\sqrt{NIR + Red}}$	Roujean & Breon 1995 [76]
Green Normalized Difference Vegetation Index	$GNDVI = \frac{NIR - Green}{NIR + Green}$	Daughtry et al. 2000 [77]
Normalized Difference Red Edge Index	$NDRE = \frac{NIR - RE}{NIR + RE}$	Fitzgerald et al. 2010 [78]
Chlorophyll Vegetation Index	$CVI = \frac{NIR}{Green} * \frac{Red}{Green}$	Vincini et al. 2008 [79]
Soil Adjusted Vegetation Index	$SAVI = \frac{NIR - Red}{NIR + Red + 0.5} * (1 + 0.5)$	Huete 1988 [80]
Modified SAVI 2	$MSAVI2 = \frac{2 * NIR + 1 - \sqrt{(2 * NIR + 1)^2 - 8 * (NIR - Red)}}{2}$	Qi et al. 1994 [81]
Modified Chlorophyll Absorption Index	$MCARI = [(RE - Red) - 0.2 * (RE - Green)] * \frac{RE}{Red}$	Daughtry et al. 2000 [77]

Table 4.5: Photogrammetric processing information.

Sampling	Date	Flight altitude (m)	RMSE (XY) of GCPs (cm)
1. sub-sampling	16.04.18	20	0.79
2. sub-sampling	03.05.18	50	0.94
1. harvest	17.05.18	50	1.27
3. sub-sampling	06.06.18	20	0.59
2. harvest	20.06.18	20	0.74
4. sub-sampling	17.07.18	20	1.43
3. harvest	03.08.18	20	0.76
5. sub-sampling	01.11.18	20	0.98

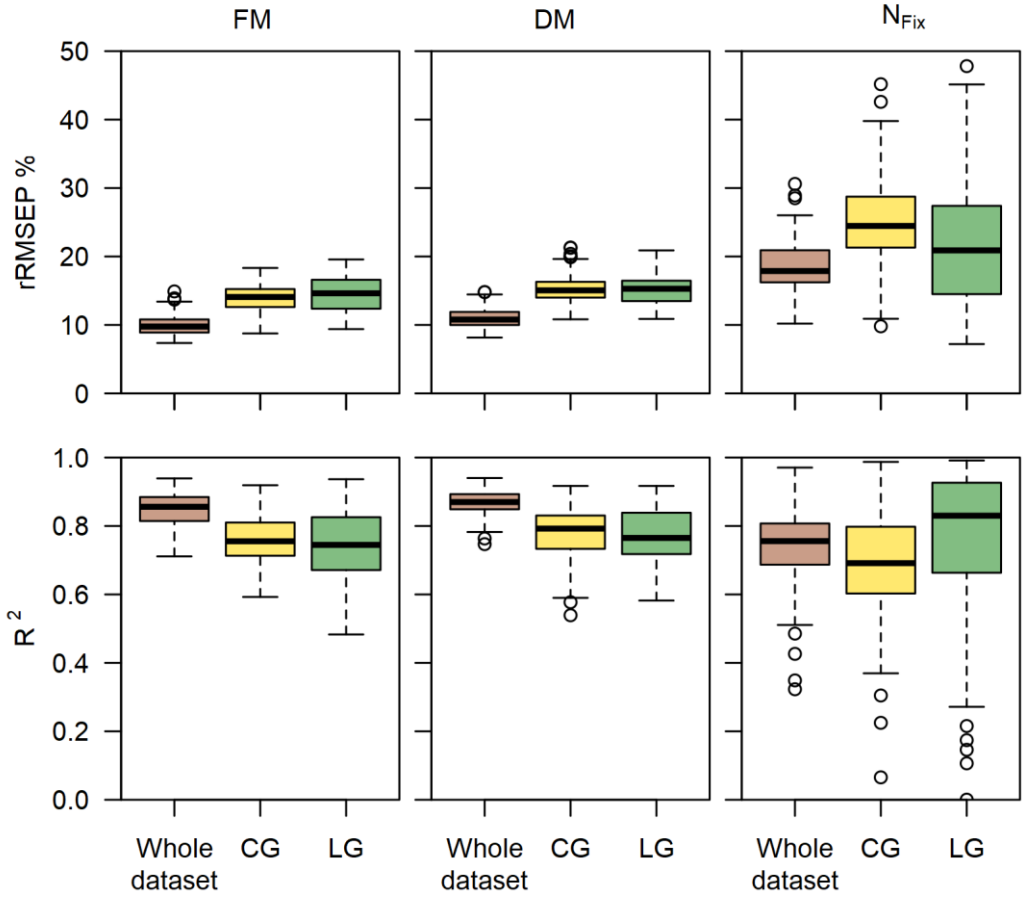

Figure 4.8: Model accuracy. Boxplots for the model accuracy created by 100 cross-validations for the whole dataset as well as crop-specific: clover-grass (CG) and lucerne-grass (LG) mixtures including the pure stands of legumes and grass. Plots show the best prediction algorithm, with 100 randomly selected test and training data sets based on data from 3 main harvests and 6 sub-sampling dates, whereas N_{Fix} contains only main harvests. Boxes show the 25 and 75% percentile, the solid line indicates the median, the whiskers represent the 5 and 95% percentile, circles show outliers.

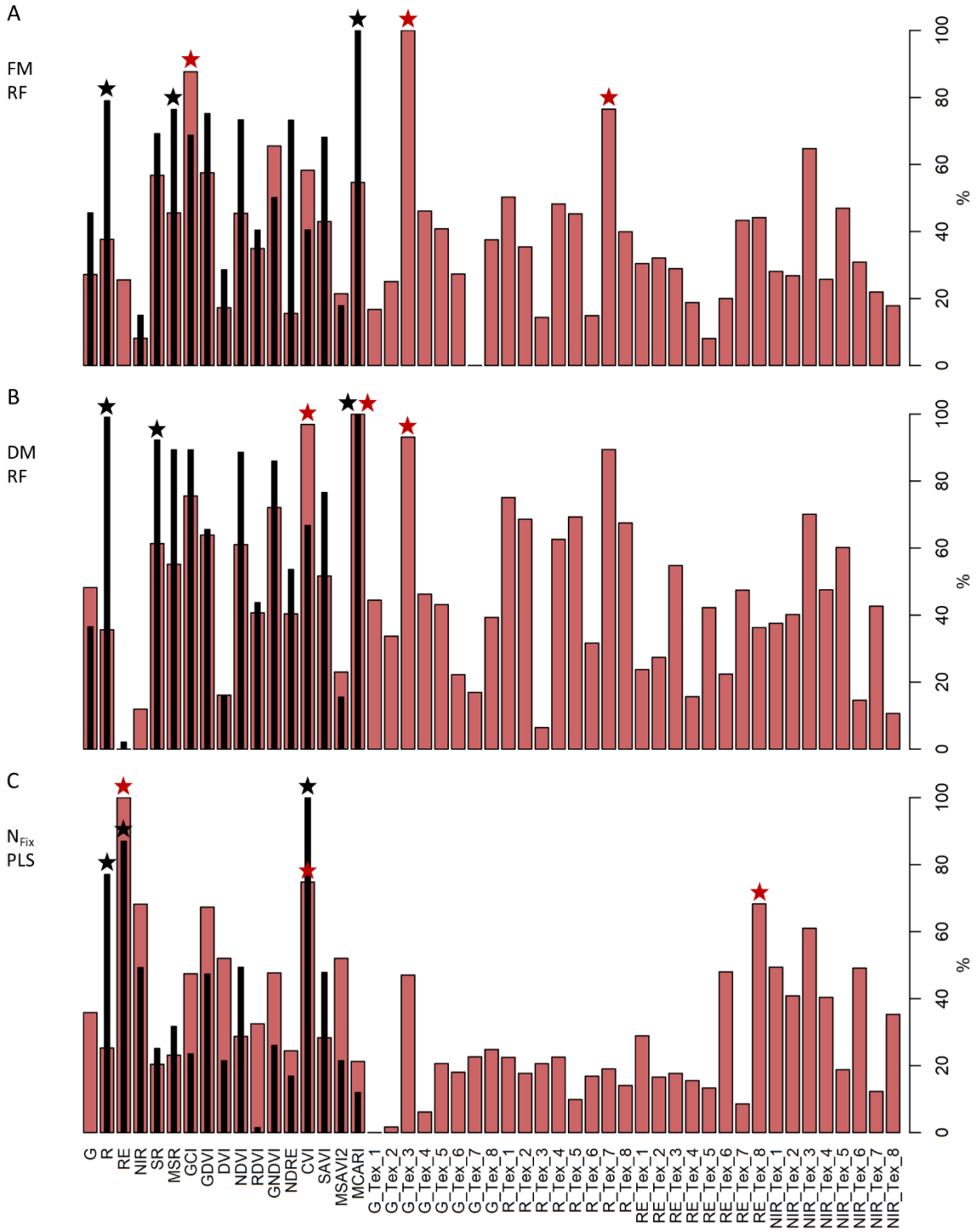

Figure 4.9: Variable importance for clover-grass. Variable importance of prediction models for fresh (FM) (A) and dry matter (DM) (B) as well as fixed N (N_{Fix}) (C) for the whole dataset built with four spectral bands, 13 vegetation indices and with (red) and without (black) 8 texture features of each band. Stars indicate the three highest rankings of variables with (red) and without texture features (black) in the model. Plots show the best prediction algorithm, Partial Least Square (PLS) or Random Forest (RF), with the best of100 randomly selected test and training data sets based on data from 3 main harvests and 6 sub-sampling dates, whereas N_{Fix} contains only main harvests.

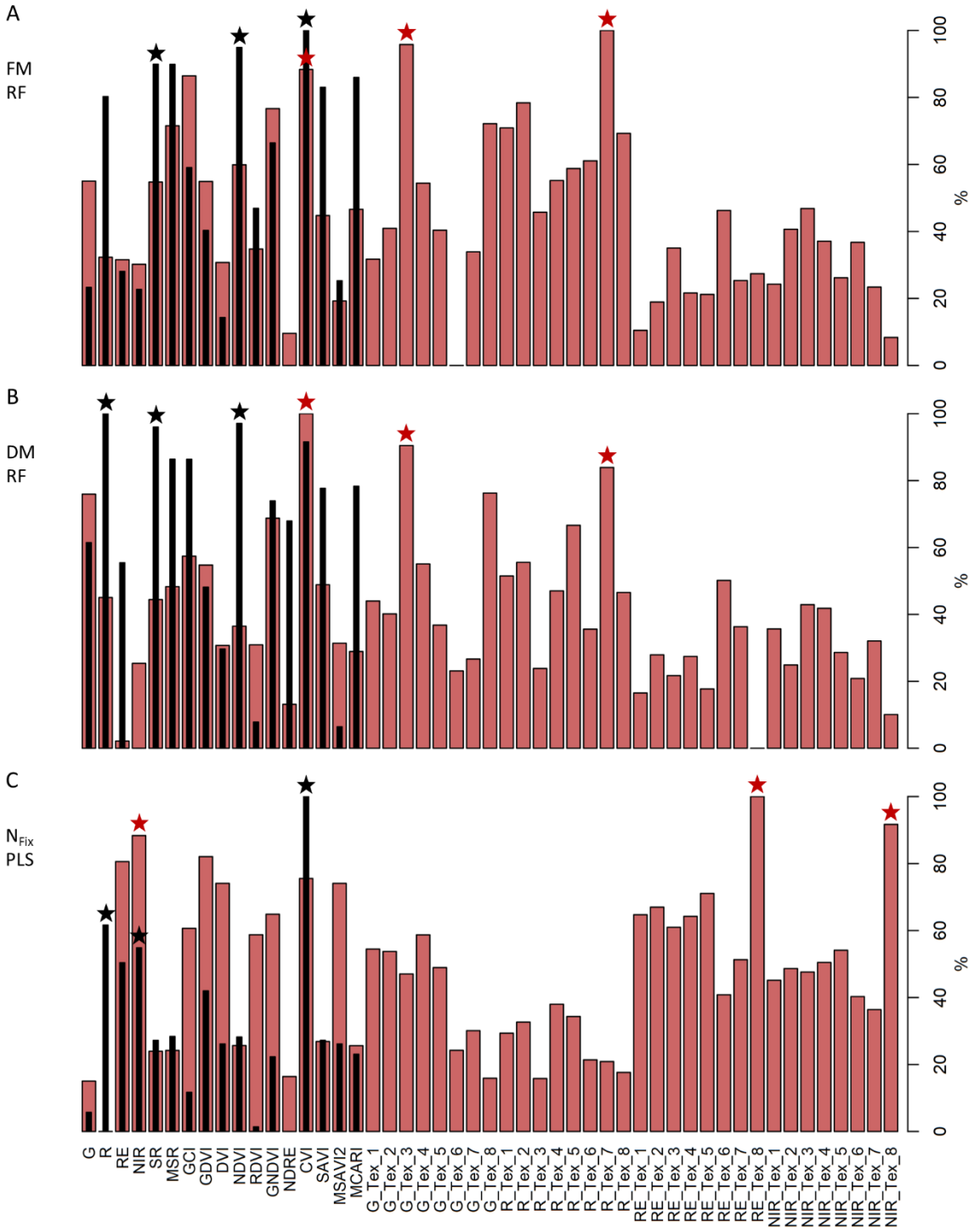

Figure 4.10: Variable importance for lucerne-grass. Variable importance of prediction models for fresh (FM) (A) and dry matter (DM) (B) as well as fixed N (N_{Fix}) (C) for the whole dataset built with four spectral bands, 13 vegetation indices and with (red) and without (black) 8 texture features of each band. Stars indicate the three highest rankings of variables with (red) and without texture features (black) in the model. Plots show the best prediction algorithm, Partial Least Square (PLS) or Random Forest (RF), with the best of100 randomly selected test and training data sets based on data from 3 main harvests and 6 sub-sampling dates, whereas N_{Fix} contains only main harvests.

5 Prediction of biomass and N fixation of legume-grass mixtures using sensor fusion

Abstract

European farmers and especially organic farmers rely on legume-grass mixtures in their crop rotation as an organic nitrogen (N) source, as legumes can fix atmospheric N, which is the most important element for plant growth. Furthermore, legume-grass serves as valuable fodder for livestock and biogas plants. Therefore, information about aboveground biomass and N fixation (N_{Fix}) are crucial for efficient farm management decisions on field level. Remote sensing, as a non-destructive and fast technique, provides different methods to quantify plant trait parameters. In our study for two legume-grass mixtures terrestrial laser scanning (TLS) for high density point clouds for crop surface height (CSH) measurements in combination with unmanned aerial vehicle (UAV)-based multispectral (MS) data were carried out. Several CSH metrics based on TLS and vegetation indices (VIs) based on the four MS bands (green, red, red edge, near infrared) were calculated. Furthermore, eight texture features based on mean CSH and the four MS bands were generated to measure horizontal spatial heterogeneity. The aim of this multi-temporal study over two vegetation periods was to create estimation models based on biomass and N fixation for two legume-grass mixtures by sensor fusion, a combination of both sensors. To represent conditions in practical farming, i. g. varying proportion of legumes, the experiment included pure stands of legume and grass of the mixtures. Sensor fusion of TLS and MS data was found to provide better estimates of biomass and N_{Fix} then separate data analysis. The study shows the important role of texture based on MS and TLS data, which contributed greatly to the estimation model generation. The applied approach offers an interesting method for improvements in precision agriculture.

5.1 Introduction

Legume-grass mixtures, sown as temporary grassland and cultivated for 1-3 years, are substantial crop rotation elements, especially for organic managed farms in European temperate climate. These crops are valuable forage for livestock and substrate for biogas plants. Furthermore, farmers utilize the ability of legumes to fix nitrogen (N), which is the main essential element for plant growth and health, to increase soil fertility and to reduce the amount of external fertilizer for the following cash crop (Fustec et al. 2010; Rasmussen et al. 2012). Total aboveground biomass and the amount of fixed N (N_{Fix}), which contributes greatly to the N cycle on field and farm level, are important input variables for sustainable management decisions (Kayser et al. 2010). Traditional methods for grassland monitoring based on destructive biomass sampling, manual plant height measurement and laboratory work are time and cost intensive. Therefore, developments of non-destructive measurement techniques from the field of remote sensing provided interesting approaches and improvements for field data acquisition (Wachendorf et al. 2018).

Remote sensing was successfully used to estimate different biophysical and chemical plant traits in grasslands. As plant height correlates with biomass, canopy surface height (CSH) of grassland can be conducted by spatial information based on 3D point clouds with an ultra-sonic sensor (Fricke et al. 2011), Light Detection and Ranging (LiDAR) (Anderson et al. 2018; Xu et al. 2020) or Structure from Motion (SfM) based on RGB (red, green, blue) images (Grüner et al. 2019; Wijesingha et al. 2018). In a previous study of Grüner et al. (2019) SfM based on RGB images captured by an unmanned aerial vehicle (UAV) with a resolution of ~ 2 cm in two legume-grass mixtures was used for biomass estimation. The authors pointed out, that a higher resolution and the inclusion of plant density information could increase model accuracy. LiDAR can generate a higher point cloud penetration and resolution and can therefore, cover also single grass tillers (Cooper et al. 2017; Madec et al. 2017). However, the sole application of LiDAR generates only spatial characteristics of vegetation traits like mean, maximum and median height metrics, as the sensor is limited to one single wavelength.

These restrictions can be compensated by spectral sensors, which quantify multi- and hyperspectral reflectance information and are used to calculate vegetation indices (VIs) (Moeckel et al. 2017; Reddersen et al. 2014). A spectral sensor mounted on a low-cost UAV serves as an interesting and simple tool for grassland monitoring. VIs were already successfully used to estimate grassland biomass, N content, N_{Fix} (Cho et al. 2007; Gao et al. 2019; Grüner et al. 2020) and are highly correlated to leaf area index (LAI) (Darvishzadeh et al. 2008; He et al. 2006; Mutanga and Skidmore 2004), which serves as a parameter for plant density (Carlson und Ripley 1997). However, the sole application of VIs for biomass estimation is affected by soil background color at low biomass levels (Huete et al. 1985) and saturates at high biomass and LAI levels (> 2-3) (Carlson and Ripley 1997; Mutanga and Skidmore 2004), as it captures reflectance only of the top surface of the canopy.

Consequently, sensor fusion of spatial and spectral information to combine different plant characteristics to overcome the above-mentioned limitations gained considerable interest as a new approach to asses forage yield and quality. Most sensor fusion studies in grasslands utilizing CSH metrics were based on ultrasonic sensors (Fricke und Wachendorf 2013; Gebremedhin et al. 2019; Moeckel et al. 2017) or UAV-based RGB SfM approaches (Geipel et al. 2014; Lussem et al. 2019; Possoch et al. 2016). Although, LiDAR provides high 3D point cloud resolution, the combination with a spectral sensor was only done by Schaefer and Lamb (2016) in a *Festuca arundinacea* dominated grassland and never done for plant traits like N fixation. The results of Wang et al. (2017a) showed an improvement of biomass estimation accuracy by LiDAR-based height metrics and VIs in maize, compared to models solely based on one sensor system. Similar results were found by Tilly et al. (2015) in a barley experiment using combined TLS and hyperspectral data. Therefore, the utilization of LiDAR in combination with VIs could further enhance prediction accuracy for forage parameter.

Grassland, as well as legume-grass mixtures can be botanically, structurally and phenologically very diverse (Biewer et al. 2009; Cho et al. 2007; Schellberg et al. 2008), as they consist of a composition of different species, compared to other agricultural crops, which are usually cultivated in monoculture. This horizontal heterogeneity within vegetation is ignored by CSH metrics and VIs. Texture features,

derived from high resolution images of vegetation, proved to serve additional structural information and correlate with heterogeneity (Gallardo-Cruz et al. 2012). The analysis of texture describes the spatial and statistical relationship of pixels (grey level values) and their variation in a defined area of interest in an image (Haralick et al. 1973; Wood et al. 2012). Texture features based on spectral data are sensitive to the phenological growth stage of the plant (Culbert et al. 2009) and increase data information of crop canopy without additional sensors. The inclusion of texture features for biomass and LAI estimation was mainly done in forests (Lu 2005; Morin et al. 2019; Wijaya et al. 2010) and to a lower degree for agricultural crops like rice (Li et al. 2019; Zheng et al. 2019; Zheng et al. 2020) and wheat (Yue et al. 2017). In grasslands the study of Grüner et al. (2020) investigated the influence of texture features based on multispectral data on model accuracy for biomass and N_{Fix} prediction in two legume-grass mixtures. The study clearly showed promising results for FM and DM estimation, whereas for N_{Fix} the results were not fully clear.

The aim of the present study was to develop a multi-temporal estimation model for aboveground biomass and N_{Fix} of two legume-grass mixtures. Estimation models were created using CSH metrics generated from TLS data and UAV-based multispectral (MS) data. Furthermore, texture features were not only extracted from MS, but also from CSH, which was never done before for grassland or other agricultural crops. As the study has a high number of predictors in combination with high multi-collinearity, a common machine learning algorithm, Random Forest (RF) (Breiman 2001), was used for model generation (Belgiu and Dră 2016. Thus, the specific objectives of this study are:

- The development of biomass (FM, DM) and N_{Fix} estimation models by RF for clover- and lucerne-grass mixtures (0-100% legumes) based on two complete growing periods.
- Comparing the exclusive model generation based on CSH from TLS and based on MS information from UAV-based multispectral imagery with the prediction model based on the fusion of both sensors.
- Identify the most important parameter for the prediction of the grass-legume mixtures and evaluate the contribution of texture features.

5.2 Material and methods

5.2.1 Experimental site

The field study was carried out on a legume-grass experiment in two consecutive growing seasons, 2018 and 2019, which is located on the research farm of the Universität Kassel in Neu-Eichenberg (51 23' N, 9 54' E, 227 m above sea level) in Hesse, Germany. The mean annual precipitation and daily temperature of the site is 661 mm and 8°C, respectively, which was not reached for the study years, especially for 2018 (Table 5.1). The research farm is managed organically and therefore, no fertilizer and chemicals were applied.

Table 5.1: Total rainfall, number of samples and UAV flight information for both research years

Year	Annual Rainfall (mm)	Harvest date	Harvest	Number of samples (n)	Flight mode	Flight altitude
2018	380	17.05.18	First harvest (H1)	72	Manually	50 m
		20.06.18	Second harvest (H2)		Manually	50 m
		03.08.18	Third harvest (H3)		Manually	20 m
2019	641	23.05.19	First harvest (H1)	68	Autopilot	20 m
		04.07.19	Second harvest (H2)		Autopilot	20 m
		22.08.18	Third harvest (H3)		Manually	20 m

The study design was adapted from (Grüner et al. 2020) and was continued for the growing season 2019. Field plots (1.5 × 12 m^2) were sown in autumn 2017 and cultivated for the following two study years with six different treatments in four replicates which were mowed 3 times a year in accordance with the common agricultural practice within the region (Table 5.1).

The six treatments were composed of two legume-grass-mixtures, clover- (CG) and lucerne-grass (LG), and pure stands of legumes (L_{CG}, L_{LG}) and grass (G_{CG}, G_{LG}) of

both mixtures with a seeding density of 35 kg ha^{-1} (Appendix Table 5.2). CG included 60% *Lolium multiflorum* (LM), 30% *Trifolium pretense* (TP), 5% *Trifolium hybridum* L. (TH) and 5% *Trifolium repens* L. (TR), whereas LG consisted of 40% *Medicago sativa* (MS), 20% *Festuca pratensis* Huds. (FP), 15% LP, 10% LM, 10% TP and 5% *Phleum pratense* L. (PP).

5.2.2 Data acquisition

TLS and UAV flight missions were done one day before every harvest. A Leica real time kinematic (RTK) global navigation satellite system (GNSS) with a measuring accuracy of 2 cm was used to measure the coordinates of the plot corners of every plot. An overview of the workflow for data acquisition and processing is given in Figure 5.1.

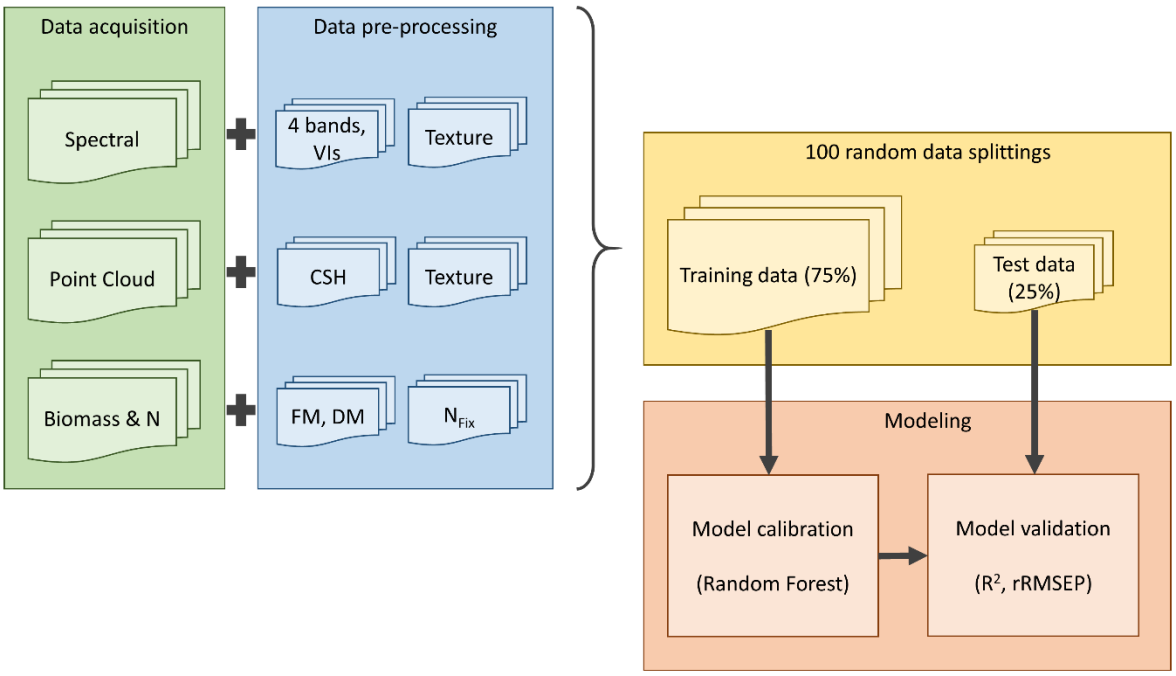

Figure 5.1: Workflow for model processing: Data acquisition (green) of spectral information (green, red, red edge, NIR), point cloud from terrestrial laser scan data as well as reference data for biomass and N_{Fix}; data pre-processing (blue): eight texture features of each spectral band (4 bands), 13 vegetation indices (VI), 15 crop surface height (CSH) parameters, eight texture features of the mean CSH, fresh (FM) and dry matter (DM), N_{Fix} calculation; 100 random data splitting (yellow); modeling (red).

Terrestrial laser scanning data collection

A Leica ScanStation P30 (Leica Geosystem, Switzerland) was used for the point cloud data collection. The laser transmits and captures 1 million pulses per second at a wavelength of 1550 nm with a resolution of 3.2 mm at 10 m distance. For each harvest date seven scans were taken, distributed in the experimental field between the blocks and at the four borders of the field to cover the plots from each side. The laser was mounted on a tripod at a height of ca. 1.70 m. Three reflective control points were used at every scan for the later point cloud alignment of the digital surface model (DSM). The coordinates of the control points were measured by the Leica RTK GNSS. One additional TLS data set was generated after the first harvest of the first study year for the later digital elevation model (DEM).

Multispectral data collection

Spectral images were taken in the morning (8:00-12:00 a.m.) with a multispectral sensor (Parrot Sequoia, MicaSense Inc, Seattle, USA) mounted on an UAV (2018: DJI Phantom 3, Advanced; 2019: DJI Phantom 4 Professional, Shenzhen, China). The sensor captures 1.2 Megapixel (MP) images in four bands (green: 530-570 nm; red: 640-680 nm; red edge: 730-740 nm; near-infrared (NIR): 770-810 nm). For automatic radiometric calibration of every image, an upwelling sunshine sensor on the top of the UAV measures the at-the-sensor irradiance. The UAV was flown manually, except for the first two cuts in 2019, where autopilot (Pix4Dcapture, Lausanne, Switzerland) was used (Table 5.1). Seven ground control points (GCPs) were evenly distributed in the pathways between and around the plots. The coordinates of the GCPs were measured by the Leica RTK GNSS.

Biomass sampling and N fixation determination

In the year 2018 the first 1.5 m of every plot were used for destructive measurements between the main harvests (Grüner et al. 2020). Therefore, this area was excluded for biomass sampling and data processing in every plot in both years. At each harvest date two destructive samples of 0.25 m^2 were taken from every plot, which were weighed for fresh matter (FM) determination and afterwards dried at 100°C for 48 h to

constant weight to determine the dry matter (DM) content. For further analysis weights were extrapolated to t ha^{-1}. Additional sub-samples of every plot were taken for N concentration analysis, which was quantified by an elemental microanalyzer (Elementar vario MAX CHN, Langenselbold, Germany) and multiplicated with DM yield. To determine NFix of the legumes and the mixtures, the difference method according to (Stülpnagel 1982) was used (Eq. 5.1):

$$N_{Fix} = N_L - N_R \quad (5.1)$$

where NL is the amount of N of legume in the pure stand and in the mixture as the N fixing crop, whereas NR represents the amount of N of the pure stand of grasses as the non-fixing reference crop. Four samples from the year 2019 were not generated due to problems in the laboratory (Table 5.1).

5.2.3 Data pre-processing

Crop surface height parameter

The point cloud processing software Leica Cyclone 3D (Leica Geosystem, Switzerland) was used for merging and geo-referencing the point clouds of the TLS datasets using the GCPs. After exporting the point clouds, R version 3.5.1 (R Core Team, Vienna, Austria) was used for further computation. To convert the 3D point cloud to 2D height information for the DSMs and DEM of every plot, a raster with 5 cm cell size was overlaid and the height values of the points (z values) within each cell were extracted. Due to geo-referencing, the DEM fitted accordingly to the DSMs and was subtracted from each other to calculate the CSH for every plot and harvest date (Eq. 5.2):

$$CSH = DSM - DEM \quad (5.2)$$

In addition to the arithmetic mean CSH value of every plot, the minimum (MIN), maximum (MAX), median, variance, standard deviation, range, mode, skewness,

kurtosis, canopy height relief and the percentiles of 25, 75, 90 and 95% were computed.

Multispectral bands and vegetation indices

For photogrammetric processing Agisoft PhotoScan Professional (Agisoft LLC, St. Petersburg, Russia) was used for multispectral orthomosaic generation. After alignment of the overlapping images of each dataset a sparse point cloud was created with the accuracy setting “high” and a key point and tie point limit of 40,000 and 1,000, respectively. Accuracy of the sparse point cloud was enhanced by including GPS coordinates of the GCPs and automatic camera calibration. To generate a dense point cloud, parameter settings were set to “high” with a “mild” depth filtering. As flight height varied (20 and 50 m), in the last step, the multispectral orthomosaics were exported as a TIFF with 4.5 cm ground resolution, for unified conditions. To extract spectral information of every band for every plot, zonal statistics in Quantum Geographical Information System (QGIS 3.4.9, QGIS Development Team, Raleigh, NC, USA) was used by creating polygon masks for each plot. Additional to the four spectral bands, 13 vegetation indices (VIs) were used in this study (Appendix Table 5.3). VIs were calculated with the original spectral mean value of every plot.

Texture features

(Haralick et al. 1973) proposed 14 texture features for the grey level co-occurrence matrix of the image texture. Based on the study of Grüner et al. (2020) eight of these GLCM texture features were used (Appendix Table 5.4). In QGIS these eight features were provided by the Orfeo Toolbox library (OTB, open source, (Grizonnet et al. 2017; Morin et al. 2019), i.e. energy, entropy, correlation, inverse difference moment, inertia, cluster shade, cluster prominence and Haralick correlation (Appendix Table 5.4). Texture feature extraction was done for the mean CSH and the four spectral bands (green, red, red edge, NIR) keeping settings on default, “simple” texture set and a radiometric resolution of 16 bits.

Cross-validation and modeling

Biomass (FM, DM) and N_{Fix} were predicted based on the CSH variables (including texture features) and multispectral reflectance information (MS, including VIs and texture features). The third model was based on a data fusion of the CSH and spectral information (fusion). Random Forest (RF) was used from the R packages *caret* (Kuhn 2008) and *randomForest* (Liaw and Wiener 2002). For the RF model the dataset was divided into two subsets, where a training dataset (75%) was used for model calibration and the remaining dataset (25%) was used as validation dataset. To prevent bias by division of the dataset only once, the data splitting was done randomly 100 times, ensuring that the validation dataset always contained samples of each year, harvest date and treatment for an even distribution. For model calibration, a cross-validation for hyper-parameter tuning of *mtry* was done, which represents the number of randomly chosen variables. *Mtry* was set by dividing the number of samples (*n*) by 3 as recommended by (Probst et al. 2018), where *n* was 140 for FM and DM (Table 5.1) and 94 for N_{Fix} (excluding pure grass-plots). For model validation the model performance between observed and predicted FM, DM and N_{Fix} was calculated using the coefficient of determination of the validation (R^2_{val}) (Eq. 5.3) and the relative root mean square error of prediction (rRMSEP) (Eq. 5.4).

$$R^2_{val} = \left[1 - \frac{\sum_{i=1}^{n}(y_i - \hat{y}_i)^2}{\sum_{i=1}^{n}(y_i - \bar{y}_i)^2}\right] \tag{5.3}$$

$$rRMSEP = \frac{\sqrt{\frac{\sum_{i=1}^{n}(y_i - \hat{y}_i)^2}{n}}}{max(y_i) - min(y_i)} \tag{5.4}$$

where y is the observed and $\hat{y}$ the predicted value, $\bar{y}$ the average predicted value and n the sample size. To determine the variable importance, the first 20 variables were identified in all 100 models and sorted by the median importance value. The importance value is the mean of squared residuals (MSE), which is the difference between calculated on out-of-bag data for every decision tree and permuted for each variable (Kuhn 2008; Liaw and Wiener 2002).

5.3 Results

5.3.1 Ground truth data

In both study years all values for FM, DM and N_{Fix} of clover-grass (mixture, legume, grass) exceeded those for lucerne-grass (Figure 5.2). Due to severe drought in 2018, biomass and N_{Fix} were higher in 2019 for both clover- and lucerne-grass in mixture and its legume, whereas the grass showed the opposite. As no fertilizer was applied, the grass suffered from nutrient deficiencies, especially in the second growing period. The average annual FM yield after the third harvest (H3) ranged between 10.36 for GLG_19 and 103.94 t ha^{-1} for LCG_19 and DM yield between 3.05 for GLG_19 and 14.70 t ha^{-1} for LCG_19. The average N_{Fix} (H3) varied between 59.73 for LG_18 and 369.24 kg ha^{-1} for LCG_18.

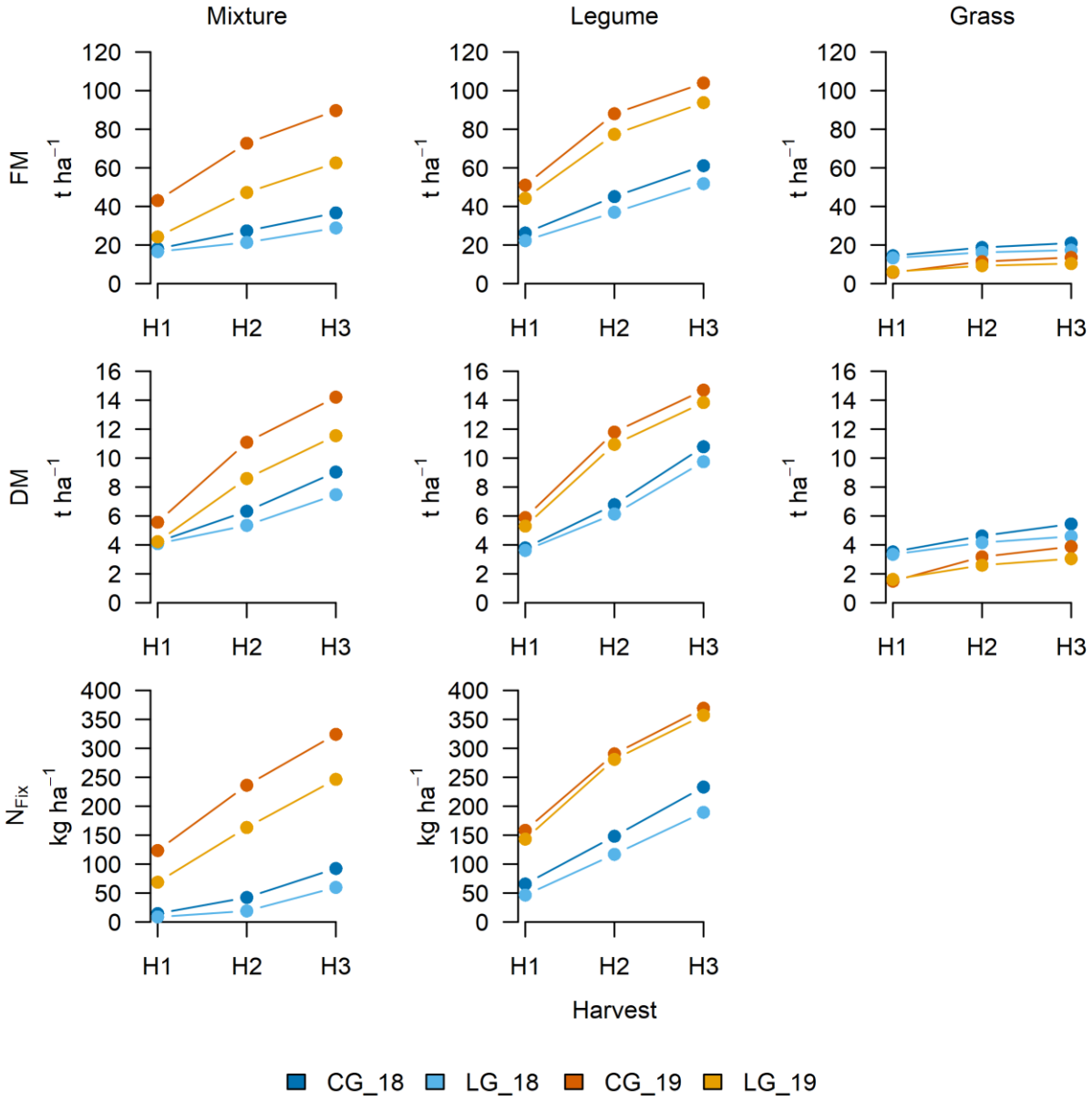

Figure 5.2: Cumulative fresh matter(FM), dry matter (DM) yield and nitrogen fixation (N_{Fix}) after the first (H1), second (H2: H1+H2) and third (H3: : H1+H2+H3) harvest in each of the two study years (2018, 2019) for clover- (CG) and lucerne-grass (LG) mixtures (left) and the pure stand of legumes (middle) and grass (right) as included in the mixtures.

5.3.2 Biomass and N_{Fix} prediction

The prediction accuracy of the models based on 100 random data splitting for calibration and validation is shown in Fig. 3. For FM CSH prediction models performed better than MS with a median rRMSEP of 13.84% and of 14.64% respectively. Sensor

fusion showed the best model accuracy with an R^2 of 0.81 and an rRMSEP of 12.40%. Similar to FM, for DM CSH showed a lower rRMSEP of 14.58% compared to MS with 16.57%. The best model performance with an R^2 of 0.82 and an rRMSEP of 13.07% was found by sensor fusion. For N_{Fix} MS showed the better model accuracy with an rRMSEP of 17.19% compared to CSH with 21.62%, although the best model was achieved again by sensor fusion with an R^2 of 0.73 and an rRMSEP of 15.18%.

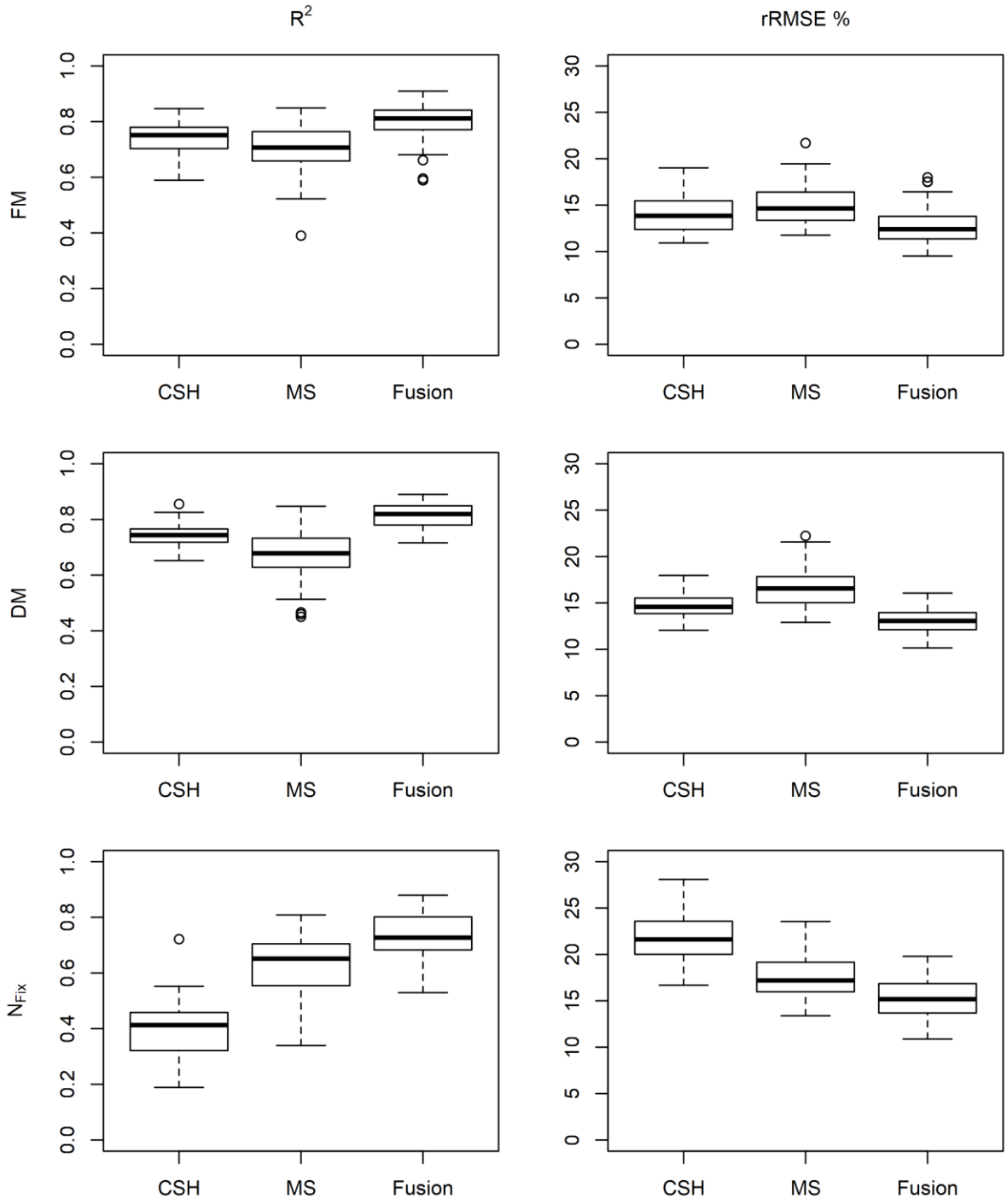

Figure 5.3: Boxplots for model accuracy based on 100 randomly divided calibration (75%) and validation (25%) subsets by treatment and year for cross-validation for the whole dataset including clover- and lucerne-grass as mixtures as well as pure stands of legume and grass of the mixtures. Model generation was done with crop surface height (CSH) information including texture features, with multispectral (MS) information including texture and vegetation indices and with sensor fusion (Fusion) based on both, CSH and MS. Boxes show the 25% and 75% percentile, the solid line indicates the median, the whiskers represent the 5 and 95% percentile, circles show outliers.

The plot of fit (Figure 5.4) of the 100 model runs for FM and DM showed no clear pattern for CSH and MS. Only a slight overestimation at low and underestimation at high yields was visible. This was reduced by the fusion of CSH and MS. For N_{Fix} the over- and underestimation at low and higher yields, respectively, was stronger, especially for CSH. This was also reduced by sensor fusion.

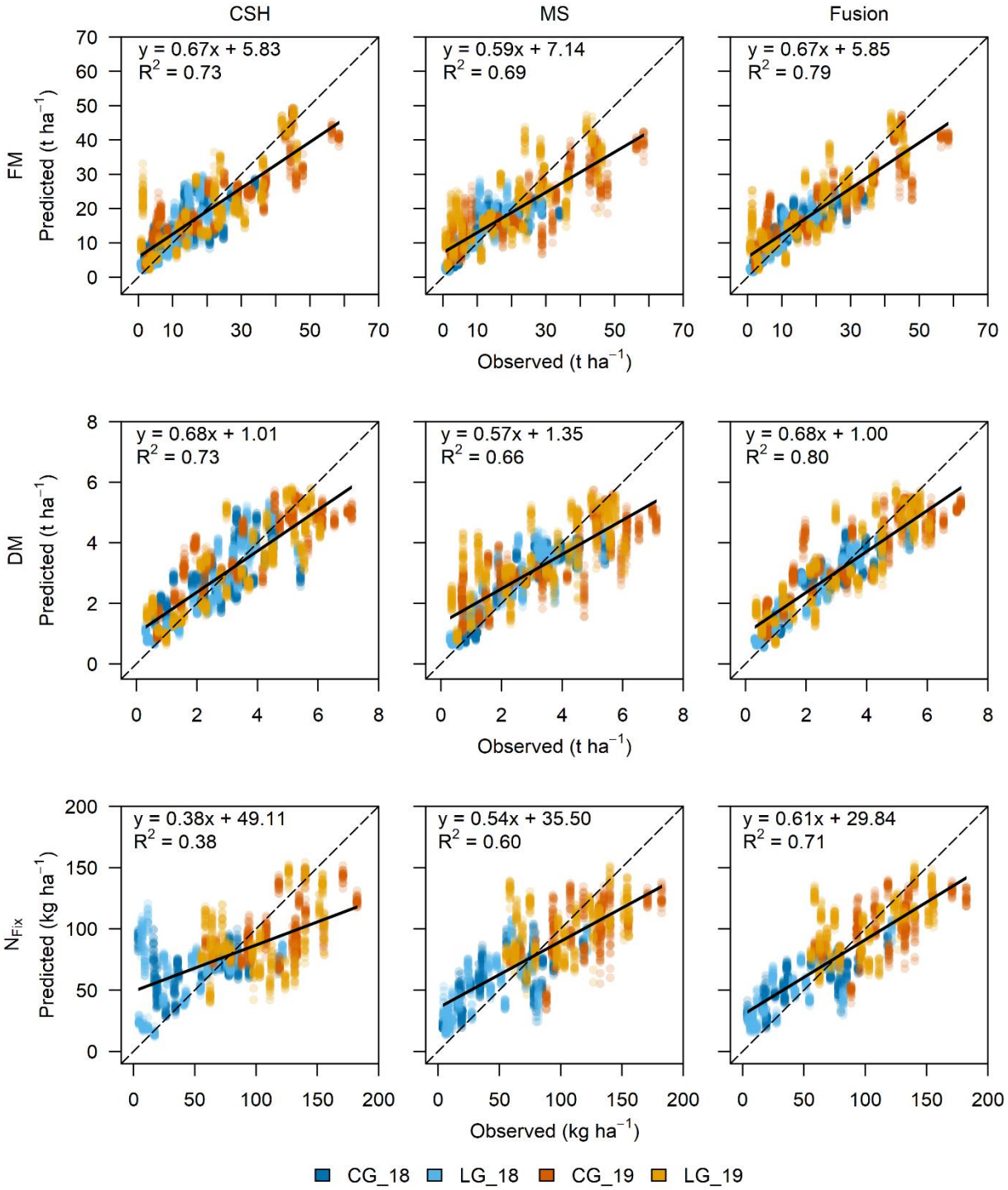

Figure 5.4: Scatterplot based on 100 randomly divided calibration (75%) and validation (25%) subsets by treatment and year for cross-validation for observed and predicted fresh (FM) as well as dry matter (DM) yield and nitrogen fixation (N_{Fix}) for the whole dataset at each of the two study years (2018, 2019) including clover- (CG) and lucerne-grass (LG) as mixtures including the corresponding pure stand of legume and grass of the mixtures. Dotted line indicates the 1:1 diagonal, whereas the solid line shows the regression line.

The importance of the first 20 RF model predictors (sorted by median) is separately shown for CSH and MS as well as for the sensor fusion in Figure 5.5. For FM, DM and N_{Fix} the variable importance for CSH showed nearly identical high rankings for texture features. For MS NIR including texture made the greatest contribution for both, FM and DM. For FM and DM the most important predictors for sensor fusion were CSH predictors, but also MS predictors, especially the NIR band including texture. For N_{Fix} MS and sensor fusion showed, that texture features especially from the green band made the greatest contribution.

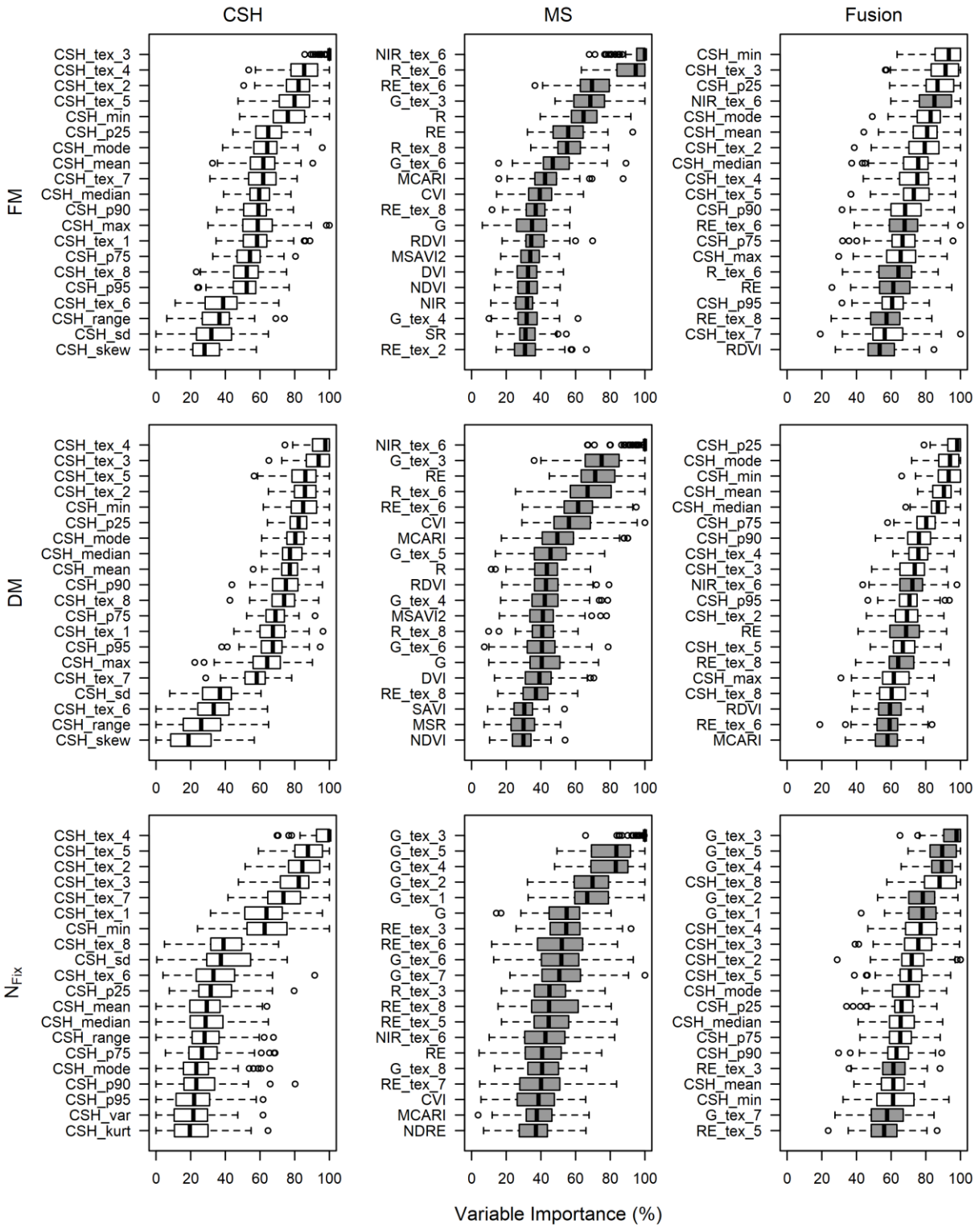
CSH
MS
Fusion
FM
DM
N_{Fix}
CSH_tex_3
CSH_tex_4
CSH_tex_2
CSH_tex_5
CSH_min
CSH_p25
CSH_mode
CSH_mean
CSH_tex_7
CSH_median
CSH_p90
CSH_max
CSH_tex_1
CSH_p75
CSH_tex_8
CSH_p95
CSH_tex_6
CSH_range
CSH_sd
CSH_skew
NIR_tex_6
R_tex_6
RE_tex_6
G_tex_3
R
RE
R_tex_8
G_tex_6
MCARI
CVI
RE_tex_8
G
RDVI
MSAVI2
DVI
NDVI
NIR
G_tex_4
SR
RE_tex_2
CSH_min
CSH_tex_3
CSH_p25
NIR_tex_6
CSH_mode
CSH_mean
CSH_tex_2
CSH_median
CSH_tex_4
CSH_tex_5
CSH_p90
RE_tex_6
CSH_p75
CSH_max
R_tex_6
RE
CSH_p95
RE_tex_8
CSH_tex_7
RDVI
CSH_tex_4
CSH_tex_3
CSH_tex_5
CSH_tex_2
CSH_min
CSH_p25
CSH_mode
CSH_median
CSH_mean
CSH_p90
CSH_tex_8
CSH_p75
CSH_tex_1
CSH_p95
CSH_max
CSH_tex_7
CSH_sd
CSH_tex_6
CSH_range
CSH_skew
NIR_tex_6
G_tex_3
RE
R_tex_6
RE_tex_6
CVI
MCARI
G_tex_5
R
RDVI
G_tex_4
MSAVI2
R_tex_8
G_tex_6
G
DVI
RE_tex_8
SAVI
MSR
NDVI
CSH_p25
CSH_mode
CSH_min
CSH_mean
CSH_median
CSH_p75
CSH_p90
CSH_tex_4
CSH_tex_3
NIR_tex_6
CSH_p95
CSH_tex_2
RE
CSH_tex_5
RE_tex_8
CSH_max
CSH_tex_8
RDVI
RE_tex_6
MCARI
CSH_tex_4
CSH_tex_5
CSH_tex_2
CSH_tex_3
CSH_tex_7
CSH_tex_1
CSH_min
CSH_tex_8
CSH_sd
CSH_tex_6
CSH_p25
CSH_mean
CSH_median
CSH_range
CSH_p75
CSH_mode
CSH_p90
CSH_p95
CSH_var
CSH_kurt
G_tex_3
G_tex_5
G_tex_4
G_tex_2
G_tex_1
G
RE_tex_3
RE_tex_6
G_tex_6
G_tex_7
R_tex_3
RE_tex_8
RE_tex_5
NIR_tex_6
RE
G_tex_8
RE_tex_7
CVI
MCARI
NDRE
G_tex_3
G_tex_5
G_tex_4
CSH_tex_8
G_tex_2
G_tex_1
CSH_tex_4
CSH_tex_3
CSH_tex_2
CSH_tex_5
CSH_mode
CSH_p25
CSH_median
CSH_p75
CSH_p90
RE_tex_3
CSH_mean
CSH_min
G_tex_7
RE_tex_5
0 20 40 60 80 100
Variable Importance (%)

Figure 5.5: The 20 most important variables in the prediction models based on 100 randomly divided calibration (75%) and validation (25%) subsets by treatment and year for cross-validation for fresh (FM) as well as dry matter (DM) and nitrogen fixation (N_{Fix}) for the whole dataset including clover- and lucerne-grass as mixtures as well as pure stands of legume and grass of the mixtures. Model generation was done with crop surface height (CSH; white box) information including texture features, with multispectral (MS; grey box) information including texture and vegetation indices and with sensor fusion (Fusion) based on both, CSH and MS. Boxes show the 25% and 75% percentile, the solid line indicates the median, the whiskers represent the 5 and 95% percentile, circles show extreme values.

5.4 Discussion

The aim of the current multi-temporal study was the development of estimation models for biomass and N_{Fix} of two legume-grass mixtures based on structural and spectral remote sensing information. RF, like other machine learning algorithms need a substantial amount of ground truth data, on the one side for calibration, but of similar importance, for validation of the model (Breiman 2001). Multi-temporal studies, which cover a wider range of plant composition, yield and vegetation periods are essential for model development (Ali et al. 2017; Psomas et al. 2011). To our best knowledge studies using machine learning based on UAV multispectral or TLS data for biomass prediction in grassland use only one-year data, like Capolupo et al. (2015), Viljanen et al. (2018), Anderson et al. (2018), Grüner et al. (2020) and Xu et al. (2020). Although Askari at al. (2019) generated UAV-based multispectral data for two years, each year included a different site. Our study consists of data based on two vegetation periods (i. e. three cuts each year) of the same experimental site. Furthermore, our study covers two legume-grass mixtures, typical for the European climate including a wide range of legume proportion (0-100%) of these mixtures, which makes our models transferable to practical farming.

Model generation was first done separately for each sensor system. For biomass estimation, CSH (14-15% rRMSEP) performed slightly better than MS (15-17% rRMSEP). Xu et al. (2020) used TLS data for aboveground biomass estimation in a heterogenous permanent grassland and showed, that TLS measurements are less effected by saturation than VIs, as the laser infiltrates deeper into the vegetation. This

might explain the advantage of TLS towards MS in our study. Grüner at al. (2020) gained an rRMSEP of 10-11% for sole MS data but containing sub-samples between the harvests from one year, which may made the model more robust but also less generalizable.

Sensor fusion of CSH and MS further improved estimation model accuracy (12-13% rRMSEP). Our finding broadly supports the work of other studies in this area linking crop height with multispectral information in grassland. Schaefer and Lamb (2016) used LiDAR for CSH and an optical reflectance sensor for measuring NDVI in a *Festuca arundinacea* dominated grassland. The sensors were both mounted on a wheeled vehicle, 1.8 m above ground, where sensor fusion reduced RMSEP from 847 (NDVI) and 708 (LiDAR) by 46 and 36%, respectively, in a linear regression model. Lussem et al. (2019) gained cross validation results from multivariate linear regression of different VIs each combined with CSH from UAV RGB (90% percentile) with similar R^2 between 0.57 and 0.75 for FM and R^2 of 0.41 and 0.81 for DM, strongly depending on harvest date. The study of Viljanen et al. (2018) in a grassland experiment with different N fertilizing levels, showed that the best model performance was given by a combination of VIs, RGB and CSH features (rRMSE = 11-15%) for multilinear regression and RF. Näsi et al. (2018) could not confirm that biomass prediction by RF of grassland based on spectral and structural (both UAV RGB) parameter performed better than separate models. Nevertheless, rRMSE was on a very low level (2-6%) due to a low sample size (n = 8) with little variability, which limits its comparability and needs further investigations. Due to the severe drought in 2018 and missing fertilizer, mature grass was growing high with very low amount of biomass, compared to mixtures and pure stands of legumes (Grüner et al. 2020). Fricke and Wachendorf (2013) showed that spectral information can compensate overestimation of CSH at low biomass levels, what might be a possible explanation of the benefit of sensor fusion in our study.

For N_{Fix} MS (rRMSEP = 17%) performed better than CSH (rRMSEP = 22%). MS results are consistent with the measurements of the study of Grüner et al. (2020) (rRMSEP = 18%). N fixation is highly correlated to DM of legumes (Carlsson and Huss-Danell 2003; Høgh-Jensen et al. 2004) and consequently also to crop height. To our best

knowledge, so far no other study used sensor fusion for N_{Fix} estimation, which further increased model accuracy (rRMSEP = 15%) in our study.

The results show that the importance of the variables differs between FM, DM and NFix for the two sensors and their fusion. Apart from mean values for crop height and reflectance from the four spectral bands, our models contain several different parameters: from both sensor systems. The most important variable of CSH and MS were based on texture features, for FM, DM and N_{Fix}. Similar findings for MS were found by Grüner et al. (2020), which is the only study so far including texture features based on spectral information biomass and N_{Fix} estimation in legume-grass mixtures. Our results further support findings in other agricultural crops. Yue et al. (2019) used texture for wheat aboveground biomass estimation based on UAV RGB imaging with an R^2 of 0.89 (RMSE = 0.82 t ha^{-1}) by multiple stepwise regression. A recent study by Zheng et al. (2020) clearly showed an improvement of N content estimation for rice by combining VIs and texture features by UAV-based multispectral data.

To our best knowledge our study is the first extracting texture features from TLS data in agriculture and furthermore, combining them with spectral information. Texture detects other image characteristics of plant structure than CSH and MS, especially differences in plant growth stages (Gao et al. 2019) and yield levels (Yue et al. 2019). Therefore, this supplementary information improves biomass and N_{Fix} estimation.

Both sensors, for TLS point clouds and UAV multispectral imaging, have their specific limitations, as they detect and measure different biophysical and -chemical properties of vegetation and furthermore, in our study from different altitude and view angle positions (nadir vs. oblique). TLS covers the area of interest in different distances within one scan due to static measurement position, whereas UAV based measurements are constant at equal flight altitude for the whole area. Therefore, UAV based RGB imaging for crop height measurement by SfM in combination with multispectral data might have advanced handling, nevertheless, point density and accuracy is lower than for TLS (Wijesingha et al. 2018). As technical and computable improvement increases rapidly, a higher image resolution is expected in the next years for spectral sensors. Due to technical issues with the UAV software, except of two flights, all remaining flights were performed manually, which leads to uneven image overlapping. Further studies must

overcome these uncertainties for unified flight missions and later analysis. Furthermore, image resolution plays a crucial role for texture feature extraction. In our study, multispectral resolution was 4.5 cm. Yue et al. (2019) showed in a winter-wheat experiment, that image resolution between 5-15 cm showed only low correlation between texture and above ground biomass due to mixed pixels of soil and green vegetation. As legume-grass is rather heterogenous compared to cereals, an image resolution enhancement could improve texture accuracy, which needs further research. In our study, the multispectral sensor covered specific wavelengths of green, red, red edge and NIRS region. As the red edge region shifts to longer wavelengths for senescent material compared to green vegetation (Gao et al. 2019), a hyperspectral sensor can cover a much broader area of wavelengths. However, this approach needs more cost intensive equipment and knowledge compared to multispectral sensors.

5.5 Conclusion

Non-destructive quantification of plant traits in grassland by remote sensing on field-level enables the famer to evaluate the status quo and to make prompt farm management decisions. The present study differs from previous studies in respect of (i) using CSH based on TLS in combination with MS data for sensor fusion, (ii) extracting and including texture features based on both TLS and MS information and (iii) using multi-temporal data based on two vegetation periods of two legume-grass mixtures. The study showed that sensor fusion increased estimation model accuracy compared to separate sensor utilization and was a suitable method for estimating biomass and N fixation in two legume-grass mixtures. Sensor fusion provides a method to overcome limits of each sensor and to improve prediction model accuracy. The variable importance analysis revealed that from a large number of available parameters, texture was an important input information. Furthermore, texture features can be easily implemented to the model, as no additional sensor is required. Selection of the most suitable texture feature for biomass and NFix estimation is important for model performance and can simplify model understanding. Nevertheless, feature selection of the optimal combination of height metrics, VIs and texture feature still needs further research, as they performed differently for FM, DM and N_{Fix}.

Our approach is not yet feasible for practical farming as TLS measurements are very time consuming and need advanced technical know-how. Nevertheless, with increasing technical and digital improvements in remote sensing, sensor fusion has great potential. Future research should focus on enhanced point cloud density and implementation to a UAV-based sensor system, which includes both CSH and MS information. Furthermore, temporal resolution in order to provide a more holistic model and deeper understanding of plant traits throughout the vegetation phase are necessary, especially for heterogeneous vegetation. The applied approach offers an interesting method for improvements in precision agriculture also for large areas.

5.6 Appendix

Table 5.2: List of treatments

Treatment		Functional group	Species	Ratio (%)
Clover-grass mixture	CG	Legumes (L)	*Trifolium pratense*	30
			Trifolium hybridum	5
			Trifolium repens	5
		Grass (G)	*Lolium multiflorum*	60
Lucerne-grass mixture	LG	L	*Medicago sativa*	40
			Trifolium pratense	10
		G	*Festuca pratensis*	20
			Lolium perenne	15
			Lolium multiflorum	10
			Phleum pratense	5
Pure clover legumes	L_{CG}	L from CG mixture	*Trifolium pratense*	75
			Trifolium hybridum	12.5
			Trifolium repens	12.5
Pure lucerne and clover legumes	L_{LG}	L from LG mixture	*Medicago sativa*	80
			Trifolium pratense	20
Pure grass sward	G_{CG}	G from CG mixture	*Lolium multiflorum*	100
Pure grass sward	G_{LG}	G from LG mixture	*Festuca pratensis*	40
			Lolium perenne	30
			Lolium multiflorum	20
			Phleum pratense	10

Table 5.3: List of vegetation indices (VIs)

Name	Definition	Reference
Simple Ratio	$SR = \frac{NIR}{Red}$	(Jordan 1969)
Modified Simple Ratio	$MSR = \frac{\frac{NIR}{Red} - 1}{\sqrt{\frac{NIR}{Red}} + 1}$	(Chen 1996)
Green Chlorophyll Index	$GCI = \left(\frac{NIR}{Green}\right) - 1$	(Gitelson et al. 2005)
Difference Vegetation Index	$DVI = NIR - Red$	(Tucker 1979)
Normalized Difference Vegetation Index	$NDVI = \frac{NIR - Red}{NIR + Red}$	(Rouse et al. 1974)
Renormalized Difference Vegetation Index	$RDVI = \frac{NIR - Red}{\sqrt{NIR + Red}}$	(Roujean und Breon 1995)
Green Normalized Difference Vegetation Index	$GNDVI = \frac{NIR - Green}{NIR + Green}$	(Daughtry et al. 2000)
Normalized Difference Red Edge Index	$NDRE = \frac{NIR - RE}{NIR + RE}$	(Fitzgerald et al. 2010)
Chlorophyll Vegetation Index	$CVI = \frac{NIR}{Green} * \frac{Red}{Green}$	(Vincini et al. 2008)
Soil Adjusted Vegetation Index	$SAVI = \frac{NIR - Red}{NIR + Red + 0.5} * (1 + 0.5)$	(Huete 1988)
Modified SAVI 2	$MSAVI2 = \frac{2 * NIR + 1 - \sqrt{(2 * NIR + 1)^2 - 8 * (NIR - Red)}}{2}$	(Qi et al. 1994)
Modified Chlorophyll Absorption Index	$MCARI = [(RE - Red) - 0.2 * (RE - Green)] * \frac{RE}{Red}$	(Daughtry et al. 2000)

Table 5.4: Haralicks texture features

Texture feature	Explanation
9. Energy	Measures the local steadiness of the grey levels
10. Entropy	Measures randomness or degree of disorder
11. Correlation	Shows the linear dependency of grey level values in the GLCM
12. Inverse Difference Moment	Measures the local homogeneity
13. Inertia	Measures the local contrast or amount of variations
14. Cluster Shade	Measures skewness of the GLCM
15. Cluster Prominence	Measures the asymmetry of the GLCM
16. Haralick Correlation	Shows the probability of two pixels with similar grey level

6 General discussion

In Europe, temporary grasslands have developed to an essential crop rotation element for organic farming and serve as a source for fodder for livestock and biogas plants. Therefore, productivity in form of aboveground biomass and N fixation are important information for successful farm management in both farming systems, organic and conventional. Research in grassland monitoring for new measurement techniques is mandatory for farmers and agronomists, as traditional methods are cost intensive and time consuming, especially for large and remote areas. Vegetation monitoring at a certain moment gives information about the actual state. Only by repeating measurements through season a trac of changes is possible. Therefore, beside spatial and spectral resolution, a high temporal resolution is of great interest. Remote sensing may offer a fast and easy technique on field and farm level to achieve the above-mentioned requirements.

So far, grassland management in precision agriculture plays only a secondary role compared to other agricultural crops. Furthermore, there exist only a few studies investigating remote sensing techniques in temporary grasslands (Biewer et al. 2008; Fricke and Wachendorf 2013; Himstedt et al. 2012; Mortensen et al. 2017; Roth and Streit 2018; Viljanen et al. 2018). However, remote sensing is a rapidly growing discipline and is used in all areas of environmental research such as geography, ecology and forestry, so that these techniques can also be tested and adapted to grassland science (Schellberg and Verbruggen 2014). In this thesis, the potential of remote sensing for aboveground biomass and N_{Fix} estimation in temporary grasslands was studied and combines the findings of three studies to evaluate general usability of these techniques.

6.1 Estimation models

6.1.1 Data acquisition

In this thesis, two different methods were used to create 3D point clouds for CSH measurement. The first study used SfM based on RGB imaging captured by a UAV, while the third study used TLS. Wijesingha et al. (2018) compared these two methods in three different permanent grasslands for biomass estimation and showed, that models based on TLS performed slightly better. This can be explained by the fact, that TLS offers a much higher point cloud resolution, which can also picture individual grass tillers (Cooper et al. 2017). Additionally, the intense processing and filtering during SfM operation on the one side reduces noises, but further reduces information content (Wallace et al. 2017; Wijesingha et al. 2018).

However, TLS measurements require more time than RGB imaging by a UAV. For TLS, seven separate scans were carried out for each harvest date to scan all plots from each side. Since the tripod had to be moved manually, the measurement took a total of 2-3 h. Schulze-Brüninghoff et al. (2019) showed in an extensive managed permanent grassland, that more than two scans do not improve model accuracy. In an intensive cultivated grassland like temporary grassland, the effect of shadows is much higher and scanning penetration into lower vegetation levels is minor, than in a low yielding grassland. Future research is needed to identify the right number of scans in temporary grasslands. UAV flight missions were done at a flight height of 20 m and lasted 30 min-1 h at each harvest date including preparation and setup. This represents a considerable time saver. Due to the steady technical improvement, spatial resolution of sensors will enhance in the near future. A higher resolution can either increase model accuracy or, by a higher flight altitude, cover a wider area of interest and decrease flight time. The rapid technical progress of sensor resolution and data quality also increased for satellites, where a much greater area of interest can be captured in a very high temporal resolution (1-18 days) (Kubitza et al. 2020). However, spatial resolution still ranges between 0.25 and several meter (Ali et al. 2016). This may not be the appropriate resolution for small structured agricultural areas and small

field sizes (Ali et al. 2016; Zeng et al. 2020). As shown in this thesis a resolution of less than 2 cm for CSH and texture analysis should be achieved to increase model accuracy. Therefore, so far, the resolution and flexible utilization made possible by UAVs has been a good compromise between ground-based measurements and satellite data on field and farm level.

6.1.2 Choice of predictor variables

Plant height is a simple but effective predictor for biomass estimation. Therefore, the first study (Chapter 3) compared CSH based on SfM using RGB images (CH_D) as an alternative to the traditional manual ruler height measurement (CH_R). CH_D provided similar results compared to CH_R, even under extreme weather conditions (drought). In our study, CH_D and CH_R was both based on the mean plot value of the maximum height of all pixels or 50 measurements within the plot, respectively. Other studies like Viljanen et al. (2018) showed, that the highest correlation between plant height metric and DM was obtained by the 90^{th} percentile, whereas for Wijesingha et al. (2018) it was obtained by the 75^{th} percentile and for Borra-Serrano et al. (2019) the 50^{th} percentile. Therefore, in the third study (Chapter 5) several height metrics were used, and variable importance showed that different height metrics for each FM, DM and N_{Fix} were in the higher rank and were also different to the above mentioned. This shows that the use of one universal variable for all grassland types is not possible.

Since grassland is a mixture of different species, it presents a higher structural complexity compared to other agricultural crops. Therefore, the results of the first study implemented that plant density and spatial resolution could have a positive influence on model accuracy. Studies using plant height for biomass estimation came to the same conclusion: additional information, e.g. spectral data, is required (Fricke und Wachendorf 2013; Moeckel et al. 2017; Wijesingha et al. 2018). Therefore, the third study combined CSH and multispectral information for enhanced model accuracy. Although, sensor fusion performed better than the separate utilization of sensors, the improvement (~ 3% rRMSEP) was not as high as expected. This might be explained by the severe drought in 2018, where yield was on a rather low level. Gao et al. (2019)

showed, that spectral reflectance of an alpine grassland changed during season and the red edge region shifted to the NIR region for senescent vegetation. A hyperspectral sensor could cover a broader range of spectral bands, which would be needed to detect important wavelengths. The second study (Chapter 4) showed, that especially the red region seemed to be important for texture features.

Beside the individual bands of a spectral sensor, VIs can be calculated, for quantification and assessment of vegetation. There exist a wide range (>100) of VIs for specific plant traits, and the number and improvement is still increasing (Xue and Su 2017). The multispectral sensor used in this thesis was limited to four bands, and therefore also the choice of VIs. With a hyperspectral sensor, more VIs can be generated and tested, than the 13 used in the second and third study. Calculating texture indices as it was done by Zheng et al. (2019), gives even more opportunities. Future research should investigate ideal bands (bandwidth and -range) and VIs for grasslands at different plant growth stages.

Especially for N_{Fix} this thesis showed a first approach, as remote sensing was never successfully used before. Nevertheless, it must be taken to account, that N_{Fix} strongly correlates to the N-content of the plant, what can explain the strong relationship in the models. Due to drought through the vegetation period (second study), soil samples could not be taken during the vegetation period for a chemical analysis to use it for the extended difference method by Stülpnagel (1982). By subtracting the amount of N in the soil, the calculation of N_{Fix} can be more accurate. Similar to destructive biomass sampling, soil analysis in the laboratory is time and cost intensive. So far, promising estimates were reported by Ji et al. (2016), using visible and NIR spectroscopy in combination with a soil spectral library. First studies already tried to estimate the N-content in the soil and other soil characteristics by satellite (Forkuor et al. 2017). In general, soil qualification and quantification by spectral reflectance is difficult, as soil is very diverse in its physical, chemical and biological properties (Ge et al. 2011).

6.1.3 Model generation

Model quality depends on the available dataset and model algorithm (Chlingaryan et al. 2018). In the first study, linear regression was used for model generation, as only one predictor, mean height, was used. In the other two studies a high number of predictor variables based on height metrics, VIs and texture were created and their performance was tested. Here (multiple-) linear regression reaches its limits, since remote sensing data is characterized by a high number of input data and multicollinearity (Chlingaryan et al. 2018). Furthermore, machine learning can handle non-linear relationships (Ali et al. 2015), what was also assumed for the relationship between spectral information and biomass in the second study, by comparing random forest (RF) and partial least square (PLS) regression. For biomass RF performed better than PLS and therefore, RF was used also in the third study solely. RF is a popular machine learning algorithm (Belgiu and Drăgut 2016; Breiman 2001). Nevertheless, there exist several other machine learning algorithms like Artificial Neural Networks (ANN) (Ali et al. 2017) or Support Vector Machine (SVM) (Zhou et al. 2019), which were also found to be suitable for biomass estimation modelling.

For N_{Fix} this pattern was not clear, as the best model algorithm was PLS for both crop-specific datasets (CG and LG). In general, the difference between PLS and RF in the second study was minor also for the models including the whole dataset. This approach should be further tested for other grassland types and machine learning algorithms. One disadvantage of machine leaning algorithms is the demand for a large dataset to split the data for calibration and validation of the model (Chlingaryan et al. 2018). Furthermore, RF over and under estimates low and high datapoints, respectively (Otgonbayar et al. 2019), what can be more prominent for small sample sizes (Fassnacht et al. 2014). Crop unspecific N_{Fix} models in the second study were based on a small dataset of 48 datapoints. The third study was based on two-year data with 94 datapoints and performed only slightly better than the previous study. Nevertheless, it is necessary to pay attention on a large sample size. Multi-temporal data, like used in the third study, can serve diverse datasets including phenological and seasonal effects for more robust models. Fassnacht et al. (2014) investigated the influence of predictor variables (used sensor), machine learning algorithm and sample size on

biomass estimation accuracy of forests based on airborne LiDAR and hyperspectral data. Interestingly, the study showed that the effects of these factors were in the presented order, but the authors pointed out that this could depend on the vegetation type and nevertheless, a minimum number of datapoints is required.

The data splitting for model calibration and validation of the second and third study was done into 75% training and 25% testing dataset, where for an even distribution at least one datapoint of each year, harvest date and treatment was part of the validation. There is no clear rule for the partition ratio of data. Furthermore, both studies used a 100 times random partition repetition to avoid bias. The wide range of the results (R^2 and rRMSEP) makes clear, how important a repetition of data splitting for model accuracy is.

Variable importance showed, that for FM, DM and N_{Fix} different variables are in the higher rankings for both studies. There might be an influence by season on variable importance, which cannot be completely explained by this thesis. The next step would be to delimit the best variables by feature selection, which is a solution for a high number of predictors. The selection reduces the number of variables, which decreases processing time and simplifies estimation models, which makes them easier to interpret (Guyon and Elisseeff 2003). Meyer et al. (2018) used forward feature selection to reduce overfitting, as overfitting can lead to high rankings in variable importance. Beside the spatial autocorrelation, especially multitemporal studies suffer from temporal autocorrelation. Therefore, the authors recommend a target-oriented cross validation of datasets, which means a Leave-Location-Out (LLO), Leave-Time-Out (LTO) or the combination of both: Leave-Location-and-Time-Out (LLTO) cross validation. Nevertheless, a target-orientated validation needs a substantial number of datapoints, like is was done in the before mentioned study, based on over 30.000 air temperature measurements from 32 sites. Otherwise, the dataset is too small for robust model calibration. As mentioned in the third study, wide and detailed multi-temporal studies for temporary grassland are missing.

6.2 Future perspectives

UAV-based monitoring is already a promising low-cost method for the assessment of biodiversity, plant height, biomass, nutrient-content and disease detection (Librán-Embid et al. 2020). Especially RGB imaging is the most popular method in research (García-Berná et al. 2020) and the first study showed, that it can serve as an promising alternative to traditional methods in grassland biomass estimation. Sensor fusion would be only feasible, if the sensors would be attached on one single platform. TLS will not be part of the on the go measurement system, but a recent study of Wang et al. (2017b) using UAV-based LiDAR for canopy height measurement showed first results with an rRMSE of 14.1% (R^2 = 0.34) for grassland biomass estimation. If sensor quality (e. g. special and temporal resolution) will increase, a combination of spatial and spectral information from a lightweight UAV seems very promising. Furthermore, combining several high spatial resolution UAV measurements based on different farm sites connected to a network in combination with satellite data could be used as a reference for regional and supra-regional monitoring.

The possibility of a high fine temporal resolution provides completely new research options. So far, monitoring vegetation is “predicting in past or present times as well as in space” (Meyer et al. 2018). A measurement gives only a snapshot of the current state. A forecast would further improve future farm management decisions and can detect upcoming dynamic changes of vegetation during day, week, month and year. Li et al. (2013) showed, that weather had an impact on grass growth in time and space based on NDVI data. The inclusion of weather forecast information like precipitation and accumulated temperature could be the basis for forecasting models in agriculture and grasslands. This would give new insights and go even beyond the current state of the harvest dates and simulations could be generated for worst- and best-case scenarios. Since weather also plays an decisive role in the N cycle (Kayser et al. 2010), this information could also contribute to N_{Fix} estimation. However, N_{Fix} is completely different from biomass related parameters like LAI, N-content and plant growth considering their structural and spectral traits. As the N fixation is part of the N cycle including soil and air, the assessment is difficult due to several environmental variables

(i. g. N content in soil, soil moisture and texture). For this reason, this thesis investigated both biomass and N_{Fix} to identify future required adaptions to establish new techniques from the field of remote sensing. Inclusion of N-content of the soil could be a first step to improve model accuracy.

Famers would only use new technologies if it can be expected to get an advantage or improvement in estimation accuracy and working time. These tools must be inexpensive and easy to handle. In addition, labor costs should not exceed the cost of improving measurement accuracy, which were not gained in a study of Sanderson et al. (2001) using the manual methods capacitance meter, rising plate meter and ruler height measurement. An economic evaluation of remote sensing techniques with high estimation accuracy for grassland monitoring would be of high interest for famers. The best biomass model in this thesis was found in the second study and was based on multispectral data including texture features for the crop unspecific dataset (rRMSEP = ~10%). The studies in this thesis were based on a small-scale experimental setup, which gives first insights, but heterogeneity is much bigger and more challenging in lager areas. Future research should check the transferability to practical fields (Gao 2006), as especially edge effects weight much greater for experimental plots.

Overall, the degree of automation in the processing chain must be increased significantly to make remote sensing attractive for farmers. Angel et al. (2020) offered a new approach for automated georectification of hyperspectral data by UAV-based SfM while reducing the number of GCPs. Taravat et al. (2019) used neural network algorithms to automatically determine the optimal harvest date for grasslands. Nevertheless, specific hardware and software knowledge is necessary. As most farmers do not have the skills to use these techniques, guidelines and education are still required. Seelan et al. (2003) successfully offered a training approach to farmers within a satellite data acquisition and processing network for improved grassland management. Although UAVs can fly in autopilot, a license or a pilot is still required, which can increase the costs. The application of UAVs for farmers would benefit of an automatic flight mission (including take-off and landing) for data acquisition and with data transmission (Lippitt and Zhang 2018). Further limiting factor for a widespread practical use is the huge amount of data (images, orthomosaics, point clouds, GPS,

etc.), which need storage space and computing power for the analysis. Since one sensor cannot serve all needed information for several target variables, like biomass and N_{Fix}, at the same time, the combination for sensor fusion requires suitable spatial, temporal, radiometric and spectral resolution (Xu and Guo 2015).

Nowadays precision agriculture also covers the wider thematic field of information technology related topics all linked to remote sensing like Machine Learning, Wireless Sensor Network, Internet of Things, Cloud Computing and Data Science (Shafi et al. 2019; Triantafyllou et al. 2019) to solve the mentioned issues. Future precision agriculture in temporary grasslands could be a comprehensive approach for the whole crop rotation, which connects remote sensing techniques with new information technologies to gain quality and quantity data. This would be a step forward to sustainable intensification of temporary grassland and consequently the food demand in the world.

7 Conclusion

The aim of this thesis was to further fill the research gap of remote sensing monitoring in heterogeneous temporary grasslands. The results of this thesis revealed the challenges and diverse possibilities of UAV-based biomass and N_{Fix} estimation of two legume-grass mixtures. Three different approaches were tested in this thesis: point cloud-based CSH measurement, multispectral information and the combination in form of sensor fusion. Based on the findings, following conclusions can be drawn:

- UAV-based point clouds were suitable for high temporal monitoring for CSH measurement as an alternative for the traditional ruler height measurement to estimate aboveground biomass (Chapter 3). Even under extreme weather conditions (drought), similar results were achieved between the two CSH measurement approaches. Nevertheless, the high variability of the canopy surface requires supplementary spectral and structural information.

- Multispectral data was suitable to estimate aboveground biomass (Chapter 4). Strong relationship was found between N_{Fix} and multispectral data. Texture analysis showed promising results to further increase model accuracy without additional sensor capacity and should be integrated in future agricultural research.

- The combination of point cloud-based CSH, multispectral data and texture features offers complementary information for aboveground biomass and N_{Fix} estimation (Chapter 5). Sensor fusion in this multi-temporal study over two vegetation seasons showed higher model accuracy compared to the separate utilization of the sensors. Nevertheless, feature selection of the optimal combination of height metrics, VIs and texture feature still needs further research, as they performed differently for FM, DM and N_{Fix}.

- Remote sensing is a valuable contribution to grassland monitoring. As there exist huge differences between the different grassland types, especially

between permanent and temporal grasslands, further research in the optimal special, spectral and temporal resolution for temporary grasslands is necessary. Furthermore, multi-temporal and long-term studies over several years to cover different environmental sites and weather conditions are needed. The rapid technical development of sensors, platforms and information technology offers constant improvements in precision agriculture and grassland monitoring.

8 References

Aasen, H.; Burkart, A.; Bolten, A.; Bareth, G. (2015): Generating 3D hyperspectral information with lightweight UAV snapshot cameras for vegetation monitoring: From camera calibration to quality assurance. In: *ISPRS Journal of Photogrammetry and Remote Sensing* 108, S. 245–259.

Aasen, H.; Honkavaara, E.; Lucieer, A.; Zarco-Tejada, P. (2018): Quantitative Remote Sensing at Ultra-High Resolution with UAV Spectroscopy: A Review of Sensor Technology, Measurement Procedures, and Data Correction Workflows. In: *Remote Sens* 10 (7), S. 1091.

Ali, I.; Cawkwell, F.; Dwyer, E.; Barrett, B.; Green, S. (2016): Satellite remote sensing of grasslands: from observation to management. In: *JPECOL* 9 (6), S. 649–671. DOI: 10.1093/jpe/rtw005.

Ali, I.; Cawkwell, F.; Dwyer, E.; Green, S. (2017): Modeling Managed Grassland Biomass Estimation by Using Multitemporal Remote Sensing Data—A Machine Learning Approach. In: *IEEE J Sel Top Appl Earth Obs Remote Sens* 10 (7), S. 3254–3264.

Ali, I.; Greifeneder, F.; Stamenkovic, J.; Neumann, M.; Notarnicola, C. (2015): Review of Machine Learning Approaches for Biomass and Soil Moisture Retrievals from Remote Sensing Data. In: *Remote Sensing* 7 (12), S. 16398–16421. DOI: 10.3390/rs71215841.

Allen, V. G.; Batello, C.; Berretta, E. J.; Hodgson, J.; Kothmann, M.; Li, X. et al. (2011): An international terminology for grazing lands and grazing animals. In: *Grass and Forage Science* 66 (1), S. 2–28. DOI: 10.1111/j.1365-2494.2010.00780.x.

Anderson, K. E.; Glenn, N. F.; Spaete, L. P.; Shinneman, D. J.; Pilliod, D. S.; Arkle, R. S. et al. (2018): Estimating vegetation biomass and cover across large plots in

shrub and grass dominated drylands using terrestrial lidar and machine learning. In: *Ecological Indicators* 84, S. 793–802.

Angel, Y.; Turner, D.; Parkes, S.; Malbeteau, Y.; Lucieer, A.; McCabe, M. F. (2020): Automated Georectification and Mosaicking of UAV-Based Hyperspectral Imagery from Push-Broom Sensors. In: *Remote Sensing* 12 (1), S. 34. DOI: 10.3390/rs12010034.

Askari, M. S.; McCarthy, T.; Magee, A.; Murphy, D. J. (2019): Evaluation of Grass Quality under Different Soil Management Scenarios Using Remote Sensing Techniques. In: *Remote Sens* 11 (15), S. 1835.

Assmann, J. J.; Kerby, J. T.; Cunliffe, A. M.; Myers-Smith, I. H. (2019): Vegetation monitoring using multispectral sensors — best practices and lessons learned from high latitudes. In: *J. Unmanned Veh. Sys.* 7 (1), S. 54–75.

Auernhammer, H. (2001): Precision farming — the environmental challenge. In: *Computers and Electronics in Agriculture* 30, S. 31–43.

Bareth, G.; Schellberg, J. (2018): Replacing Manual Rising Plate Meter Measurements with Low-cost UAV-Derived Sward Height Data in Grasslands for Spatial Monitoring. In: *PFG* 86 (3-4), S. 157–168.

Barrett, B.; Nitze, I.; Green, S.; Cawkwell, F. (2014): Assessment of multi-temporal, multi-sensor radar and ancillary spatial data for grasslands monitoring in Ireland using machine learning approaches. In: *Remote Sens Environ* 152, S. 109–124.

Belgiu, M.; Drăguţ, L. (2016): Random forest in remote sensing: A review of applications and future directions. In: *ISPRS J Photogramm Remote Sens* 114, S. 24–31.

Bellis, L. M.; Pidgeon, A. M.; Radeloff, V. C.; St.-Louis, V.; Navarro, J. L.; Martella, M. B. (2008): Modeling Habitat Suitability for greater Rheas Based on Satellite Image Texture. In: *Ecol Appl* 18 (8), S. 1956–1966.

Bendig, J.; Bolten, A.; Bennertz, S.; Broscheit, J.; Eichfuss, S.; Bareth, G. (2014): Estimating Biomass of Barley Using Crop Surface Models (CSMs) Derived from UAV-Based RGB Imaging. In: *Remote Sensing* 6 (11), S. 10395–10412.

Bendig, J.; Yu, K.; Aasen, H.; Bolten, A.; Bennertz, S.; Broscheit, J. et al. (2015): Combining UAV-based plant height from crop surface models, visible, and near infrared vegetation indices for biomass monitoring in barley. In: *Int J Appl Earth Obs Geoinf* 39, S. 79–87.

Bengtsson, J.; Bullock, J. M.; Egoh, B.; Everson, C.; Everson, T.; O'Connor, T. et al. (2019): Grasslands-more important for ecosystem services than you might think. In: *Ecosphere* 10 (2), e02582. DOI: 10.1002/ecs2.2582.

Berry, P. M.; Sylvester-Bradley, R.; Philipps, L.; Hatch, D. J.; Cuttle, S. P.; Rayns, F. W.; Gosling, P. (2002): Is the productivity of organic farms restricted by the supply of available nitrogen? In: *Soil Use Manag* 18, S. 248–255.

Bhakta, I.; Phadikar, S.; Majumder, K. (2019): State-of-the-art technologies in precision agriculture: a systematic review. In: *Journal of the science of food and agriculture* 99 (11), S. 4878–4888. DOI: 10.1002/jsfa.9693.

Biewer, S.; Erasmi, S.; Fricke, T.; Wachendorf, M. (2008): Prediction of yield and the contribution of legumes in legume-grass mixtures using field spectrometry. In: *Precision Agric* 10 (2), S. 128–144.

Biewer, S.; Fricke, T.; Wachendorf, M. (2009): Determination of Dry Matter Yield from Legume–Grass Swards by Field Spectroscopy. In: *Crop Science* 49 (5), S. 1927–1936.

Boller, B. C.; Nösberger, J. (1987): Symbiotically fixed nitrogen from field- grown white and red clover mixed with ryegrasses at low levels of15N-fertilization. In: *Plant Soil* 104 (2), S. 219–226.

Borra-Serrano, I.; Swaef, T. d.; Muylle, H.; Nuyttens, D.; Vangeyte, J.; Mertens, K. et al. (2019): Canopy height measurements and non-destructive biomass

estimation of Lolium perenne swards using UAV imagery. In: *Grass Forage Sci* 10, S. 233.

Boyd, D. S.; Foody, G. M. (2011): An overview of recent remote sensing and GIS based research in ecological informatics. In: *Ecological Informatics* 6 (1), S. 25–36. DOI: 10.1016/j.ecoinf.2010.07.007.

Breiman, L. (2001): Random Forests. In: *Mach Learn* 45, S. 5–32.

Bueren, S. K. von; Burkart, A.; Hueni, A.; Rascher, U.; Tuohy, M. P.; Yule, I. J. (2015): Deploying four optical UAV-based sensors over grassland. Challenges and limitations. In: *Biogeosciences* 12 (1), S. 163–175.

Campbell, N. A.; Arnold, G. W. (1973): The visual assessment of pasture yield. In: *Australian Journal of Experimental Agriculture* 13 (62).

Capolupo, A.; Kooistra, L.; Berendonk, C.; Boccia, L.; Suomalainen, J. (2015): Estimating Plant Traits of Grasslands from UAV-Acquired Hyperspectral Images: A Comparison of Statistical Approaches. In: *IJGI* 4 (4), S. 2792–2820.

Carlson, T. N.; Ripley, D. A. (1997): On the Relation between NDVI, Fractional Vegetation Cover, and Leaf Area Index. In: *Remote Sensing of Environment* 62, S. 241–252.

Carlsson, G.; Huss-Danell, K. (2003): Nitrogen fixation in perennial forage legumes in the field. In: *Plant Soil* 253, S. 353–372.

Catchpole, E. R.; Wheeler, C. J. (1992): Estimating plant biomass: A review of techniques. In: *Australian Journal of Ecology* (17), S. 121–131, zuletzt geprüft am 25.10.2018.

Chen, J. M. (1996): Evaluation of Vegetation Indices and a Modified Simple Ratio for Boreal Applications. In: *Canadian Journal of Remote Sensing* 22 (3), S. 229–242.

Chlingaryan, A.; Sukkarieh, S.; Whelan, B. (2018): Machine learning approaches for crop yield prediction and nitrogen status estimation in precision agriculture: A review. In: *Computers and Electronics in Agriculture* 151, S. 61–69.

Cho, M. A.; Skidmore, A.; Corsi, F.; van Wieren, S. E.; Sobhan, I. (2007): Estimation of green grass/herb biomass from airborne hyperspectral imagery using spectral indices and partial least squares regression. In: *Int J Appl Earth Obs Geoinf* 9 (4), S. 414–424.

Coburn, C. A.; Roberts, A. C. B. (2004): A multiscale texture analysis procedure for improved forest stand classification. In: *Int J Remote Sens* 25 (20), S. 4287–4308.

Cohen, W. B.; Maiersperger, T. K.; Gower, S. T.; Turner, D. P. (2003): An improved strategy for regression of biophysical variables and Landsat ETM+ data. In: *Remote Sensing of Environment* 84 (4), S. 561–571.

Cooper, Sam; Roy, D.; Schaaf, C.; Paynter, I. (2017): Examination of the Potential of Terrestrial Laser Scanning and Structure-from-Motion Photogrammetry for Rapid Nondestructive Field Measurement of Grass Biomass. In: *Remote Sensing* 9 (6), S. 531.

Critchley, C.; Nigel, R.; Poulton, S. M. C. (1998): A method to optimize precision and scale in grassland monitoring. In: *Journal of Vegetation Science* 9, S. 837–846.

Crookston, R. K. (2006): A Top 10 List of Developments and Issues Impacting Crop Management and Ecology During the Past 50 Years. In: *Crop Sci.* 46 (5), S. 2253–2262. DOI: 10.2135/cropsci2005.11.0416gas.

Cudlín, O.; Hakl, J.; Hejcman, M.; Cudlín, P. (2018): The use of compressed height to estimate the yield of a differently fertilized meadow. In: *Plant Soil Environ.* 64 (No. 2), S. 76–81.

Culbert, P. D.; Pidgeon, A. M.; St.-Louis, V.; Bash, D.; Radeloff, V. C. (2009): The Impact of Phenological Variation on Texture Measures of Remotely Sensed Imagery. In: *IEEE J Sel Top Appl Earth Obs Remote Sens* 2 (4), S. 299–309.

Cunliffe, A. M.; Brazier, R. E.; Anderson, K. (2016): Ultra-fine grain landscape-scale quantification of dryland vegetation structure with drone-acquired structure-from-motion photogrammetry. In: *Remote Sensing of Environment* 183, S. 129–143.

Darvishzadeh, R.; Skidmore, A.; Schlerf, M.; Atzberger, C.; Corsi, F.; Cho, M. (2008): LAI and chlorophyll estimation for a heterogeneous grassland using hyperspectral measurements. In: *ISPRS Journal of Photogrammetry and Remote Sensing* 63 (4), S. 409–426. DOI: 10.1016/j.isprsjprs.2008.01.001.

Daughtry, C. S. T.; Walthall, C. L.; Kim, M. S.; Brown de Colstoun, E.; McMurtrey, J. E. (2000): Estimating Corn Leaf Chlorophyll Concentration from Leaf and Canopy Reflectance. In: *Remote Sens Environ* 74, S. 229–239.

Dittmann, S.; Thiessen, E.; Hartung, E. (2017): Applicability of different non-invasive methods for tree mass estimation: A review. In: *Forest Ecology and Management* 398, S. 208–215.

Dixon, A. P.; Faber-Langendoen, D.; Josse, C.; Morrison, J.; Loucks, C. J. (2014): Distribution mapping of world grassland types. In: *J. Biogeogr.* 41 (11), S. 2003–2019. DOI: 10.1111/jbi.12381.

Elgersma, A.; Søegaard, K. (2018): Changes in nutritive value and herbage yield during extended growth intervals in grass-legume mixtures. Effects of species, maturity at harvest, and relationships between productivity and components of feed quality. In: *Grass Forage Sci* 73 (1), S. 78–93.

Ergon, Å.; Kirwan, L.; Bleken, M. A.; Skjelvåg, A. O.; Collins, R. P.; Rognli, O. A. (2016): Species interactions in a grassland mixture under low nitrogen fertilization and two cutting frequencies. 1. dry-matter yield and dynamics of species composition. In: *Grass Forage Sci* 71 (4), S. 667–682.

Eriksen, J.; Pedersen, L.; Jørgensen, J. R. (2006): Nitrate leaching and bread-making quality of spring wheat following cultivation of different grasslands. In: *Agric Ecosyst Environ* 116 (3-4), S. 165–175.

Fan, L.; Gao, Y.; Brück, H.; Bernhofer, Ch. (2009): Investigating the relationship between NDVI and LAI in semi-arid grassland in Inner Mongolia using in-situ measurements. In: *Theor Appl Climatol* 95 (1-2), S. 151–156. DOI: 10.1007/s00704-007-0369-2.

Fassnacht, F. E.; Hartig, F.; Latifi, H.; Berger, C.; Hernández, J.; Corvalán, P.; Koch, B. (2014): Importance of sample size, data type and prediction method for remote sensing-based estimations of aboveground forest biomass. In: *Remote Sensing of Environment* 154, S. 102–114. DOI: 10.1016/j.rse.2014.07.028.

Fitzgerald, G.; Rodriguez, D.; O'Leary, G. (2010): Measuring and predicting canopy nitrogen nutrition in wheat using a spectral index—The canopy chlorophyll content index (CCCI). In: *Field Crops Res* 116 (3), S. 318–324.

Forkuor, G.; Hounkpatin, O. K. L.; Welp, G.; Thiel, M. (2017): High Resolution Mapping of Soil Properties Using Remote Sensing Variables in South-Western Burkina Faso: A Comparison of Machine Learning and Multiple Linear Regression Models. In: *PloS one* 12 (1), e0170478. DOI: 10.1371/journal.pone.0170478.

Forsmoo, J.; Anderson, K.; Macleod, C. J. A.; Wilkinson, M. E.; Brazier, R.; Smit, I. (2018): Drone-based structure-from-motion photogrammetry captures grassland sward height variability. In: *J Appl Ecol* 94, S. 237.

Fricke, T.; Richter, F.; Wachendorf, M. (2011): Assessment of forage mass from grassland swards by height measurement using an ultrasonic sensor. In: *Computers and Electronics in Agriculture* 79 (2), S. 142–152. DOI: 10.1016/j.compag.2011.09.005.

Fricke, T.; Wachendorf, M. (2013): Combining ultrasonic sward height and spectral signatures to assess the biomass of legume–grass swards. In: *Computers and Electronics in Agriculture* 99, S. 236–247.

Fustec, J.; Lesuffleur, F.; Mahieu, S.; Cliquet, J.-B. (2010): Nitrogen rhizodeposition of legumes. A review. In: *Agron Sustain Dev* 30 (1), S. 57–66.

Gallardo-Cruz, J. A.; Meave, J. A.; González, E. J.; Lebrija-Trejos, E. E.; Romero-Romero, M. A.; Pérez-García, E. A. et al. (2012): Predicting tropical dry forest successional attributes from space: is the key hidden in image texture? In: *PloS one* 7 (2), e30506.

Galloway, J. N.; Schlesinger, W. H.; Levy II, H.; Michaels, A.; Schnoor, J. L. (1995): Nitrogen fixation: Anthropogenic enhancement-environmental response. In: *Global Biogeochemical Cycles* 9 (2), S. 235–252.

Gao, J. (2006): Quantification of grassland properties: how it can benefit from geoinformatic technologies? In: *International Journal of Remote Sensing* 27 (7), S. 1351–1365. DOI: 10.1080/01431160500474357.

Gao, J.; Liang, T.; Yin, J.; Ge, J.; Feng, Q.; Wu, C. et al. (2019): Estimation of Alpine Grassland Forage Nitrogen Coupled with Hyperspectral Characteristics during Different Growth Periods on the Tibetan Plateau. In: *Remote Sensing* 11 (18), S. 2085. DOI: 10.3390/rs11182085.

García-Berná, J. A.; Ouhbi, S.; Benmouna, B.; García-Mateos, G.; Fernández-Alemán, J. L.; Molina-Martínez, J. M. (2020): Systematic Mapping Study on Remote Sensing in Agriculture. In: *Applied Sciences* 10 (10), S. 3456. DOI: 10.3390/app10103456.

Ge, Y.; Thomasson, J. A.; Sui, R. (2011): Remote sensing of soil properties in precision agriculture: A review. In: *Front. Earth Sci.* 33 (2), S. 149. DOI: 10.1007/s11707-011-0175-0.

Gebhardt, S.; Kühbauch, W. (2007): A new algorithm for automatic Rumex obtusifolius detection in digital images using colour and texture features and the influence of image resolution. In: *Precision Agric* 8 (1-2), S. 1–13, zuletzt geprüft am 24.09.2019.

Gebremedhin, A.; Badenhorst, P.; Wang, J.; Giri, K.; Spangenberg, G.; Smith, K. (2019): Development and Validation of a Model to Combine NDVI and Plant

Height for High-Throughput Phenotyping of Herbage Yield in a Perennial Ryegrass Breeding Program. In: *Remote Sensing* 11 (21), S. 2494.

Geipel, J.; Link, J.; Claupein, W. (2014): Combined Spectral and Spatial Modeling of Corn Yield Based on Aerial Images and Crop Surface Models Acquired with an Unmanned Aircraft System. In: *Remote Sensing* 6 (11), S. 10335–10355.

Geladi, P.; Kowalski, B. R. (1986): Partial Least-Square Regression: A Toutorial. In: *Analytica Chimica Acta* 185, S. 1–17.

Gierus, M.; Kleen, J.; Loges, R.; Taube, F. (2012): Forage legume species determine the nutritional quality of binary mixtures with perennial ryegrass in the first production year. In: *Animal Feed Science and Technology* 172 (3-4), S. 150–161.

Gillan, J. K.; Karl, J. W.; Duniway, M.; Elaksher, A. (2014): Modeling vegetation heights from high resolution stereo aerial photography. An application for broad-scale rangeland monitoring. In: *Journal of environmental management* 144, S. 226–235.

Gitelson, A. A.; Vina, A.; Ciganda, V.; Rundquist, D. C.; Arkebauer, T. J. (2005): Remote estimation of canopy chlorophyll content in crops. In: *Geophys Res Lett* 32 (8), S. 1–4.

Green, K.; Kempka, D.; Lackey, L. (1994): Using Remote Sensing to Detect and Monitor Land-Cover and Land-Use Change. In: *Photogrammetic Engineering & Remote Sensing* 60, S. 331–337.

Grenzdörffer, G. J. (2014): Crop height determination with UAS point clouds. In: *Int. Arch. Photogramm. Remote Sens. Spatial Inf. Sci.* XL-1, S. 135–140.

Grizonnet, M.; Michel, J.; Poughon, V.; Inglada, J.; Savinaud, M.; Cresson, R. (2017): Orfeo ToolBox: open source processing of remote sensing images. In: *Open geospatial data, softw. stand.* 2 (1), S. 993.

Grüner, E.; Astor, T.; Wachendorf, M. (2019): Biomass Prediction of Heterogeneous Temperate Grasslands Using an SfM Approach Based on UAV Imaging. In: *Agronomy* 9 (2), S. 54.

Grüner, E.; Wachendorf, M.; Astor, T. (2020): The potential of UAV-borne spectral and textural information for predicting aboveground biomass and N fixation in legume-grass mixtures. In: *PLoS ONE* 15 (6), e0234703. DOI: 10.1371/journal.pone.0234703.

Guo, X.; Wilmshurst, J.; McCanny, S.; Fargey, P.; Richard, P. (2004): Measuring Spatial and Vertical Heterogeneity of Grasslands Using Remote Sensing Techniques. In: *Journal of Environmental Informatics* 3 (1), S. 24–32.

Guyon, I.; Elisseeff, A. (2003): An Introduction to Variable and Feature Selection. In: *Journal of Machine Leraning Research* 3, S. 1157–1182.

Hakl, J.; Hrevušová, Z.; Hejcman, M.; Fuksa, P. (2012): The use of a rising plate meter to evaluate lucerne (Medicago sativa L.) height as an important agronomic trait enabling yield estimation. In: *Grass Forage Sci* 67 (4), S. 589–596.

Haralick, R.; Shanmugam, K.; Dinstein, I. (1973): Textural Features for Image Classification. In: *IEEE Trans Syst Man Cybern* 3 (6), S. 610–621.

Harmoney, K. R.; Moore, K. J.; George, J. R.; Brummer, E. C.; Russell, J. R. (1997): Determination of Pasture Biomass Using Four Indirect Methods. In: *Agronomy Journal* 89 (4), S. 665.

He, Y.; Guo, X.; Wilmshurst, J. (2006): Studying mixed grassland ecosystems I: suitable hyperspectral vegetation indices. In: *Can J Remote Sensing* 32 (2), S. 98–107.

Heady, H. F. (1957): The Measurement and Value of Plant Height in the Study of Herbaceous Vegetation. In: *Ecology* 38 (2), S. 313–320.

Himstedt, M.; Fricke, T.; Wachendorf, M. (2012): The Benefit of Color Information in Digital Image Analysis for the Estimation of Legume Contribution in Legume–Grass Mixtures. In: *Crop Science* 52 (2), S. 943–950.

Høgh-Jensen, H.; Loges, R.; Jørgensen, F. V.; Vinther, F. P.; Jensen, E. S. (2004): An empirical model for quantification of symbiotic nitrogen fixation in grass-clover mixtures. In: *Agric Syst* 82 (2), S. 181–194.

Holman, F.; Riche, A.; Michalski, A.; Castle, M.; Wooster, M.; Hawkesford, M. (2016): High Throughput Field Phenotyping of Wheat Plant Height and Growth Rate in Field Plot Trials Using UAV Based Remote Sensing. In: *Remote Sensing* 8 (12), S. 1031.

Huete, A. R.; Jackson, R. D.; Post. D. F. (1985): Spectral Response of a Plant Canopy with Different Soil Backgrounds. In: *Remote Sens Environ* 17, S. 37–53.

Huete, A.R (1988): A soil-adjusted vegetation index (SAVI). In: *Remote Sens Environ* 25 (3), S. 295–309.

Jackson, R. D.; Huete, A. R. (1991): Interpreting vegetation indices. In: *Prev Vet Med* 11, S. 185–200.

Jay, S.; Rabatel, G.; Hadoux, X.; Moura, D.; Gorretta, N. (2015): In-field crop row phenotyping from 3D modeling performed using Structure from Motion. In: *Computers and Electronics in Agriculture* 110, S. 70–77.

Ji, W.; Li, S.; Chen, S.; Shi, Z.; Viscarra Rossel, R. A.; Mouazen, A. M. (2016): Prediction of soil attributes using the Chinese soil spectral library and standardized spectra recorded at field conditions. In: *Soil and Tillage Research* 155, S. 492–500. DOI: 10.1016/j.still.2015.06.004.

Jordan, C. F. (1969): Derivation of Leaf-Area Index from Quality of Light on the Forest Floor. In: *Ecology* 50 (4), S. 663–666.

Kaufman, Y. J.; Tanre, D.; Holben, B. N.; Markham, B.; Gitelson, A. (1992): Atmospheric Effects on the Ndvi - Strategies for its Removal. In: *Geoscience and Remote Sensing Symposium*, S. 1238–1241.

Kayser, M.; Müller, J.; Isselstein, J. (2010): Nitrogen management in organic farming: comparison of crop rotation residual effects on yields, N leaching and soil conditions. In: *Nutr Cycl Agroecosyst* 87 (1), S. 21–31. DOI: 10.1007/s10705-009-9309-0.

Kearney, J. (2010): Food consumption trends and drivers. In: *Philosophical transactions of the Royal Society of London. Series B, Biological sciences* 365 (1554), S. 2793–2807. DOI: 10.1098/rstb.2010.0149.

Knoblauch, C.; Watson, C.; Berendonk, C.; Becker, R.; Wrage-Mönnig, N.; Wichern, F. (2017): Relationship between Remote Sensing Data, Plant Biomass and Soil Nitrogen Dynamics in Intensively Managed Grasslands under Controlled Conditions. In: *Sensors* 17 (7).

Köpke, U. (1995): Nutrient Management in Organic Farming Systems: the Case of Nitrogen. In: *Biological Agriculture & Horticulture* 11 (1-4), S. 15–29.

Kubitza, C.; Krishna, V. V.; Schulthess, U.; Jain, M. (2020): Estimating adoption and impacts of agricultural management practices in developing countries using satellite data. A scoping review. In: *Agron. Sustain. Dev.* 40 (3), S. 127. DOI: 10.1007/s13593-020-0610-2.

Kuhn, M. (2008): Building Predictive Models in R Using the caret Package. In: *J Stat Softw* 28 (5), S. 1–26.

Künnemeyer, R.; Schaare, P. N.; Hanna, M. M. (2001): A simple reflectometer for on-farm pasture assessment. In: *Computers and Electronics in Agriculture* 31 (2), S. 125–136.

Kuo, S.; Jellum, E. J. (2002): Cropping systems. Influence of Winter Cover Crop and Residue Management on Soil Nitrogen Availability and Corn. In: *Agronomy Journal* 94, S. 501–508.

Kupidura, P. (2019): The Comparison of Different Methods of Texture Analysis for Their Efficacy for Land Use Classification in Satellite Imagery. In: *Remote Sens* 11 (10), S. 1233.

Kusumo, B. H.; Hedley, M. J.; Hedley, C. B.; Tuohy, M. P. (2011): Measuring carbon dynamics in field soils using soil spectral reflectance: prediction of maize root density, soil organic carbon and nitrogen content. In: *Plant Soil* 338 (1-2), S. 233–245.

Kyere, I.; Astor, T.; Graß, R.; Wachendorf, M. (2019): Multi-Temporal Agricultural Land-Cover Mapping Using Single-Year and Multi-Year Models Based on Landsat Imagery and IACS Data. In: *Agronomy* 9 (6), S. 309.

Laliberte, A. S.; Goforth, M. A.; Steele, C. M.; Rango, A. (2011): Multispectral Remote Sensing from Unmanned Aircraft: Image Processing Workflows and Applications for Rangeland Environments. In: *Remote Sensing* 3 (11), S. 2529–2551. DOI: 10.3390/rs3112529.

Laliberte, A. S.; Rango, A. (2009): Texture and Scale in Object-Based Analysis of Subdecimeter Resolution Unmanned Aerial Vehicle (UAV) Imagery. In: *IEEE Trans Geosci Remote Sens* 47 (3), S. 761–770.

Lati, R. N.; Filin, S.; Eizenberg, H. (2013): Estimating plant growth parameters using an energy minimization-based stereovision model. In: *Computers and Electronics in Agriculture* 98, S. 260–271.

Ledgard, S. F.; Steele, K. W. (1992): Biological nitrogen fixation in mixed legume/grass pastures. In: *Plant Soil* 141, S. 137–153.

Lesschen, J. P.; van den Berg, M.; Westhoek, H. J.; Witzke, H. P.; Oenema, O. (2011): Greenhouse gas emission profiles of European livestock sectors. In: *Animal Feed Science and Technology* 166-167, S. 16–28. DOI: 10.1016/j.anifeedsci.2011.04.058.

Li, S.; Yuan, F.; Ata-UI-Karim, S. T.; Zheng, H.; Cheng, T.; Liu, X. et al. (2019): Combining Color Indices and Textures of UAV-Based Digital Imagery for Rice LAI Estimation. In: *Remote Sens* 11 (15), S. 1763.

Li, W.; Niu, Z.; Chen, H.; Li, D.; Wu, M.; Zhao, W. (2016): Remote estimation of canopy height and aboveground biomass of maize using high-resolution stereo images from a low-cost unmanned aerial vehicle system. In: *Ecological Indicators* 67, S. 637–648.

Li, Z.; Huffman, T.; McConkey, B.; Townley-Smith, L. (2013): Monitoring and modeling spatial and temporal patterns of grassland dynamics using time-series MODIS NDVI with climate and stocking data. In: *Remote Sensing of Environment* 138, S. 232–244. DOI: 10.1016/j.rse.2013.07.020.

Liaw, A.; Wiener, M. (2002): Classification and Regression by randomForest. In: *R News* 2 (3), S. 18–22.

Librán-Embid, F.; Klaus, F.; Tscharntke, T.; Grass, I. (2020): Unmanned aerial vehicles for biodiversity-friendly agricultural landscapes - A systematic review. In: *The Science of the total environment* 732, S. 139204. DOI: 10.1016/j.scitotenv.2020.139204.

Lippitt, C. D.; Zhang, S. (2018): The impact of small unmanned airborne platforms on passive optical remote sensing: a conceptual perspective. In: *International Journal of Remote Sensing* 39 (15-16), S. 4852–4868. DOI: 10.1080/01431161.2018.1490504.

Lu, D. (2005): Aboveground biomass estimation using Landsat TM data in the Brazilian Amazon. In: *Int J Remote Sens* 26 (12), S. 2509–2525.

Lu, D. (2006): The potential and challenge of remote sensing-based biomass estimation. In: *International Journal of Remote Sensing* 27 (7), S. 1297–1328.

Lussem, U.; Bolten, A.; Menne, J.; Gnyp, M. L.; Schellberg, J.; Bareth, G. (2019): Estimating biomass in temperate grassland with high resolution canopy surface

models from UAV-based RGB images and vegetation indices. In: *J. Appl. Rem. Sens.* 13 (03), S. 1.

Madec, S.; Baret, F.; Solan, B. de; Thomas, S.; Dutartre, D.; Jezequel, S. et al. (2017): High-Throughput Phenotyping of Plant Height: Comparing Unmanned Aerial Vehicles and Ground LiDAR Estimates. In: *Frontiers in plant science* 8, S. 2002.

Malambo, L.; Popescu, S. C.; Murray, S. C.; Putman, E.; Pugh, N. A.; Horne, D. W. et al. (2018): Multitemporal field-based plant height estimation using 3D point clouds generated from small unmanned aerial systems high-resolution imagery. In: *International Journal of Applied Earth Observation and Geoinformation* 64, S. 31–42.

McKendry, P. (2002): Energy production from biomass (part 1): overview of biomass. In: *Bioresouce Technology* 83, S. 37–46, zuletzt geprüft am 07.05.2020.

Melander, B.; Rasmussen, I. A.; Olesen, J. E. (2016): Incompatibility between fertility building measures and the management of perennial weeds in organic cropping systems. In: *Agric Ecosyst Environ* 220, S. 184–192.

Meyer, H.; Reudenbach, C.; Hengl, T.; Katurji, M.; Nauss, T. (2018): Improving performance of spatio-temporal machine learning models using forward feature selection and target-oriented validation. In: *Environmental Modelling & Software* 101, S. 1–9.

Moeckel, T.; Dayananda, S.; Nidamanuri, R.; Nautiyal, S.; Hanumaiah, N.; Buerkert, A.; Wachendorf, M. (2018): Estimation of Vegetable Crop Parameter by Multi-temporal UAV-Borne Images. In: *Remote Sensing* 10 (5), S. 805.

Moeckel, T.; Safari, H.; Reddersen, B.; Fricke, T.; Wachendorf, M. (2017): Fusion of Ultrasonic and Spectral Sensor Data for Improving the Estimation of Biomass in Grasslands with Heterogeneous Sward Structure. In: *Remote Sensing* 9 (1), S. 98.

Möller, K.; Stinner, W.; Leithold, G. (2008): Growth, composition, biological N2 fixation and nutrient uptake of a leguminous cover crop mixture and the effect of their removal on field nitrogen balances and nitrate leaching risk. In: *Nutr Cycl Agroecosyst* 82 (3), S. 233–249.

Morin, D.; Planells, M.; Guyon, D.; Villard, L.; Mermoz, S.; Bouvet, A. et al. (2019): Estimation and Mapping of Forest Structure Parameters from Open Access Satellite Images: Development of a Generic Method with a Study Case on Coniferous Plantation. In: *Remote Sens* 11 (11), S. 1275.

Mortensen, A.; Karstoft, H.; Søegaard, K.; Gislum, R.; Jørgensen, R. (2017): Preliminary Results of Clover and Grass Coverage and Total Dry Matter Estimation in Clover-Grass Crops Using Image Analysis. In: *J. Imaging* 3 (4), S. 59.

Mulla, D. J. (2013): Twenty five years of remote sensing in precision agriculture. Key advances and remaining knowledge gaps. In: *Biosystems Engineering* 114 (4), S. 358–371.

Mutanga, O.; Skidmore, A. K. (2004): Hyperspectral band depth analysis for a better estimation of grass biomass (Cenchrus ciliaris) measured under controlled laboratory conditions. In: *International Journal of Applied Earth Observation and Geoinformation* 5 (2), S. 87–96. DOI: 10.1016/j.jag.2004.01.001.

Näsi, R.; Viljanen, N.; Kaivosoja, J.; Alhonoja, K.; Hakala, T.; Markelin, L.; Honkavaara, E. (2018): Estimating Biomass and Nitrogen Amount of Barley and Grass Using UAV and Aircraft Based Spectral and Photogrammetric 3D Features. In: *Remote Sensing* 10 (7), S. 1082.

Nyfeler, D.; Huguenin-Elie, O.; Suter, M.; Frossard, E.; Lüscher, A. (2011): Grass–legume mixtures can yield more nitrogen than legume pure stands due to mutual stimulation of nitrogen uptake from symbiotic and non-symbiotic sources. In: *Agric Ecosyst Environ* 140 (1-2), S. 155–163.

Oenema, O.; Klein, C. de; Alfaro, M. (2014): Intensification of grassland and forage use: driving forces and constraints. In: *Crop Pasture Sci.* 65 (6), S. 524. DOI: 10.1071/CP14001.

Olesen, J. E.; Askegaard, M.; Rasmussen, I. A. (2009): Winter cereal yields as affected by animal manure and green manure in organic arable farming. In: *European Journal of Agronomy* 30 (2), S. 119–128. DOI: 10.1016/j.eja.2008.08.002.

Ollinger, S. V. (2011): Sources of variability in canopy reflectance and the convergent properties of plants. In: *The New phytologist* 189 (2), S. 375–394.

O'Mara, F. P. (2012): The role of grasslands in food security and climate change. In: *Annals of botany* 110 (6), S. 1263–1270. DOI: 10.1093/aob/mcs209.

Otgonbayar, M.; Atzberger, C.; Chambers, J.; Damdinsuren, A. (2019): Mapping pasture biomass in Mongolia using Partial Least Squares, Random Forest regression and Landsat 8 imagery. In: *International Journal of Remote Sensing* 40 (8), S. 3204–3226. DOI: 10.1080/01431161.2018.1541110.

Peeters, A. (2009): Importance, evolution, environmental impact and future challenges of grasslands and grassland-based systems in Europe. In: *Grassland Science* 55 (3), S. 113–125. DOI: 10.1111/j.1744-697X.2009.00154.x.

Peterson, D. L.; Price, K. P.; Martinko, E. A. (2002): Discriminating between cool season and warm season grassland cover types in northeastern Kansas. In: *International Journal of Remote Sensing* 23 (23), S. 5015–5030. DOI: 10.1080/01431160210142833.

Possoch, M.; Bieker, S.; Hoffmeister, D.; Bolten, A.; Schellberg, J.; Bareth, G. (2016): Multi-Temporal Crop Surface Models combined with the RGB Vegetation Index from UAV-based Images for Forage Monitoring in Grassland. In: *Int. Arch. Photogramm. Remote Sens. Spatial Inf. Sci.* XLI-B1, S. 991–998.

Probst, P.; Wright, M.; Boulesteix, A.-L. (2018): Hyperparameters and Tuning Strategies for Random Forest. In: *WIREs Data Mining Knowl Discov* 9 (3), S. 281. DOI: 10.1002/widm.1301.

Psomas, A.; Kneubühler, M.; Huber, S.; Itten, K.; Zimmermann, N. E. (2011): Hyperspectral remote sensing for estimating aboveground biomass and for exploring species richness patterns of grassland habitats. In: *Int J Remote Sens* 32 (24), S. 9007–9031.

Qi, J.; Chehbouni, A.; Huete, A. R.; Kerr, Y. H.; Sorooshian, S. (1994): A Modified Soil Adjusted Vegetation Index. In: *Remote Sens Environ* 48, S. 119–126.

Rasmussen, J.; Ntakos, G.; Nielsen, J.; Svensgaard, J.; Poulsen, R. N.; Christensen, S. (2016): Are vegetation indices derived from consumer-grade cameras mounted on UAVs sufficiently reliable for assessing experimental plots? In: *Eur J Agron* 74, S. 75–92.

Rasmussen, J.; Søegaard, K.; Pirhofer-Walzl, K.; Eriksen, J. (2012): N2-fixation and residual N effect of four legume species and four companion grass species. In: *Eur J Agron* 36 (1), S. 66–74.

Reay, D. S.; Davidson, E. A.; Smith, K. A.; Smith, P.; Melillo, J. M.; Dentener, F.; Crutzen, P. J. (2012): Global agriculture and nitrous oxide emissions. In: *Nature Clim Change* 2 (6), S. 410–416.

Reddersen, B.; Fricke, T.; Wachendorf, M. (2014): A multi-sensor approach for predicting biomass of extensively managed grassland. In: *Computers and Electronics in Agriculture* 109, S. 247–260. DOI: 10.1016/j.compag.2014.10.011.

Roth, L.; Streit, B. (2018): Predicting cover crop biomass by lightweight UAS-based RGB and NIR photography. An applied photogrammetric approach. In: *Precision Agric* 19 (1), S. 93–114.

Roujean, J.-L.; Breon, F.-M. (1995): Estimating PAR Absorbed by Vegetation from Bidirectional Reflectance Measurements. In: *Remote Sens Environ* 51, S. 375–384.

Rouse, J. W.; Haase, R. H.; Schell, A.; Deering, D. W. (1974): Monitoring Vegetation Systems in the Great Plains with ERTS. Proceedings Third ERTS Symposium, NASA SP-351, 10–14 December 1973, Washington, DC (Washington: NASA Scientific and Technical Information Office), S. 309–317.

Sanderson, M. A.; Rotz, C. A.; Fultz, S. W.; Rayburn, E. B. (2001): Estimating Forage Mass with a Commercial Capacitance Meter, Rising Plate Meter, and Pasture Ruler. In: *Agronomy Journal* 93 (6), S. 1281.

Schaefer, M.; Lamb, D. (2016): A Combination of Plant NDVI and LiDAR Measurements Improve the Estimation of Pasture Biomass in Tall Fescue (Festuca arundinacea var. Fletcher). In: *Remote Sensing* 8 (2), S. 109. DOI: 10.3390/rs8020109.

Schellberg, J.; Hill, M. J.; Gerhards, R.; Rothmund, M.; Braun, M. (2008): Precision agriculture on grassland. Applications, perspectives and constraints. In: *Eur J Agron* 29 (2-3), S. 59–71.

Schellberg, J.; Verbruggen, E. (2014): Frontiers and perspectives on research strategies in grassland technology. In: *Crop Pasture Sci.* 65 (6), S. 508. DOI: 10.1071/CP13429.

Schirrmann, M.; Giebel, A.; Gleiniger, F.; Pflanz, M.; Lentschke, J.; Dammer, K.-H. (2016): Monitoring Agronomic Parameters of Winter Wheat Crops with Low-Cost UAV Imagery. In: *Remote Sensing* 8 (9), S. 706.

Schröder, J. J.; Scholefield, D.; Cabral, F.; Hofman, G. (2004): The effects of nutrient losses from agriculture on ground and surface water quality: the position of science in developing indicators for regulation. In: *Environ Sci Policy* 7 (1), S. 15–23.

Schulze-Brüninghoff, D.; Hensgen, F.; Wachendorf, M.; Astor, T. (2019): Methods for LiDAR-based estimation of extensive grassland biomass. In: *Computers and Electronics in Agriculture* 156, S. 693–699. DOI: 10.1016/j.compag.2018.11.041.

Schut, A. G.T.; Traore, P. C. S.; Blaes, X.; By, R. A. de (2018): Assessing yield and fertilizer response in heterogeneous smallholder fields with UAVs and satellites. In: *Field Crops Research* 221, S. 98–107.

Seelan, S. K.; Laguette, S.; Casady, G. M.; Seielstad, G. A. (2003): Remote sensing applications for precision agriculture: A learning community approach. In: *Remote Sensing of Environment* 88 (1-2), S. 157–169. DOI: 10.1016/j.rse.2003.04.007.

Shafi, U.; Mumtaz, R.; García-Nieto, J.; Hassan, S. A.; Zaidi, S. A. R.; Iqbal, N. (2019): Precision Agriculture Techniques and Practices: From Considerations to Applications. In: *Sensors (Basel, Switzerland)* 19 (17). DOI: 10.3390/s19173796.

Shah, A.; Askegaard, M.; Rasmussen, I. A.; Jimenez, E. M. C.; Olesen, J. E. (2017): Productivity of organic and conventional arable cropping systems in long-term experiments in Denmark. In: *Eur J Agron* 90, S. 12–22.

Simin, C.; Rongqun, Z.; Liming, L.; De, Z. (2010): A method of salt-affected soil information extraction based on a support vector machine with texture features. In: *Math Comput Model* 51 (11-12), S. 1319–1325.

Stinner, Walter; Möller, Kurt; Leithold, Günter (2008): Effects of biogas digestion of clover/grass-leys, cover crops and crop residues on nitrogen cycle and crop yield in organic stockless farming systems. In: *European Journal of Agronomy* 29 (2-3), S. 125–134. DOI: 10.1016/j.eja.2008.04.006.

Stülpnagel, R. (1982): Schätzung der von Ackerbohnen symbiontisch fixierten Stickstoffmenge im Feldversuch mit der erweiterten Differenzmethode. In: *Zeitschrift für Acker- und Pflanzenbau* 151, S. 446–458.

Suter, M.; Connolly, J.; Finn, J. A.; Loges, R.; Kirwan, L.; Sebastià, M.-T.; Lüscher, A. (2015): Nitrogen yield advantage from grass-legume mixtures is robust over a wide range of legume proportions and environmental conditions. In: *Global change biology* 21 (6), S. 2424–2438.

Taravat, A.; Wagner, M.; Oppelt, N. (2019): Automatic Grassland Cutting Status Detection in the Context of Spatiotemporal Sentinel-1 Imagery Analysis and Artificial Neural Networks. In: *Remote Sensing* 11 (6), S. 711. DOI: 10.3390/rs11060711.

Thilakarathna, M.; Raizada, M. (2018): Challenges in Using Precision Agriculture to Optimize Symbiotic Nitrogen Fixation in Legumes: Progress, Limitations, and Future Improvements Needed in Diagnostic Testing. In: *Agronomy* 8 (5), S. 78.

Tilly, N.; Aasen, H.; Bareth, G. (2015): Fusion of Plant Height and Vegetation Indices for the Estimation of Barley Biomass. In: *Remote Sensing* 7 (9), S. 11449–11480. DOI: 10.3390/rs70911449.

Toupet, R.; Gibbons, A. T.; Goodacre, S. L.; Bell, M. J. (2020): Effect of Herbage Density, Height and Age on Nutrient and Invertebrate Generalist Predator Abundance in Permanent and Temporary Pastures. In: *Land* 9 (5), S. 164. DOI: 10.3390/land9050164.

Triantafyllou, A.; Sarigiannidis, P.; Bibi, S. (2019): Precision Agriculture: A Remote Sensing Monitoring System Architecture †. In: *Information* 10 (11), S. 348. DOI: 10.3390/info10110348.

Tucker, C. J. (1979): Red and Photographic Infrared Linear Combinations for Monitoring Vegetation. In: *Remote Sens Environ* 8, S. 127–150.

United Nations (2019): World Population Prospect 2019: Highlights. ST/ESA. Department of Economic and Social Affairs, Population Division.

van Eekeren, N.; van Liere, D.; Vries, F. de; Rutgers, M.; Goede, R. de; Brussaard, Li. (2009): A mixture of grass and clover combines the positive effects of both plant species on selected soil biota. In: *Appl Soil Ecol* 42 (3), S. 254–263.

van Evert, F. K.; Polder, G.; van der Heijden, G. W. A. M.; Kempenaar, C.; Lotz, L. A. P. (2009): Real-time vision-based detection of Rumex obtusifolius in grassland. In: *Weed Res* 49 (2), S. 164–174.

van Iersel, W.; Straatsma, M.; Addink, E.; Middelkoop, H. (2018): Monitoring height and greenness of non-woody floodplain vegetation with UAV time series. In: *ISPRS Journal of Photogrammetry and Remote Sensing* 141, S. 112–123.

Velthof, G. L.; Lesschen, J. P.; Schils, R.; Smit, A.; Elbersen, B.; Hazeu, G. et al. (2014): Final report: Grassland areas, production and use. Lot 2. Methodological studies in the field of Agro-Environmental Indicators. European Commission, EUROSTAT.

Viljanen, N.; Honkavaara, E.; Näsi, R.; Hakala, T.; Niemeläinen, O.; Kaivosoja, J. (2018): A Novel Machine Learning Method for Estimating Biomass of Grass Swards Using a Photogrammetric Canopy Height Model, Images and Vegetation Indices Captured by a Drone. In: *Agriculture* 8 (5), S. 70.

Vincini, M.; Frazzi, E.; D'Alessio, P. (2008): A broad-band leaf chlorophyll vegetation index at the canopy scale. In: *Precision Agric* 9 (5), S. 303–319.

Wachendorf, M.; Fricke, T.; Möckel, T. (2018): Remote sensing as a tool to assess botanical composition, structure, quantity and quality of temperate grasslands. In: *Grass Forage Sci* 35 (4), S. 201.

Wallace, L.; Hillman, S.; Reinke, K.; Hally, B.; Kriticos, D. (2017): Non-destructive estimation of above-ground surface and near-surface biomass using 3D terrestrial remote sensing techniques. In: *Methods Ecol Evol* 257, S. 1684.

Wan, S.; Chang, S.-H. (2018): Crop classification with WorldView-2 imagery using Support Vector Machine comparing texture analysis approaches and grey relational analysis in Jianan Plain, Taiwan. In: *Int J Remote Sens* 40 (21), S. 8076–8092.

Wang, C.; Nie, S.; Xi, X.; Luo, S.; Sun, X. (2017a): Estimating the Biomass of Maize with Hyperspectral and LiDAR Data. In: *Remote Sensing* 9 (1), S. 11. DOI: 10.3390/rs9010011.

Wang, D.; Xin, X.; Shao, Q.; Brolly, M.; Zhu, Z.; Chen, J. (2017b): Modeling Aboveground Biomass in Hulunber Grassland Ecosystem by Using Unmanned

Aerial Vehicle Discrete Lidar. In: *Sensors (Basel, Switzerland)* 17 (1). DOI: 10.3390/s17010180.

Wang, X.; Gao, X.; Zhang, Y.; Fei, X.; Chen, Z.; Wang, J. et al. (2019): Land-Cover Classification of Coastal Wetlands Using the RF Algorithm for Worldview-2 and Landsat 8 Images. In: *Remote Sens* 11 (16), S. 1927.

Watanabe, K.; Guo, W.; Arai, K.; Takanashi, H.; Kajiya-Kanegae, H.; Kobayashi, M. et al. (2017): High-Throughput Phenotyping of Sorghum Plant Height Using an Unmanned Aerial Vehicle and Its Application to Genomic Prediction Modeling. In: *Frontiers in plant science* 8, S. 421.

Wijaya, A.; Kusnadi, S.; Gloaguen, R.; Heilmeier, H. (2010): Improved strategy for estimating stem volume and forest biomass using moderate resolution remote sensing data and GIS. In: *J For Res* 21 (1), S. 1–12.

Wijesingha, J.; Astor, T.; Schulze-Brüninghoff, D.; Wengert, M.; Wachendorf, M. (2020): Predicting Forage Quality of Grasslands Using UAV-Borne Imaging Spectroscopy. In: *Remote Sensing* 12 (1), S. 126. DOI: 10.3390/rs12010126.

Wijesingha, J.; Moeckel, T.; Hensgen, F.; Wachendorf, M. (2018): Evaluation of 3D point cloud-based models for the prediction of grassland biomass. In: *International Journal of Applied Earth Observation and Geoinformation* 78, S. 352–359.

Willmott, C. J. (1981): On the validation of models. In: *Physical Geography* (2), S. 184–194.

Wood, E. M.; Pidgeon, A. M.; Radeloff, V. C.; Keuler, N. S. (2012): Image texture as a remotely sensed measure of vegetation structure. In: *Remote Sens Environ* 121, S. 516–526.

Wood, E. M.; Pidgeon, A. M.; Radeloff, V. C.; Keuler, N. S. (2013): Image Texture Predicts Avian Density and Species Richness. In: *PloS one* 8 (5).

Xu, D.; Guo, X. (2015): Some insights on grassland health assessment based on remote sensing. In: *Sensors (Basel, Switzerland)* 15 (2), S. 3070–3089. DOI: 10.3390/s150203070.

Xu, K.; Su, Y.; Liu, J.; Hu, T.; Jin, S.; Ma, Q. et al. (2020): Estimation of degraded grassland aboveground biomass using machine learning methods from terrestrial laser scanning data. In: *Ecological Indicators* 108, S. 105747. DOI: 10.1016/j.ecolind.2019.105747.

Xue, J.; Su, B. (2017): Significant Remote Sensing Vegetation Indices: A Review of Developments and Applications. In: *J Sens* 2017 (1), S. 1–17.

Yang, X.; Tridandapani, S.; Beitler, J. J.; Yu, D. S.; Yoshida, E. J.; Curran, W. J.; Liu, T. (2012): Ultrasound GLCM texture analysis of radiation-induced parotid-gland injury in head-and-nech cancer radiotherapy: An in vivo study of late toxicity. In: *Med. Phys.* 39 (9).

Yao, H.; Qin, R.; Chen, X. (2019): Unmanned Aerial Vehicle for Remote Sensing Applications—A Review. In: *Remote Sens* 11 (12), S. 1443.

Yu, X.; Liu, Q.; Liu, X.; Wang, Y. (2017): A physical-based atmospheric correction algorithm of unmanned aerial vehicles images and its utility analysis. In: *International Journal of Remote Sensing* 38 (8-10), S. 3101–3112. DOI: 10.1080/01431161.2016.1230291.

Yue, J.; Yang, G.; Li, C.; Li, Z.; Wang, Y.; Feng, H.; Xu, B. (2017): Estimation of Winter Wheat Above-Ground Biomass Using Unmanned Aerial Vehicle-Based Snapshot Hyperspectral Sensor and Crop Height Improved Models. In: *Remote Sensing* 9 (7), S. 708. DOI: 10.3390/rs9070708.

Yue, J.; Yang, G.; Tian, Q.; Feng, H.; Xu, K.; Zhou, C. (2019): Estimate of winter-wheat above-ground biomass based on UAV ultrahigh-ground-resolution image textures and vegetation indices. In: *ISPRS Journal of Photogrammetry and Remote Sensing* 150, S. 226–244. DOI: 10.1016/j.isprsjprs.2019.02.022.

Zeng, L.; Wardlow, B. D.; Xiang, D.; Hu, S.; Li, D. (2020): A review of vegetation phenological metrics extraction using time-series, multispectral satellite data. In: *Remote Sensing of Environment* 237, S. 111511. DOI: 10.1016/j.rse.2019.111511.

Zhang, N.; Wang, M.; Wang, N. (2002): Precision agriculture*a worldwide overview. In: *Computers and Electronics in Agriculture* 36, S. 113–132.

Zheng, H.; Cheng, T.; Zhou, M.; Li, D.; Yao, X.; Tian, Y. et al. (2019): Improved estimation of rice aboveground biomass combining textural and spectral analysis of UAV imagery. In: *Precision Agric* 20 (3), S. 611–629.

Zheng, H.; Ma, J.; Zhou, M.; Li, D.; Yao, X.; Cao, W. et al. (2020): Enhancing the Nitrogen Signals of Rice Canopies across Critical Growth Stages through the Integration of Textural and Spectral Information from Unmanned Aerial Vehicle (UAV) Multispectral Imagery. In: *Remote Sensing* 12 (6), S. 957. DOI: 10.3390/rs12060957.

Zhou, J.; Yan Guo, R.; Sun, M.; Di, T. T.; Wang, S.; Zhai, J.; Zhao, Z. (2017): The Effects of GLCM parameters on LAI estimation using texture values from Quickbird Satellite Imagery. In: *Scientific reports* 7 (1), S. 7366.

Zhou, Z.; Morel, J.; Parsons, D.; Kucheryavskiy, S. V.; Gustavsson, A.-M. (2019): Estimation of yield and quality of legume and grass mixtures using partial least squares and support vector machine analysis of spectral data. In: *Comput Electron Agric* 162, S. 246–253.